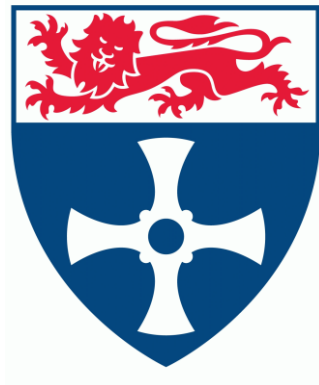


---

# **On The Design And Construction Of Modulated Pole Machines**



**Edwin Pinguey**

A thesis submitted for the degree of  
Engineering Doctorate in Power Electronics,  
Drives and Machines

University of Newcastle Upon Tyne  
School of Electrical, Electronic and Computer Engineering  
December 2010

---

---

**To my family,  
for their support and love**

---

**Abstract**

This thesis presents two designs for modulated pole machines from concept through to validating prototypes, each comparing favourably with other modulated pole machines. The key feature to these designs is that they employ novel fabrication techniques which are realisable in low cost manufacture without compromise in performance. This is achieved by reviewing the specific properties of soft magnetic composite and laminated steel. Each material was then utilised in such a way as to take best advantage of its distinguishing properties leading to the development of novel fabrication and construction techniques.

The designs are each presented in three stages. Firstly the development of the concept is presented and the use of finite element simulation to reach a design worthy of construction is documented. The development of fabrication techniques for the various parts is then presented along with the assembly into a working single phase prototype. Finally testing and comparison of results with simulated and other existing published designs is presented.

## Acknowledgement

This EngD thesis would never have been conceived without my supervisor Professor Alan Jack who set up the EngD centre at Newcastle and made the phone call to me, bringing it to my attention. For this, along with the large amount of knowledge and support he has passed on to me, I am truly grateful.

Secondly, I wish to thank Höganäs AB for their sponsorship of the project, their support and technical guidance with their product. The months I spent at the company HQ in Sweden gave me my first insight into industry and also Swedish culture.

I'd like to thank all those that have worked with me in the school, including the technicians in the mechanical workshop who endured my endless requests for jigs and assemblies, specifically Chris and Stuart. Those from the UG Lab and later CAED, both past and present, that have listened to my endless descriptions of problems and then suggested we think it over in the pub.

A special thank you goes to the IT guys for their assistance throughout with random non-standard software requests and endless requirements for more processing power.

I'd like to thank my current employer Dyson Ltd who has allowed me the time and flexibility to finalise this theses. Without which it may never have come to light.

Finally I would like to thank my family, especially my wife Mhairi and my two children, Maia and Ethan. Over the last couple of years they have been deprived of my time while I was writing up. They have shown me endless support and love. I look forward to spending more time with you all.

## Table of Contents

Chapter 1. Introduction .....	1
1.1 The Engineering Doctorate .....	1
1.2 Höganäs AB .....	1
1.3 What is a Modulated Pole Machine? .....	1
1.3.1 Modulated Poles - the pole number effect .....	2
1.3.2 History and Development of Modulated Pole Machines .....	5
1.3.3 Modern day machines - Incorporation of Permanent Magnets. ....	7
1.3.4 Power Factor .....	9
1.3.5 Magnet Utilisation .....	10
1.3.6 Multiple Phase Machines .....	13
1.4 Materials for Manufacturing MP Machines .....	14
1.5 Material Hybrid Concept .....	16
1.5.1 Material Hybrid Machines .....	16
1.5.2 Forming Laminations .....	18
1.5.3 Flux Concentrated Rotor .....	18
1.5.4 Toroidal Winding .....	19
1.6 Material Hybrid MP Concept .....	19
1.7 Objectives and Overview of the Thesis .....	20
Chapter 2. Electromagnetic Design Development Using Finite Element Analysis .....	22
2.1. Finite Element Analysis .....	22
2.2. Electromagnetic Finite Element Analysis (FEA) in ANSYS .....	22
2.3. ANSYS FE Model .....	23
2.3.1. Model Symmetry .....	23
2.3.2. Mesh Refinement .....	26
2.4. Pole Number .....	26

---

2.5.	Torque Calculation using Co-energy from D-axis Flux.....	27
2.6.	Material Properties .....	28
2.6.1.	Magnet .....	28
2.6.2.	SMC and Laminations.....	28
2.7.	12 Pole Design.....	29
2.7.1.	Geometry Development.....	29
2.7.2.	Design Analysis .....	32
2.8.	Leakage path assessment .....	33
2.9.	Fifty pole design.....	35
2.9.1.	First Fifty Pole Design with a 20-10-20 stator ratio .....	36
2.9.2.	Reducing the Axial Length .....	38
2.9.3.	Stator ratio 8-8-8 with straight teeth.....	41
2.9.4.	Larger SMC cross section area.....	44
2.10.	Final Design summary .....	46
Chapter 3.	Construction of the Material Hybrid Prototype .....	50
3.1	Stator .....	50
3.1.1	Introduction.....	50
3.1.2	Laminations .....	50
3.1.3	SMC core-back sections.....	52
3.2	Rotor .....	54
3.2.1	SMC Flux Concentration Blocks.....	54
3.2.2	Magnets .....	55
3.2.3	Shaft and Rotor Mount.....	55
3.3	Coil.....	58
3.4	Casing and Shaft .....	62
3.4.1	Outer Casing .....	62
3.4.2	End Caps .....	62

---

---

3.4.3	Shaft .....	64
3.5	Assembly .....	64
3.5.1	Stator Assembly .....	64
3.5.2	Rotor Assembly.....	66
3.5.3	Final Assembly.....	67
Chapter 4.	Testing and Comparison with Calculations for the Material Hybrid Prototype..	69
4.1	Thermal Testing.....	69
4.2	Static Torque Measurements.....	72
4.2.1	Rig set-up.....	72
4.2.2	Cogging Torque .....	72
4.2.3	Aligned Cogging Torque.....	74
4.2.4	Unaligned Cogging Torque .....	75
4.2.5	Combined Aligned and Unaligned Cogging Torque Effects .....	76
4.2.6	Retrospective FE investigation of Construction Issues .....	77
4.2.7	Armature excited torques .....	82
4.2.8	Average torque.....	84
4.3	Torque per unit mass .....	85
4.4	Inductance Measurements and Computed Power factor .....	86
Chapter 5.	Development of the Formed Lamination Machine.....	90
5.1	The Approach.....	90
5.2	Design Development.....	90
5.2.1	Solid Core-back with projecting teeth.....	90
5.2.2	Replace SMC arcs with lamination links .....	93
5.2.3	Overcoming the Increased Length Due to Bending .....	94
5.2.4	Introduction of Skew.....	95
5.2.5	A Better Skew Position .....	96
5.2.6	Bending order.....	97

---

5.2.7	Creating Bend B.....	97
5.3	Creating Bend A .....	98
5.4	Three section test.....	99
Chapter 6.	Construction of the Formed Lamination Machine.....	103
6.1	Lamination Production .....	103
6.2	Bending the laminations .....	105
6.3	The Winding .....	111
6.4	Forming the Laminations around the coil.....	114
6.5	Casing and end caps .....	115
6.6	Assembly and Final Machining.....	116
Chapter 7.	Testing of Formed Lamination Prototype and Comparison with the MH Prototype. ....	119
7.1	Thermal Testing.....	119
7.2	Rotor Failure.....	122
7.3	Back EMF .....	123
7.3.1	Measurements .....	123
7.3.2	Air-gap measurement .....	124
7.3.3	Finite Element Calculated effect of air-gap differences.....	125
7.4	Static Torque Measurements.....	129
7.4.1	Cogging Torque .....	129
7.4.2	Armature Excited Torque .....	132
7.4.3	Average torque.....	133
7.5	Loss Measurements.....	134
7.6	Torque per unit Mass .....	136
7.7	Inductance measurement and Computed Power Factor.....	137
Chapter 8.	Conclusions .....	140
8.1	Design .....	140
8.2	Construction of the first prototype .....	140

8.3	Measured Results.....	142
8.4	Formed Lamination Concept .....	144
8.5	Measured Results FL prototype .....	145
8.6	Closing Statement .....	147
	References.....	148

**List of Symbols and Abbreviations**

FL	Formed Lamination
MH	Material Hybrid
EngD	Engineering Doctorate
PM	Powder Metallurgy
SMC	Soft Magnetic Composite
MP	Modulated Pole
MMF	Magneto Motive Force
TFM	Transverse Flux Machine
DC	Direct Current
AC	Alternating Current
BLPM	Brushless Permanent Magnet
BLDC	Brushless Direct Current
MPPM	Modulated Pole Permanent Magnet
NdFeB	Neodymium Iron Boron
Nm	Newton Meter
Kg	Kilogramme
FEA	Finite Element Analysis
2D	Two Dimensional
3D	Three Dimensional
FE	Finite Element
CAD	Computer Aided Design
$\Phi$	Power Factor Angle
PF	Power Factor
$\Psi$	Flux Linkage
I	Current
E / emf	Back Electro Motive Force
X	Reactance

T	Tesla
$T_c$	Case Temperature
$T_w$	Winding Temperature
$\tau$	Time constant
MDF	Medium Density Fibreboard
CMM	Co-ordinate Measuring Machine

## **Chapter 1. Introduction**

### **1.1 The Engineering Doctorate**

The Engineering Doctorate (EngD) program is structured to deliver research of PhD level, but with current industrial relevance. This is achieved by the sponsorship of the 'research engineer' by an industrial partner which will appoint a supervisor to compliment the academic supervisor and help direct the research. The EngD takes an additional year compared to a standard 3 year PhD in which time the student undertakes taught modules, this allows the transfer of a student into the EngD from a neighbouring engineering discipline.

### **1.2 Höganäs AB**

This EngD was sponsored by Höganäs AB, Sweden who's principal activities are developing, manufacturing and marketing iron and metal powders [1] (an area of technology commonly known as powder metallurgy, (PM)) . The products are used for the production of precision components for the automotive industry, white goods, computers and power tools. Within the array of products is a group of powder products that go by the trade name of Somaloy® and fall into the internationally recognized name classification of soft magnetic composites (SMC). SMC is commonly used in the cores of high frequency components such as inductors, where it easily out performs laminated steel. The Somaloy® range is different and has a target use in lower frequency electrical machines. Direct replacement of laminations with SMC will generally result in poor results and the machine design engineer has to aim to take full advantage of the isotropic properties of SMC to achieve designs with benefits over the use of laminations. A more in depth comparison of laminations and SMC is given later in this chapter.

### **1.3 What is a Modulated Pole Machine?**

The concept of modulated pole machines (MP) is to use highly permeable iron structures around a single homopolar coil to create a multiplex of poles, each with an MMF equal to that of the homopolar coil, i.e. increasing the pole number without changing the volume or rotational speed of the machine will result in an increase in the magnetic field strength produced by the poles and this in turn results in an increase in the specific torque. This term is introduced to gather together a range of machines known by a variety of titles which use this principle. A particular example is machines described as transverse flux (TFM) which have their origins in two papers presented by Weh [2, 3] in the 1980's in which he makes reference to the fact that flux links with the windings in a direction which is 'transverse' to the direction of motion of the machine whereas, conventional layouts used for instance in

commonplace induction and synchronous machines have major elements of their flux paths which are more in alignment with the motion of the machine. It is commonly recognised that TFM is an inadequate name as it fails to recognise the crux of this family of machines which is in the method of making multiple poles from single coils. To unify the set of machines the term Modulated Pole (MP), will be used throughout the thesis.

### 1.3.1 Modulated Poles - the pole number effect

To help understand how changing the pole number increases the specific force (or torque) output for a given machine dimension, it is good to first consider the fundamentals of electromagnetic force generation. From the general expression for the force acting on a conductor in a magnetic field,

$$F = Bil \quad (1-1)$$

it can be derived [4] that the force per unit volume of a machine,  $F$ , is

$$T = kAB_{g\max}r^2l \quad (1-2)$$

Where  $k$  is a constant for a specific operating point,  $r$  is the rotor radius and  $l$  the rotor axial length.  $A$  represents the electrical loading and is normally defined as the magneto motive force (MMF) per unit periphery of the machine.  $B_{g\max}$  represents the magnetic loading of the machine and is usually defined as the peak flux density in the air-gap of the machine.

Equation (1-2) gives an indication of the energy density of the machine and for conventional machines directly relates to the capability of the machine to convert energy between the electrical and mechanical systems. As will be explained in more detail shortly, changing the internal geometry of a conventional machine does not (significantly) increase the conversion of energy and so the equation is a useful means of classification for conventional machines. However, this is not the case for a MP machine where the specific output can be changed by altering the internal geometry of the machine, i.e. increasing the pole number and hence increasing the electrical loading without any change in cooling or volume.  $A$  is thus not a fixed number for a particular size and cooling regime and hence the possibilities for increased torque are rather hidden by equation (1-2).

An alternative is to write the equation for force in terms of the change in co-energy [5] as in equation (1-3).

$$F = \frac{\partial W'}{\partial x} \quad (1-3)$$

If forces not related to current (i.e. cogging) are ignored, equation (1-3) can be written as

$$F = i \frac{\partial \psi}{\partial x} \quad (1-4)$$

An attempt will now be made to explain in detail the ability of an MP machine to increase specific output by altering the pole number by comparing the idealised linear machines presented in Figure 1-1. Linear machines are used here as they simplify the description of flux modulation [6, 7], but the same theory can be applied to rotational machines by replacing force and distance with torque and angle respectively.

Consider first the four pole section of a conventional machine topology, Figure 1-1(a) and an MP machine topology, Figure 1-1(b). It is clearly evident that a displacement at a fixed speed between the field producing magnets and the armature teeth results in a change in flux linking the armature winding,  $\psi$ . Maintaining a fixed current  $i$ , and noting that the winding flux linkage alternates with position, it is seen from equation (1-4) that an alternating force with change in position of peak value  $\hat{F}$  is produced.

Now consider the case where the pole number is doubled to eight for the same length of machine, shown for the conventional machine in Figure 1-1(c) and the MP machine Figure 1-1(d). For the same displacement and fixed speed as before, the rate of change of the flux linkage has increased by a factor of two. i.e. work is being done twice as fast if the current does not change. However, this does not result in a doubling of the peak force output of the conventional machine as the doubling of the pole number halved the area available for the armature conductor. This means that for the same thermal limits of the machine, the MMF per pole must be reduced by a factor of two to prevent overheating. The net result is the specific output of the machine is not altered significantly by a change in pole number. The topology of the MP machine means that alteration to the pole number has no direct effect on the space for the armature winding, so the electrical loading can stay the same. Couple this with the increased rate of change of flux linkage and it is seen that the peak force output of the MP machine changes directly with the pole number.

This is not strictly fair to the conventional machine, as an increase in pole number results in a corresponding drop in the flux carried by the armature core back and hence the core back can be made smaller and the area available for conductors made correspondingly larger. However this is an effect which gets smaller as the pole number rises and at typical pole numbers does not match the rise in force inherent in the MP structure.

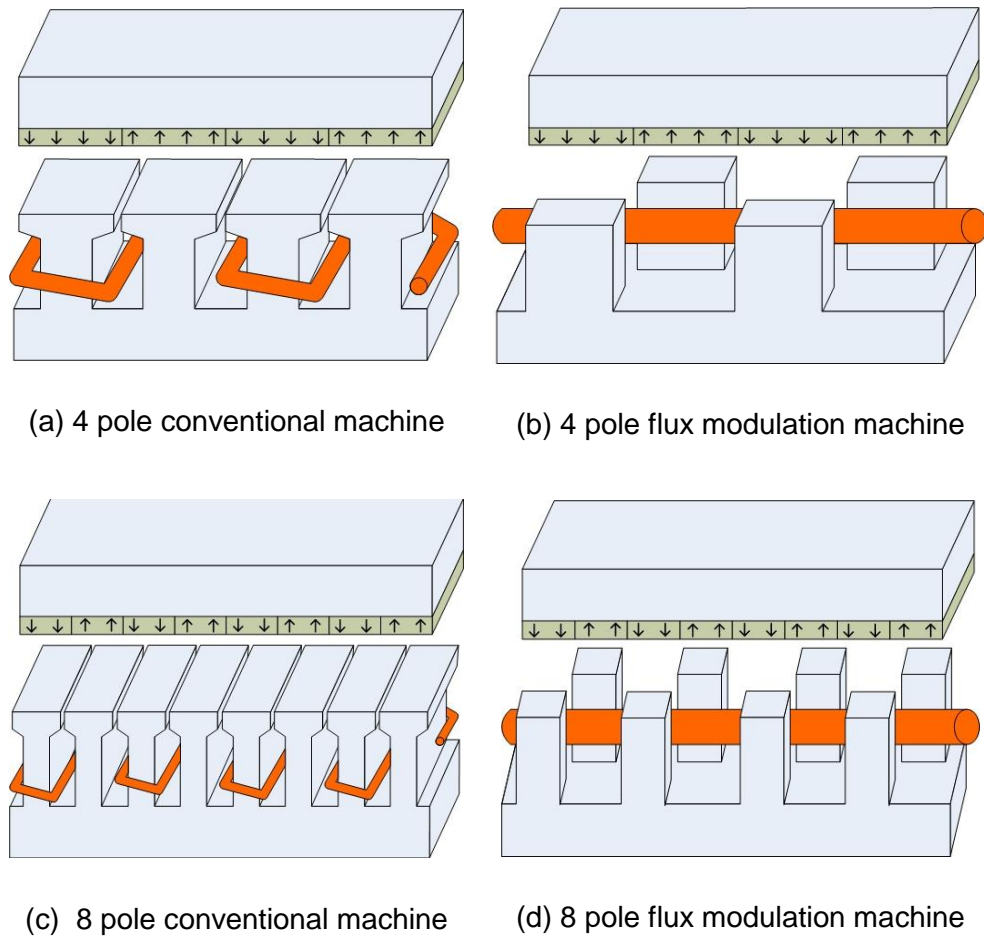


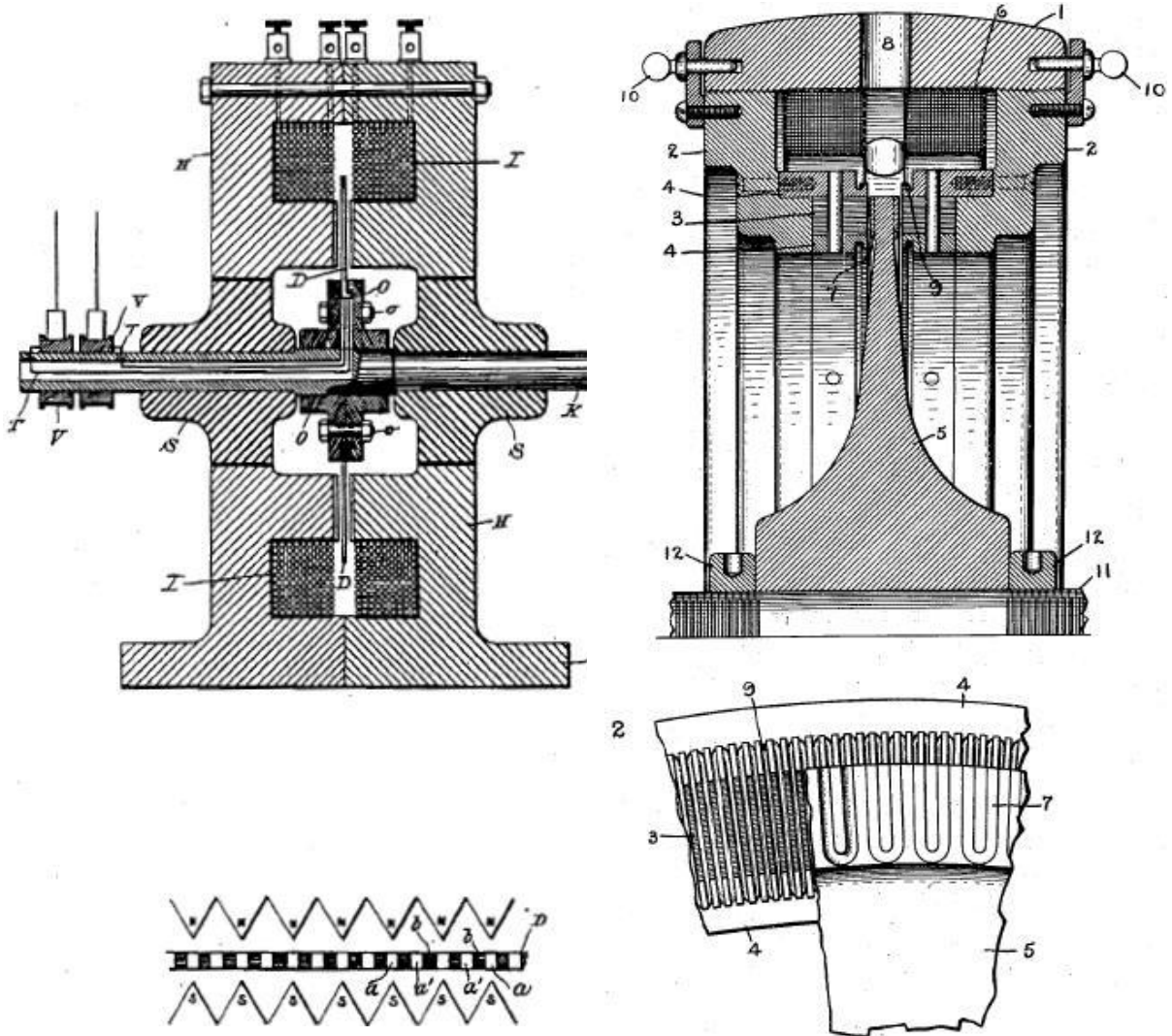
**Figure 1-1 Diagrams showing the effects of changing the pole number for conventional and MP machines**

By this definition, an MP machine with infinite specific output is achievable, but of course this is not true. As the pole number increases and the distance between adjacent teeth starts to approach that of the air-gap between the stator and rotor, the amount of field flux leaking without linking the armature winding starts to dominate and the advantages of the flux modulation are lost. However, it has been shown [8] that pragmatic limits in terms of manufacturability and the switching frequency of the converter are more probable to dominate, limiting the pole number well below any magnetic limit.

Another major problem associated with a high electric loading is a high armature reactance which is exacerbated in an MP machine by the leakage fields created by the complex magnetic circuit necessary to produce the poles via modulating the flux. This has negative implications for the VA rating of the converter and for the limits imposed by saturation of the core.

### 1.3.2 History and Development of Modulated Pole Machines

The idea of using an iron structure to modulate the flux of a single coil can easily be traced back to around the turn of the 20<sup>th</sup> century. The growth in interest of electrical power distribution and wireless communications led to numerous inventions and patents for continuous wave generation. Nicola Tesla's patent [9], a diagram from which is reproduced in Figure 1-2(a) uses a homopolar winding (I) in an iron 'C' core (N) with a serrated surface in the air-gap to produce a multitude of poles. A rotating winding is placed between the two sides of the serrated air-gap of the stator, wound such (bottom Figure 1-2(a)) that the rotation induces an alternating voltage. A very similar idea is used by Ernest Alexanderson in his patent [10] of a 100kHz inductor alternator for radio communications, Figure 1-2(b). The difference being that the armature winding (3) is integrated into the stator (4) and a variable permeance rotor (5) is used to create the alternating field, the idea for which Alexanderson took from William Stanley's invention in 1887, "a novel rotating electric machine that used 'iron projections' to produce a fluctuating magnetic flux" [11, 12]. The result is that unlike Tesla's machine this one is a 'brushless' solution.



(a) Tesla's high frequency generator [9]      (b) Alexanderson's 100kHz Alternator [10]

Figure 1-2 diagrams from patents of N. Tesla and E. F. W. Alexanderson showing high frequency machines

At the same time as the afore mentioned patent of Tesla's being granted, William Mordey filed a patent [13] that is much more akin to the machines that will be presented as the focus for this thesis. The patent itself contains a range of variants about the same concept "a method of constructing an alternate-current machine having only a single pole or winding" [13]. He then goes on to state that "Thus I am able to construct alternate-current machines for any speed and required rate of alternations in which there is but one simple annular armature-coil and one annular field-magnet coil", which is a very concise way of describing that Mordey has realised the advantage of modulated poles given in section 1.3.1. The simplest variant in the patent to understand is reproduced in Figure 1-3. The inner structure has a simple annular DC winding and an iron structure to modulate this into multiple poles. The outer armature consists of two types of iron structures (I + K) alternating in position around a second annular winding. As the machine rotates the iron structures labelled I that

form a U shape around the armature winding see changing level of flux as the field rotates. The “magnet short-circuiting pieces” labelled k, keep the reluctance path for the field winding fairly constant, preventing the need to laminate the iron structure of the rotor. However, the alternating field seen by the iron parts of the armature mean that these must be laminated to prevent excessive iron loss.

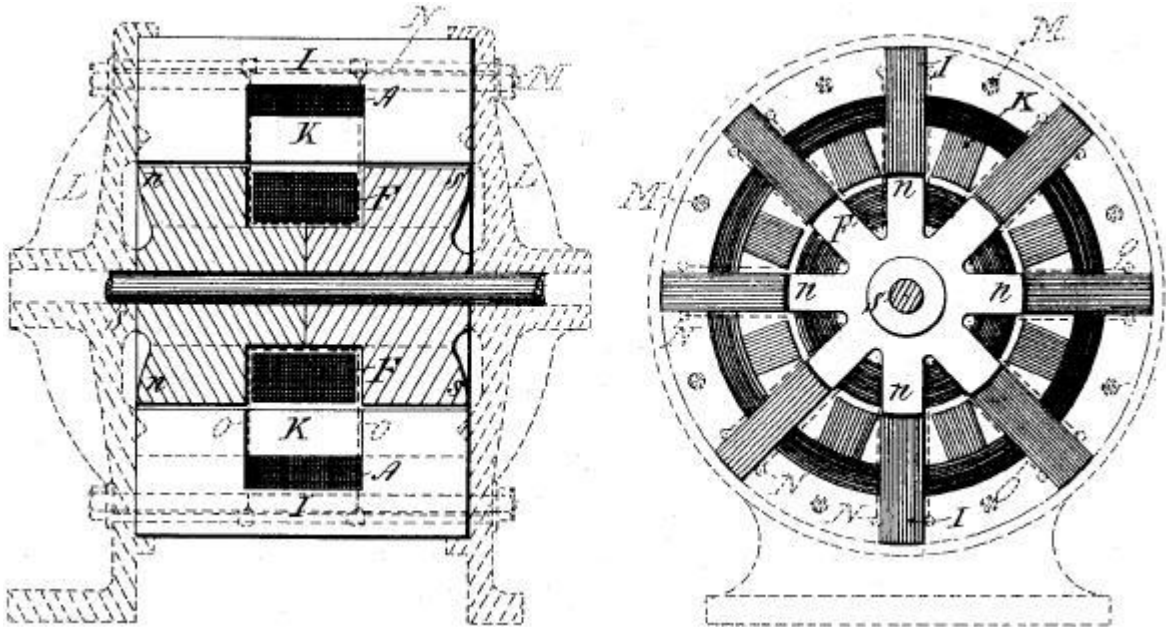


**Figure 1-3 A variant from Mordey's patent [13] for a construction method of an electric generator with only one annular coil**

### **The Lundell ‘claw-pole’ Alternator**

The Lundell ‘claw pole’ induction alternator is the basis of the modern day automotive alternator and is one of the most widely found examples of modulated poles in the modern day. The basis of the iron claw like structure modulating the flux of a single dc stator winding was invented by Robert Lundell while working for an Edison affiliated company, but the idea did not take off until the company was bought by General Electric in 1902 who paid Lundell royalties for every one made. It was later adapted for a source of electric power in tanks, and with the introduction of silicon diodes in 1960 in the form of a diode bridge, the modern day automotive alternator was conceived [14]. Interestingly while the introduction of affordable silicon components allowed the realisation of the modern automotive alternator, it spelled the end for the final application of induction alternators as the silicon thyristor replaced them.

### **1.3.3 Modern day machines - Incorporation of Permanent Magnets.**

With the introduction in the second half of the twentieth century of higher energy density magnets [15] and semiconductors replacing valves, the brushless permanent magnet (BLPM) machine became increasingly popular. Attention was turned back to the modulated

pole topologies developed at the turn of the century and the question asked, what happens when the field winding is replaced by permanent magnets?

Claw pole armature structures had been common place for many years in permanent magnet synchronous machines of the small power range, such as clock motors. They look very similar in configuration to that shown in Figure 1-4 which is a multi phase BLPM machine commonly found in hard disk drives. More in depth study into the operations of these machines is given by [16] and [17].



**Figure 1-4 Claw pole armature in a small BLPM machine taken from a hard disc drive**

One of the earliest references this author can find relating to the use of modulated pole in medium power permanent magnet brushless direct current (BLDC) machines is G.W. Mclean [7] in 1979. The machine presented in this paper, the topology of which is shown reproduced from the paper in Figure 1-5a, uses 'C' shaped iron sections arranged alternately around a single coil to produce a disc armature with a double claw pole structure resulting in the machine requiring two rotors. The paper is of specific relevance to this thesis as it highlights the problems associated with trying to laminate the iron structures of a rotating MP machine. Lamination is required in this situation due to the MP component being located in the armature of the machine, unlike the automotive alternator [14] where the MP structure is used for the DC field allowing construction from solid steel. Increasing the pole number of an MP machine to increase the specific output results in a high frequency in the armature thus making laminations essential to minimise eddy current loss. McLean's solution to achieve lamination in the circumferential direction is presented in Figure 1-5(b) (also reproduced from [7]). The outer and inner C sections have different dimensions in terms of the surface area

presented to the active air-gap. The sections linking the outer part of the coil present a radially short and circumferentially long rectangle to the air-gap, while the opposite is true for the sections linking the inner surface of the coil. It is shown that carefully selecting the ratio of these sizes, can result in a balanced net effect in terms of flux linking the coil. However, this makes a poor utilisation of the magnets, something that will later be shown to be critical in achieving a good power factor in MP permanent magnet (MPPM) machines.

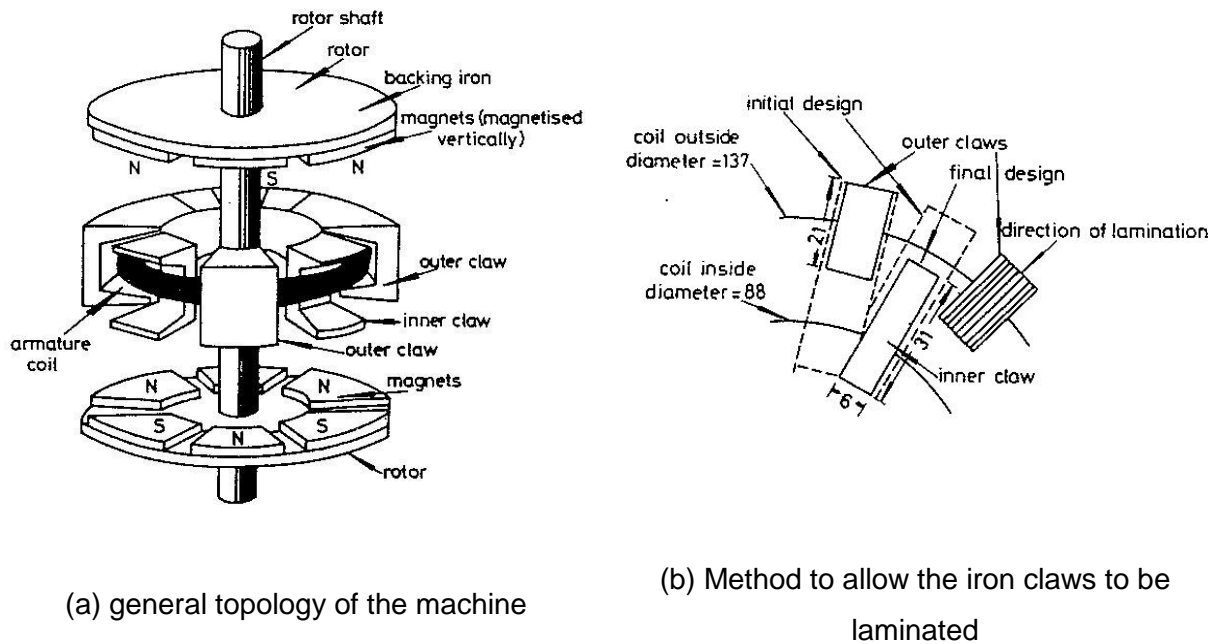


Figure 1-5 McLean's double air-gap/rotor clawpole machine taken from [7]

### 1.3.4 Power Factor

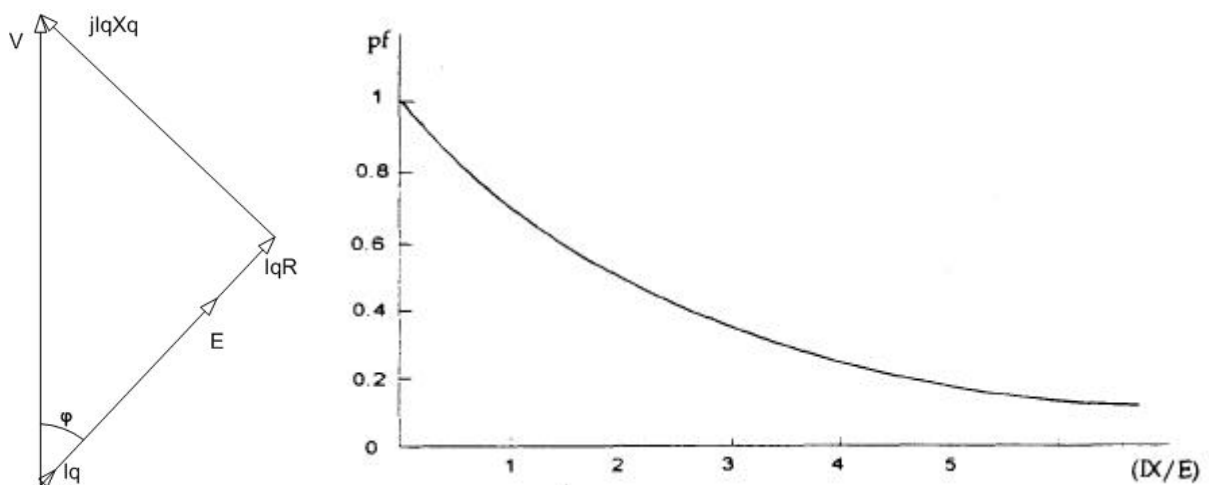
Here power factor refers only to the angle between voltage and current in an alternating system (i.e displacement power factor) and no account is taken of the effects of harmonic distortion (i.e. the distortion power factor is assumed unity). This is clearly shown as the angle  $\phi$  in Figure 1-6(a) which is a generic vector diagram of a synchronous machine operating with only q-axis current. It is defined from this by Harris [18] that if the  $IR$  voltage drop is small and ignored, then the power angle can be defined as

$$\phi = \arctan\left(\frac{IX}{E}\right) \tag{1-5}$$

Harris termed this the 'flux ratio' and can be easier perceived as the ratio of flux linkage due to the armature acting alone and the flux linkage due to the magnets acting alone, neglecting saturation effects.

It is commonly referenced that the high torque densities in an MP machine are at the sacrifice of a low power factor [18], and this is to a certain extent true. The cause of this reduced power factor is directly related to the increase in pole numbers and the effect this has upon the inductance. More poles mean a higher electric loading and in addition the leakage paths for the armature flux to link the winding are proliferated which also increases the inductance. As the reactance,  $X$ , of the armature winding is directly proportional to the inductance, by observation of equation (1-5) it can be seen that the power factor angle increases. The increase in the power factor angle means that the VA rating of any power electronics used to drive the machine need to be overrated by the ratio of  $1:\cos(\phi)$ .

$\cos(\phi)$  is termed the power factor and the relationship between this and the flux ratio defined by Harris et al [18] is shown in Figure 1-6(b). While this shows the fall off in power factor as the flux ratio is increased due to greater reactance, it also shows that for a conventional machine to reach the torque densities achievable in naturally cooled MP machines, the power factor would also drop off, as this would require increased electrical loading and some form of forced cooling would need to be implemented.



(a) Vector diagram

(b) Harris's [18] graph relating 'flux ratio' and power factor

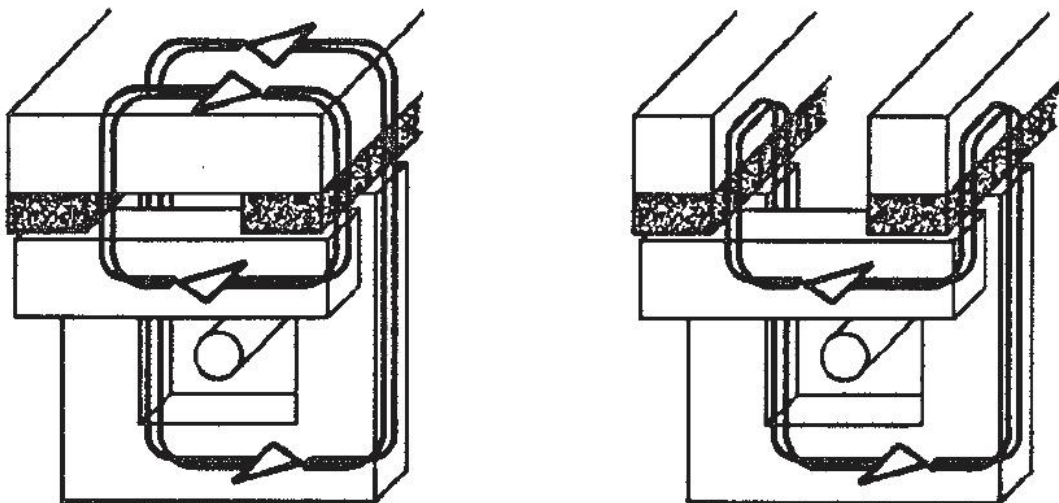
**Figure 1-6 Explanation for the low power factor commonly seen in MP machines**

### 1.3.5 Magnet Utilisation

While the description of power factor in MP machines above focused on the electrical side, it is also apparent that anything which results in a greater amount of flux linkage due to the field magnets without increasing the  $IX$  term will also improve the power factor. There are some very obvious things which may be done to improve things such as the use of high energy permanent magnets, namely Neodymium Iron Boron (NdFeB). It was also visible in Figure 1-5(b) that McLean's machine [7] has an armature iron structure which at the air-gap

is not optimal for collecting the flux of the magnet, i.e. there is a large discrepancy in the shape of the magnet and the armature poles, a compromise made to allow lamination of the armature iron to reduce iron loss. The utilisation of magnet flux has led to the development of different topologies of MPPM machines which tend to fall into one of two categories:

**Single sided machines:** These refer to structures similar to the generic MP machine in Figure 1-1(c), where the armature only takes flux from one side of the ‘surface mounted’ magnets and a return flux path is provided in the form of an iron core-back. In this specific example there is a 50% redundancy in magnets at any one time and as the magnets move in and out of alignment with the iron of the armature they are constantly being driven up and down in the second quadrant of their B-H characteristics [19]. To prevent the constant change of the magnet operating point, return paths in the form of Mordey’s [13] magnetic short-circuiting bars can be implemented. An example of which is shown in Figure 1-7(a) reproduced from Bork et al [20] a concept which has been adopted into many machines [3, 21]. Bork took the design a step further and removed the linking iron between magnets at different axial ends of the machine. The result shown in the diagram reproduced from [20] in Figure 1-7(b) shows that the main path for the field flux now links all the magnets. However, the advantage is counteracted to some extent by the presence of two air-gaps which the field flux must cross.



(a) Redundant magnets shorted

(b) Utilising redundant magnets

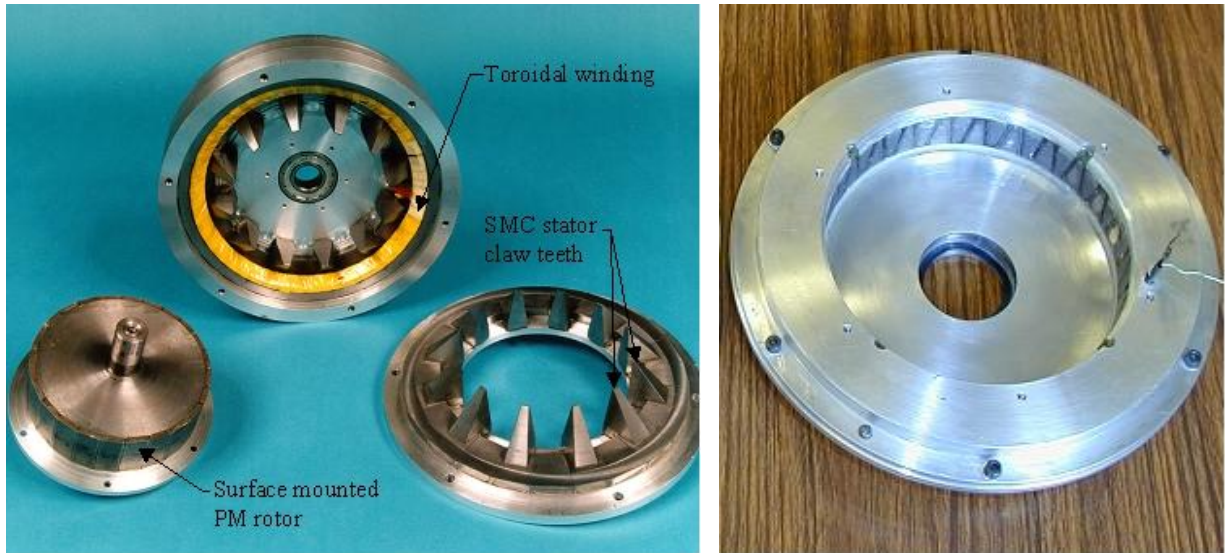
**Figure 1-7 100% magnet utilisation in a single sided MP machine taken from M. Bork et al [20]**

**Double sided machines:** Considering the single sided machine in Figure 1-7(a), removing the magnet core-back and replacing it with a second stator, Weh [3] revealed the double sided concept, another means by which the magnets can be 100% utilised. Two years later,

Weh published [22] the concept of using a flux concentrated rotor which utilises both sides of the magnet at all times, but removes the need for magnetic short-circuiting bars in the stator.

As with conventional machines, and documented by Weh et al's patent on MP machines [3], flux concentration provides great benefits in the performance of any machine as the flux density in the air-gap can be greater than the residual value of the magnet which provided it. When combined with a stator utilising an MP topology, high force density values can be achieved with substantially improved power factors.

Another method to reduce redundancy of magnets was developed and built by Jack et al [23] and tested by Madison [24] and prototypes are shown in Figure 1-8. Similar in concept to McLean's machine, Figure 1-5, discussed earlier, with a surface mounted magnet rotor and a claw pole structure in the armature stator achieved by the use of SMC and taking full advantage of its' isotropic permeability. By opting for a radial air-gap, rather than an axial one, [7] the structure of the claw teeth was equal throughout, allowing each tooth to be exposed to an identical magnetic field of the rotor. In comparison to [20, 21] method of utilising the flux, Jack' et al's [23] machine has a reduced the net air-gap length for the field flux. However, the close complex structure of the claw teeth does result in a high amount of armature flux reducing the power factor. The simplified structure of the armature does lend itself better to ease of manufacture. This prototype had a low torque density for active material of 3.3Nm/kg. Work by Dickenson [8, 25] optimised the machine design by increasing the pole number to 50 and reducing armature flux by altering the claw topology, Figure 1-8(b), this resulted in an increase in torque density of 9.3Nm/kg.



(a) Jack's single sided 'claw pole' MP machine [23]

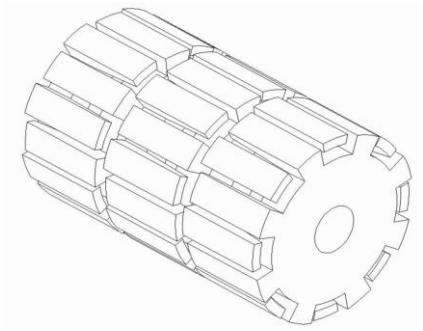
(b) Dickinson's optimised 50pole machine [8, 25]

**Figure 1-8 Claw pole MP machines developed by Newcastle University**

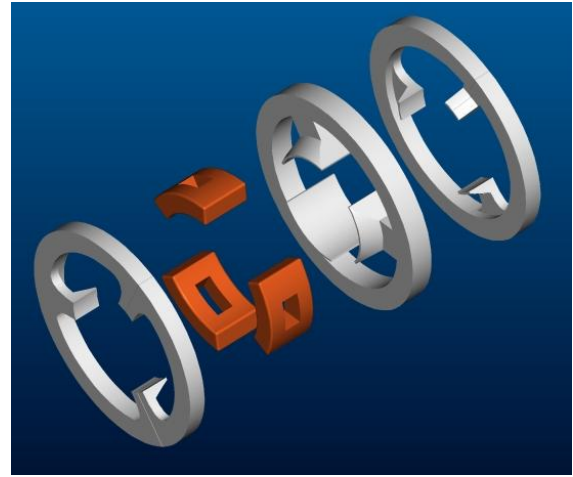
### 1.3.6 Multiple Phase Machines

The topologies of the machines presented so far have generally only considered single phase synchronous machines. Operation of these machines in a motoring sense would be difficult: starting and guarantee of operational direction requires feedback and complex control of the converter feeding the machine, also the mechanical output torque would have a 100% ripple. It is therefore more ideal to operate these machines with multiple phases. The simplest method is to stack multiple machines in series with the appropriate displacement between each phase producing a smooth net output. A good example of this is presented by Mecrow et al [26], and is recreated from the paper in Figure 1-9(a). The same concept of stacking phases is used in [27, 28] while [29] uses a more integrated variation in the stator of an induction machine.

A machine which has an armature that is more of a hybrid topology of conventional and MP machines is presented by Cros et al [30], and is recreated from the paper in Figure 1-9(b). This is a multi phase machine but is less segmented than that of Mecrow.



(a) Mecrow's stacked multiple phase MP machine



(b) Cros's hybrid multiple phase MP machine

**Figure 1-9 Example of multiple phase MP machines**

### **1.4 Materials for Manufacturing MP Machines**

In the overview of MP machines that has been presented, three forms of iron have been used to create the high permeability parts which carry flux, namely solid iron, laminated iron and SMC.

Solid iron is the best option mechanically for manufacturing MP structures. Different amounts of processing and alloy content of solid iron can produce a range of grades with different B-H characteristics. It is commonly used in areas of machines where there is no or little alternation in the flux, such as the core-back to close the magnetic loop for surface mounted magnet rotors, and the claw structure in the field of Lundell alternators. Its use within MP armature structures is limited due the presence of alternating flux, which results in loss and thence heat being generated within the iron, the majority of which is as a result of eddy currents.

Hysteresis loss is generally reduced by controlled processes in the manufacture of the iron itself, such as the reduction in contamination of certain elements. Reduction of eddy current loss is more in the hands of the machine designer. The conventional method of limiting eddy currents is to laminate the iron structures with electrical insulation between each lamination. This limits the size of the path an eddy current can take and reduces the resistive loss it contributes. This is demonstrated in a 2D sense by comparing Figure 1-10 (a) and (b). While the dielectric used to insulate adjacent laminations is normally applied as a thin coating and is a small fraction of the thickness of the lamination, the process of stacking laminations creates air-gaps. These gaps between adjacent laminations result in anisotropic permeability and thermal conductivity properties, lower across the lamination stack than in the plane of a

lamination. This lends laminations well to topologies which are a linear extrapolation of a 2D geometry, such as most conventional cylindrical machines. However, in cylindrical MP machines, the geometry for the lamination is normally extrapolated in the circumferential direction, which is difficult to realise in manufacturing.

The MP machines built by Newcastle University [8, 23-26, 31] take advantage of the isotropic properties of SMC to produce machines that still have modular construction, but the individual parts are in contact with each other, utilising space better in the machine. The isotropic properties of SMC are achieved by performing the same process of laminating, but in all three dimensions and at a much smaller level [32-34]. Powdered iron with grain sizes of the order of 50µm is mixed with a dielectric, insulating the individual grains from each other. The powder is then compressed at high pressures to form a solid and heat treated (at low enough temperatures to avoid sintering – which would destroy the insulation) to stress relieve the part and hence reduce hysteresis loss and this also develops the insulation (which in part is an oxide) [35-37]. The result is a part that requires no post processing and is laminated in all directions at a microscopic level, limiting eddy current flow within individual grains as shown in Figure 1-10(c).

There are drawbacks to the SMC material. While the properties are isotropic, the final part is not as dense as a stack of laminations meaning that the permeability is lower than that in the plane of a lamination. The low density - circa 7500 kg/m<sup>3</sup> depending upon topology - results from limits on the compaction pressure during manufacture. If the pressure is too high, it starts to significantly breakdown the insulation between adjacent particles, allowing larger eddy currents paths to be formed. Another drawback with SMC reveals itself in prototyping. The tools for pressing parts are expensive so prototype parts are usually machined from larger blanks of material. The machining process tends to produce micro-cracks in the SMC and hence reduce the permeability. This effect has been reduced by machining in the green state (pre-heat-treatment) while the material is softer and, since the SMC components in this thesis were produced, a special material for prototyping has been developed.

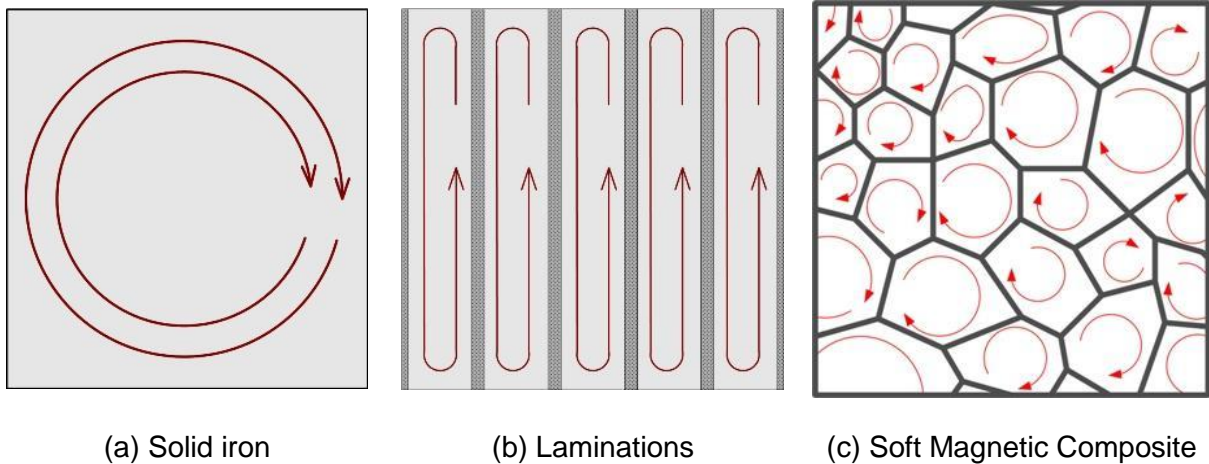


Figure 1-10 eddy current path in different iron materials (not to scale)

### 1.5 Material Hybrid Concept

From the description of the different physical forms of iron above, it is clear that each one has unique properties which are best utilised in different situations of electrical machines, depending upon the requirements for the flux. It is clear, comparing the MP machines discussed above, that manufacturing a machine solely from one material results in a compromise at some point in the design, be it poor power factor, torque density, magnet utilisation etc. This leads to the question, can a machine be produced that uses different materials in locations where they are best suited to the flux requirements at that point, a 'Material Hybrid'? This is not a new idea, as will be shown in the following sections. However, the author believes it is a new concept for MPPM machines, and it also requires the bringing together of several technologies also discussed in the following sections, along with innovative applications of them, to produce a viable concept that is not compromised in performance due to a singular material use.

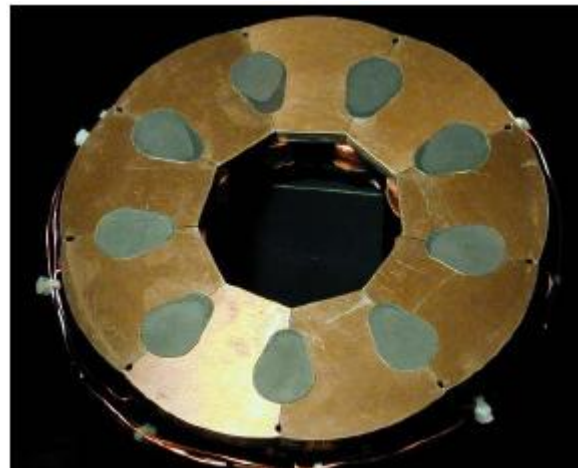
#### 1.5.1 Material Hybrid Machines

While machines like automotive alternators [14] could be termed material hybrids, as they use laminations for the armature and solid iron for the claw pole field MP structure, in the context of this thesis, material hybrid more specifically refers to the use of laminations and SMC in the same structure within a machine, particularly the use of both materials within the stator.

An example of a hybrid stator is presented by Jack et al [38, 39], pictures from which are reproduced in Figure 1-11. The machine comprises of teeth pressed from SMC which gather field flux from an entirely magnet rotor. Each tooth entails a productive feature, utilising the isotropic permeability of the SMC by radically changing the shape of the tooth as it moves away from the air-gap, creating a more efficient shape for the winding, Figure 1-11(a). To

form the core-back between the SMC teeth, laminations are used. The final required shape for the laminations is not greatly different from that used in conventional machines, but instead of directly producing them in that shape, they are produced as a strip of teeth with a small mechanical hinge joining adjacent sections, Figure 1-11(a). This strip can then be bent to form the final shape with an interfering fit with the SMC teeth producing a solid, adhesive free coupling between the two, Figure 1-11(b).

Combining laminations and SMC enables the use of pre-wound coils which are slid onto the teeth during construction. While the same result could maybe have been achieved by SMC alone, winding directly onto each tooth, the use of laminations to clamp the whole structure together is appealing as a viable, low cost, manufacturing solution.

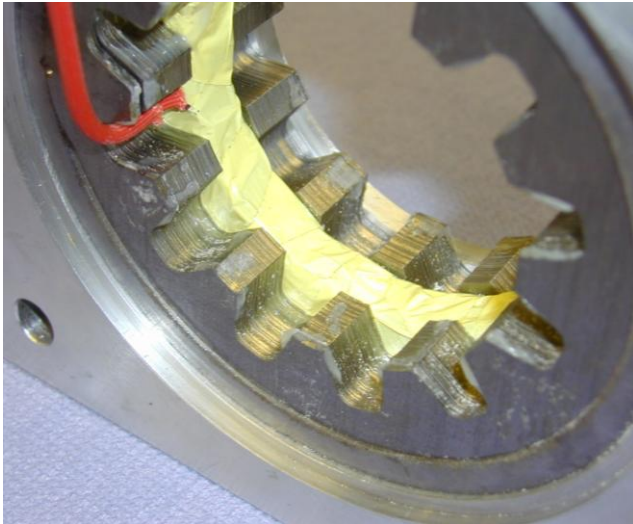


(a) Pre bend laminations and pressed teeth with a pre wound coil

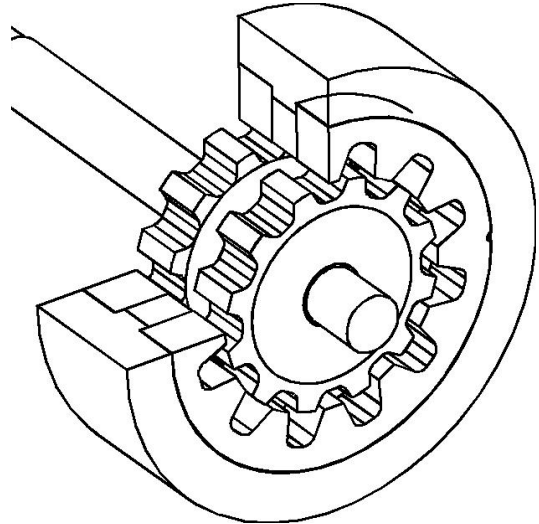
(b) Laminations bent to form the core-back and gripping onto the SMC teeth

**Figure 1-11 Photos of Jack et al [39] axial flux machine**

Another example of combining two materials in one stator is presented by Hassan et al [40, 41] where an MP has been integrated into a switched reluctance machine. Images of the machine are reproduced from [41] in Figure 1-12 showing the stator (a) and the whole machine assembled (b). It is the method of construction in the stator that is of real interest. The teeth are constructed from laminations stacked in the axial direction with one stack located either side of the winding. However, a core-back connecting these two sections is difficult to realise from laminations, as it would require the stacking direction to be circumferential. If the stacking direction were axial, the flux would need to travel across the laminations, which will have poor permeability and high eddy current loss. The solution implemented is to use an SMC cylinder for the core-back, which is a simple part to construct and allows the flux to curve out of the laminations and travel axially to the other set of laminations.



(a) photograph showing the laminations with SMC core-back



(b) schematic drawing of the whole machine

**Figure 1-12 switched reluctance machine with a simple hoop winding [41]**

### 1.5.2 Forming Laminations

The idea of drawing a strip of lamination into a circle discussed above has great ability to reduce the amount of scrap in stamping the laminations, as well as opening opportunities for improved winding structures with high copper fill factors. Considering the final shape of the laminations in Figure 1-11(b), if the laminations were produced directly in this final shape, the central air region and the gaps for the teeth would all result in large quantities of scrap material. Reductions in scrap of this kind can become very significant when applied to large diameter machines, which can have largely redundant air spaces in the rotor region. Many patents highlighting this type of construction to reduce waste have been filed [42-45] all using a form of hinge, as in [38] to link adjacent sections together. Alternatively, Kazama et al [46] and Grundfos [47], achieve similar savings, by implementing dovetail style joints which has the benefit of reducing stress in the lamination which is known to reduce magnetic performance, but is more complex in construction.

In further embodiments of the idea of forming circular structures from a strip of lamination, the ability to improve the winding structure have been noted, either by using slip on pre-wound coils [38, 48], or by increasing the space such that a high precision CNC winding machine can be utilised [43, 49].

### 1.5.3 Flux Concentrated Rotor

Previous work discussed earlier in this chapter shows that the flux concentrated rotor can give great advantages in terms of the specific output of a machine and improvement in the power factor by its ability to produce an air-gap flux density which is greater than the residual

flux density of the magnet. The flux concentrated rotor design from Weh [22, 50] was successfully integrated into a single stator and air-gap prototype by Madison [24].

#### **1.5.4 Toroidal Winding**

The toroidal or annular homopolar winding which is present in nearly all of the radial MP machines presented in this chapter lends itself well to very good copper fill factors due to its simplicity. Although there are no visible end windings, there are sections where the coil is not in proximity to an armature tooth and this could be classed as an end winding. Structures like the 100 pole claw pole hybrid machine by Madison [24] greatly reduces this compared to the double stator machines of Weh [2].

Toroidal coils naturally lend themselves to the use of ribbon copper. However, insulating ribbon copper is difficult and requires production of ribbon that has rounded edges. It is becoming more available in the market place but is still quite expensive. Because of the simplicity in shape of an annular homopolar winding, high fill factors can be achieved using conventional round wire.

#### **1.6 Material Hybrid MP Concept**

By taking the four technologies presented above and combining them, a concept for a material hybrid machine has been developed and patented [51]. Figure 1-13 shows an exploded diagram of the concept. The rotor structure uses the magnet and SMC concept used by Madison [24]. The stator uses the structure used by Amreiz [40] consisting of two laminations stacks. But instead of producing the laminations as a solid ring, the rolled up strip concept is applied. These two laminations stacks are mounted either side of a toroidal coil with a pole pitch displacement circumferentially between them such that the rotor does not have to be skewed. To link the lamination rings, they are inserted into an SMC ring to form the core-back. This ring allows the flux to spread evenly across the laminations and take the shortest route across the core-back, which is not parallel to the axial direction. The use of laminations in the axial direction will hopefully result in reduced armature leakage flux flowing axially across the machine, which will in turn improve the power factor.

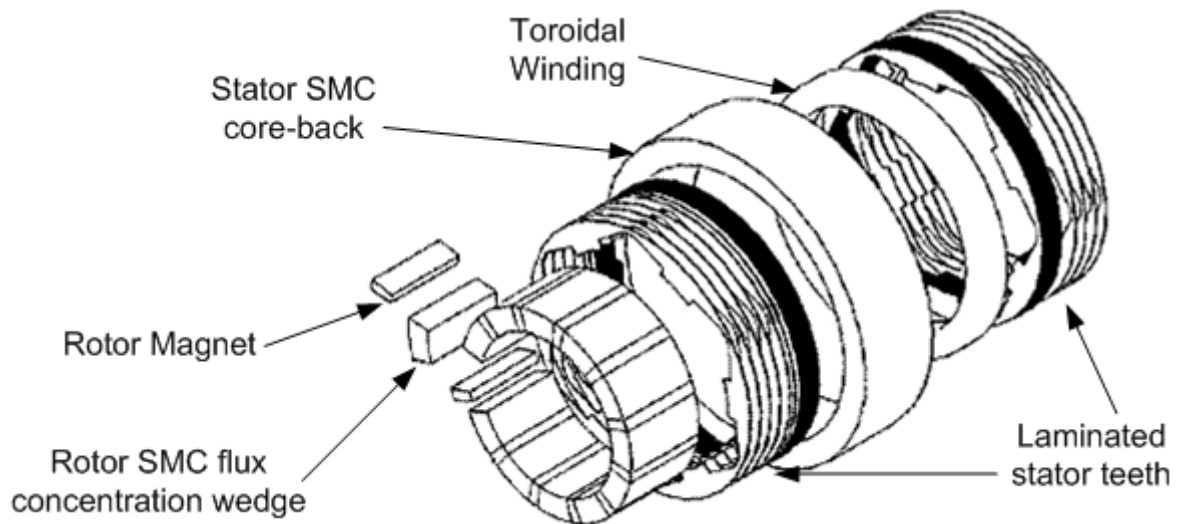


**Figure 1-13 Material Hybrid MP machine concept**

This concept is the first of two structures examined in the thesis. The second concept uses entirely laminations for the armature core.

### ***1.7 Objectives and Overview of the Thesis***

The objective behind this thesis was to develop structures for MP machines which use materials in locations where their characteristics are best utilised. This is achieved by employing materials in unorthodox ways and combinations. Two prototype machines formed from the material hybrid MP machine concept above have been designed, built and tested.

Chapter 2 describes the development of design concepts using finite element (FE) simulation, of the concept presented in section 1.6 into a sensible fifty pole design. Chapter 3 discusses the process of converting the FE design into a working prototype and the construction methods used. Methods of testing the prototype and results are then presented in Chapter 4.

Chapter 5 shows the evolution of the first prototype stator into an idea for a second construction method. Chapter 6 presents the construction of a second stator using the new method and the testing and results are presented in chapter 7.

Finally conclusions are drawn for the two machines covering their performance relative to other MP and conventional machines, and the relative merits of the methods of construction are discussed.

This thesis makes the following contributions to knowledge:

- (a) A fuller understanding of the mechanism of cogging torque in modulated pole machines.

- (b) Knowledge of how to hybridise machines using soft magnetic composites and laminations in tandem.
- (c) New construction techniques for modulated pole machines
- (d) Knowledge of how to take the desirable properties of modulated pole machines and harness them in designs that are realisable in the manufacturing industry.

## **Chapter 2. Electromagnetic Design Development Using Finite Element Analysis**

### **2.1. Finite Element Analysis**

Finite element analysis (FEA) is a very accurate way of modelling and simulating engineering systems. Its use in low frequency electromagnetic systems such as electrical machines (as with mechanical and thermal systems) has been constrained more by the processing power of the computers running the software than the maths and algorithms within it. At the start of this work in 2003, computer processing power had advanced to a level that allowed larger three dimensional (3D) models (greater than 30000 nodes) to be processed in a few hours. Before then the use of two dimensional (2D) finite element (FE) was very common place and quite a comprehensive design could be attained by accounting for 3D effects within the 2D model. For example, all 2D simulations produce results based on a unit length of the machine, by adjusting the unit length value in different parts of the simulation, 3D saturations effects can be modelled. It is also worth noting that a combination of 2D and 3D FE can be a useful approach. The 2D FE, requiring less computation resource, is ideal for design space scoping work, while the 3D FE can used to refine and explore chosen designs in more detail, giving accurate results of machine end effects such as fringing of the flux.

Where a 2D model falls down and a 3D model excels is in the calculation of truly 3D effects of flux leakage paths and circulating currents and or fluxes. It is the ability to truly simulate 3D problems that lends itself to the design of modulated pole machines. The iron structures for modulation of the flux in these types of machine, results in the creation of a multiple of leakage paths that are truly 3D by nature.

### **2.2. Electromagnetic Finite Element Analysis (FEA) in ANSYS**

The ANSYS Finite Element suite [52] is a very extensive software package with its roots lying in mechanical and thermal modelling. To allow more complex systems to be modelled, a multi-physics package was released which included electromagnetism. The reason this series of events is important is that while the package is quite capable of modelling electromagnetic problems, the software itself and the tools it provides for processing results are angled towards mechanical analysis problems. For example mesh refinement tools all increase mesh densities in areas of high (mechanical) stress, which, when translated into the magnetic equivalent, is not always what is required to increase the accuracy of the result. Another aspect of the software that was found to be a hindrance was the modelling of airspaces. Obviously, in mechanical systems this is not required, and as a result it was found difficult to create effective transitions from very fine air-gap mesh densities (to avoid element

aspect ratio issues) to larger element sizes in the iron parts and surrounding air. This often resulted in large element counts which became costly in terms of processor power. Despite these shortcomings, ANSYS was only one of two 3D software packages available to the author at the start of this work. The second was written in-house and is used extensively by Maddison [24] in his PhD work. Although this software is very functional for electromagnetic machines simulation, it is limited in the shapes that can be modelled as it uses extrusion of 2D shapes for both geometry and mesh creation. So purely for the ability to model more complex structures, ANSYS was chosen. At several points in the analysis the in-house software (which was better understood in terms of the maths it was using) was used to validate results when ANSYS produced unexpected results.

After the initial FEA work was performed and the design decided upon for the prototype, a different software suite has been purchased by the research group, Infolytica's, MAGNET [53]. This software has been developed around the simulation of low frequency electromagnetics, and has been proven well suited to electrical machine design. Using MAGNET some retrospective simulation work was performed to help understand the prototype results. This simulation work is presented with the results of the prototypes.

It should also be noted that since the original FEA work in ANSYS was performed, the ANSYS software has been developed to include more tools for the electromagnetics designer. The problems stated above are purely observations made during the course of design with the software and hence are by no means meant to be a review of its ability.

### **2.3. ANSYS FE Model**

As 3D FE models require large amounts of processing power, resulting in long solution times in comparison to 2D models, it is a key requirement to minimise the size (node and element count) of the model. This can be split into two areas; partial modelling of the machine by taking advantage of symmetry; and balancing mesh refinement with solve-time and accuracy.

#### **2.3.1. Model Symmetry**

The symmetry available in this machine is cyclic in the circumferential direction, meaning that it is independent of the number of poles; which is different from conventional radial field topologies. In fact the same model can be used for different pole numbers by scaling the model by the ratio of the angle spanned and maintaining all radial dimensions, although this is not as straight forward with a flux concentrated rotor, as will become apparent in this chapter.

The ANSYS model will be a static model and as such only magnetic parts need to be included. The non-magnetic parts such as the casing, and magnetic components remote from the field such as the shaft and bearings do not need to be modelled. If the model was of a transient, then there may be need to model close proximity conducting materials such as the casing and shaft. The active parts of a fifty pole machine; that actually is taken from the CAD model of the final design are shown in Figure 2-1. A four pole cut away section is shown within the centre, labelling the different active components. The stator consists of a toroidal winding sandwiched between two lamination packs which perform the flux modulation of the coil's field. The lamination stacks are connected magnetically on the outer diameter by an SMC core-back. The rotor consists of a series of magnets, magnetised in a circumferential direction, alternating in direction between adjacent magnets. Between each magnet there is an SMC "flux concentration" wedge that orientates the flux for delivery to the stator tooth across the air-gap.

Focusing back on the symmetry in the machine, looking at the four pole section in Figure 2-1 and considering the stator, the teeth of a single lamination pack (one side of the coil) have the same magnetic polarity. So in a partial model, for flux to flow around the stator, there must be a tooth from each side of the coil and associated SMC core-back. Now considering the rotor, as the SMC wedge delivers the flux from the magnet to the tooth, there needs to be a matching number of SMC wedges and stator teeth. Each SMC wedge takes the flux from two sides of two different magnets, if this is examined on a more global level, considering only a case with flux from the magnets, not the coil, then the MMF of one magnet drives half the flux of the two adjacent SMC wedges. This equates to one magnet per SMC wedge, and indeed in Figure 2-1 there are matching numbers of SMC wedges and magnets in the rotor.

From this discussion it can be concluded that a model spanning only two pole pitches is achievable using periodic boundary conditions. Where the model is cut in the stator is not important, as the flux source here is the coil and will be the same wherever the cut. It also does not matter where the rotor is split as long as full two poles are spanned and an even periodicity boundary condition is used. Having said this, it makes sense where possible to split the model in a way that produces more interpretable results by maintaining geometrical symmetry in the model, e.g. centring a prominent feature such as a magnet in the middle of the model.

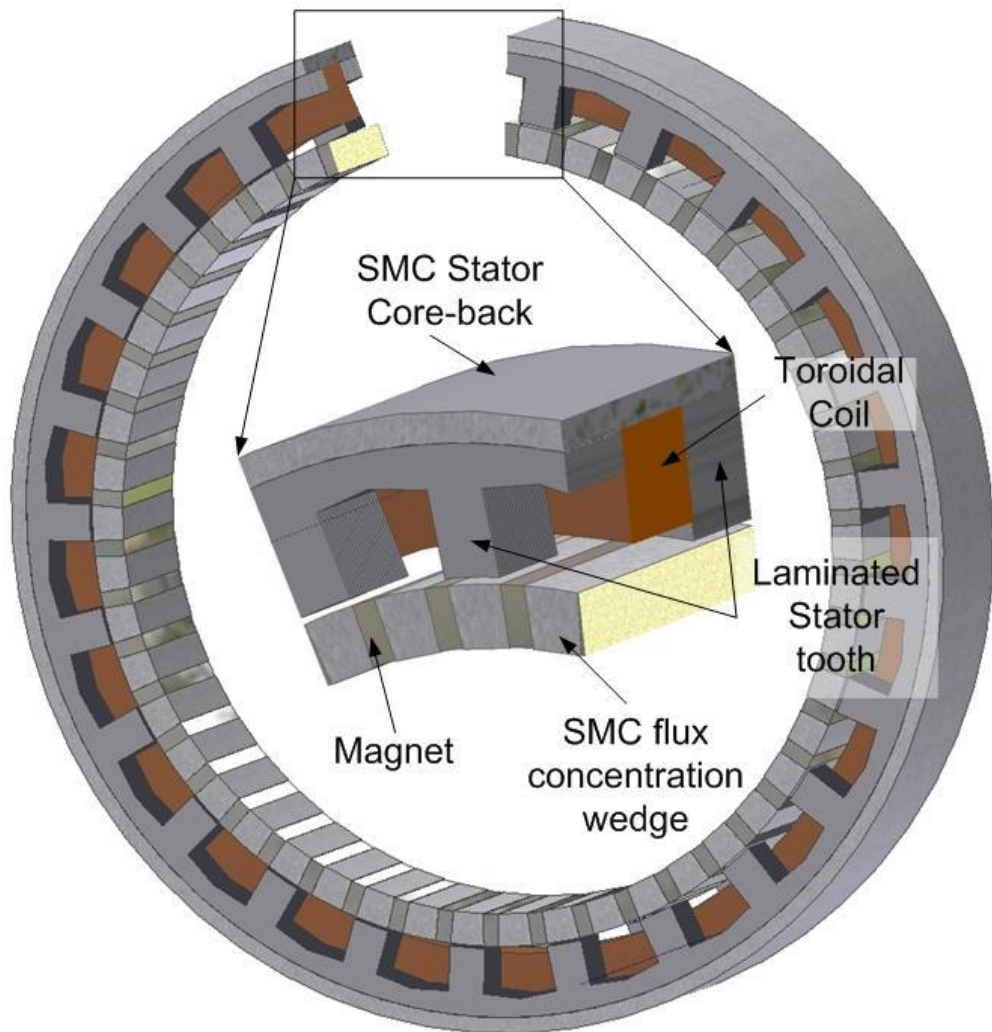


**Figure 2-1 Active parts of a fifty pole design with four pole close up labelled view in the centre**

Solving a 3D two pole model in multiple positions still requires large amounts of computer time (>24 hours), a further reduction in the section of the model was performed, that although limited somewhat the amount of data that could be attained, produces a much more manageable means of investigating designs. This reduction is to take the model from two poles to a single pole. Instead of using periodic boundaries, this model utilises symmetry of the flux flow in the parts when arranged in the aligned (maximum flux linkage) position. At this point to help understanding, it is worth jumping ahead in the text and taking a look at Figure 2-6 & Figure 2-7 which show the single pole model that was used. As already stated there are no periodic boundary conditions, instead the surfaces (radial-axial plane) that would adjoin with the rest of the machine, have a flux tangential boundary condition forced upon them. This can be used, as, in this position all the flux carrying parts have a central line of symmetry in the axial-radial plane. The only other rotor position where this can be done is the unaligned (minimum flux linkage) position. More discussion as to how torque calculations can be obtained from this model is given in section 2.5.

### **2.3.2. Mesh Refinement**

The amount of mesh refinement in a model is governed by a compromise between the time taken to solve the model and the accuracy of the results. In manual control of element size, the key to efficient use of elements is to refine in areas of high stored energy (i.e. air gaps and heavily saturated regions) and where the flux is changing direction, as more elements gives a better resolution of the path of the flux. So in air regions away from the main active components the elements can be very large (as the field is rather low and varying slowly): several orders of magnitude of say the ones in the air-gap between the stator and rotor. The gap between the stator and rotor has high fields and the flux can be quite tortuous in its path as it travels between the sharp edges of the teeth, magnets and rotor poles and hence needs many elements.

Examples of different refinements can be seen in Figure 2-6, which as a model had 36181 elements connecting 20321 nodes. Not all of these are shown in the figure as the air regions have been omitted for clarity. The mesh was created by first performing a 2D mesh of a surface in the axial-circumferential plane that took into account all the material boundaries throughout the model when viewed in the axial direction. This mesh was then extruded through the model at varying step sizes to create the 3D mesh. It can be seen that the elements around the air-gap are smaller than those around the outer edges of the parts.

By refining the mesh in successive steps and comparing the change in resulting values (flux linkage) an understanding of the quality of the mesh can be developed. This process has already been performed in several steps to produce the mesh in Figure 2-6, further refinement of this mesh for the final design resulted in less than 1% change in the flux linkage.

### **2.4. Pole Number**

The effect of pole number on the machine has already been discussed in detail in the previous chapter, so just to recap and remind the reader. The specific torque of a modulated pole machine below a limit is directly proportional to the pole number [7]. The limit as the pole number increases is governed by three factors; increased flux leakage due to reduced distance between poles in the structure; electrical frequency of the supply as the pole number increases for a fixed running speed; and physical constraints on the size of the components. Previous work in the field shows that the first two constraints dominate the final one. Increasing leakage means less effective use of the magnets, but it also means a higher inductance which increases the cost of the converter to drive the machine. Increasing

frequency means higher iron loss and also challenges the limits imposed by device switching speed in the converter. Leakage flux also has the effect of increasing the flux carried by the core and hence leads to saturation imposing a limit on the specific torque output from the machine.

In previous work by Dickinson [8] and Madison [24] the iron parts of the machines carrying alternating flux were built entirely from SMC. Due to the isotropic nature of the SMC, there was a large quantity of significant leakage paths. In addition SMC has a rather low permeability and this too leads to leakage paths having a relatively lower reluctance than they would if the permeability were higher. In this design it is hoped that the use of laminations in combination with the SMC will help stem the leakage and improve the specific torque of the machine.

Power output is the multiple of torque and speed and hence limiting pole number would be very beneficial if good specific torque output could still be achieved. Based on that logic, the initial design work was based on 12 poles, far lower than Dickinson's machines which had 50 poles and Madison's machine which had 100.

### ***2.5. Torque Calculation using Co-energy from D-axis Flux***

The side effect of having a one pole model is that it only gives results for the aligned (d axis) and unaligned (q-axis) axes and can't be solved for positions in between, so instantaneous torque values over a range of positions to give the profile shape of the torque are not possible. However, ignoring cogging torque effects and assuming a square wave excitation, an estimate for the mean torque of the machine can be calculated. The square wave implies turning the current on in the negative d axis position (i.e. with the magnet aligned with the armature) and turning it off in the positive d axis position. By simulating the machine with a range of winding MMFs from positive to negative rated current a flux linkage  $\psi$ 's MMF characteristic for the d axis position can be determined. If the same is done for the opposite pole position and plotted on the same graph, an area is defined. The area enclosed by this graph, is the co-energy, (equation (2-1)). Dividing the co-energy by the angle between the two positions gives the mean torque produced by the machine over that half cycle as in equation (2-2). This gives the torque of one pole of the machine, to get the mean torque for the whole machine, it needs to be multiplied by the number of poles in the machine.

$$A = \Psi I = W \tag{2-1}$$

$$T = \frac{W}{d\theta} \quad (2-2)$$

## 2.6. Material Properties

### 2.6.1. Magnet

The design is based on using a Neodymium Iron Boron (NdFeB) magnet, grade N38H. The properties for this material at 20°C can be found in Table 2-1. The ANSYS software requires the values of  $H_c$  and  $\mu_r$  and assumes a linear relationship between them to calculate  $B_r$ .

**Table 2-1 Material data for Magnet used in finite element simulations.**

Material Property	Value
Coercive Intrinsic Magnetic Field Strength, $H_c$ (A/m)	-918202
Relative Permeability, $\mu_r$ (H/m)	1.04
Residual Flux Density, $B_r$ (T)	1.2

### 2.6.2. SMC and Laminations

The flux density against electric field strength (B-H) data for the lamination material and the SMC material is shown in Figure 2-2, where it can be clearly seen that the SMC saturates much earlier than the lamination material. As usual the measured data does not reach high enough levels and the software is forced into some form of extrapolation of the measured data. The point being that care needs to be taken in assuming that accuracy is maintained when very high fields are present.

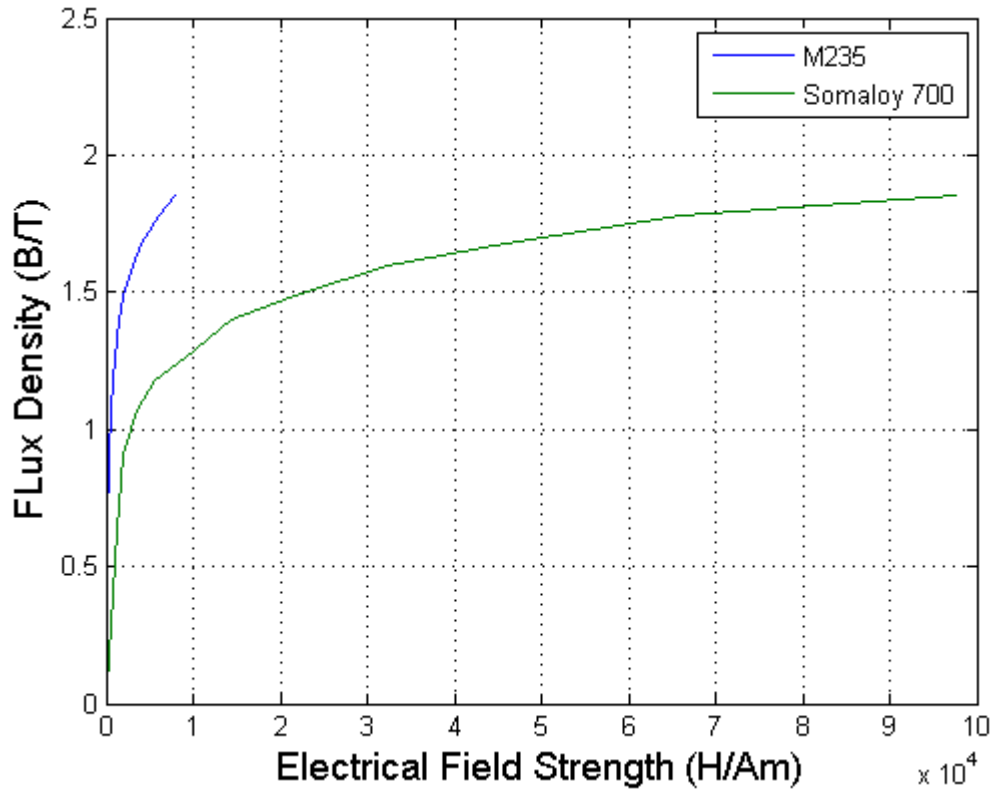


Figure 2-2 Graph showing the B-H characteristics of the iron parts of the machine

## 2.7. 12 Pole Design

### 2.7.1. Geometry Development

With the aim of finding a design capable of high power output and hoping to exploit the possible savings in leakage flux from using laminations, the first design had twelve poles as explained above. This design and the following fifty pole design are scaled circumferentially and axially so the same material boundary image shown in Figure 2-7 (actually from the fifty pole design) can be used to describe both designs.

The view in the top right of Figure 2-7 is with the axial direction of the machine into the page, and is probably the best of the four views to describe the different parts. The red outer arc is the SMC core-back. The blue sections connecting to the core-back inner radius are the laminations, separated in the axial direction by the coil space. Moving radially inwards, there is a 0.5mm air-gap which is shown as a white gap in the model. The two inner red sections are half (split in the axial-radial planes) of two separate SMC flux concentration wedges. Sandwiched between these is a single magnet, shown in yellow, which is magnetised in the pseudo circumferential (horizontal) plane.

This and future designs are purely for proof of concept and there is no specific application to help constrain the design, making it difficult to choose parameters. A stock of 12.5x3x50mm

NdFeB magnets was available and these dimensions define to a large extent the rotor, and give an anchor for choosing the rest of the machine's dimensions. Choosing these magnets also means that the machine comes out close to the diameter of Jack et al [23] and Dickinson's [25] machines (which allows fair comparisons between the different topologies). The air gap was chosen as 0.5mm (again as per the earlier machines).

The key feature to note about this design is the tapered profile of the laminated tooth when viewed from the axial direction (top right, Figure 2-7). At the air-gap, the tooth spans a slightly bigger angle than the field pole formed by the SMC wedge. This overlap helps catch more of the magnet fringing flux to improve the peak flux linkage. Moving radially out from the air-gap, the tooth starts to widen in the circumferential direction. The idea of this is to help the flux in the tooth spread before entering the SMC, which has a lower saturation level than the lamination, and hence needs to be operated at a slightly lower flux density. The widening of the tooth does not really start until a third of the radial length of the tooth. This is to limit leakage from the tooth back into the opposite polarity rotor parts without linking the coil.

By fixing the dimensions of the magnet (and hence the axial length of the machine), the outer diameter and the air-gap length, much of the basic geometry of the machine is fixed. The three leading dimensions that are left to choose are pole number, working air-gap diameter, and tooth-coil slot-tooth ratio in the axial direction; which is shown in Figure 2-3. The design that produced the results in Figure 2-4 has an air-gap central diameter of 125.5mm. This coupled with a 20-10-20 ratio of the stator teeth and coil in the axial direction left a coil cross section (viewing circumferentially) of  $185\text{mm}^2$ . The leading details for this design are presented in Table 2-2.

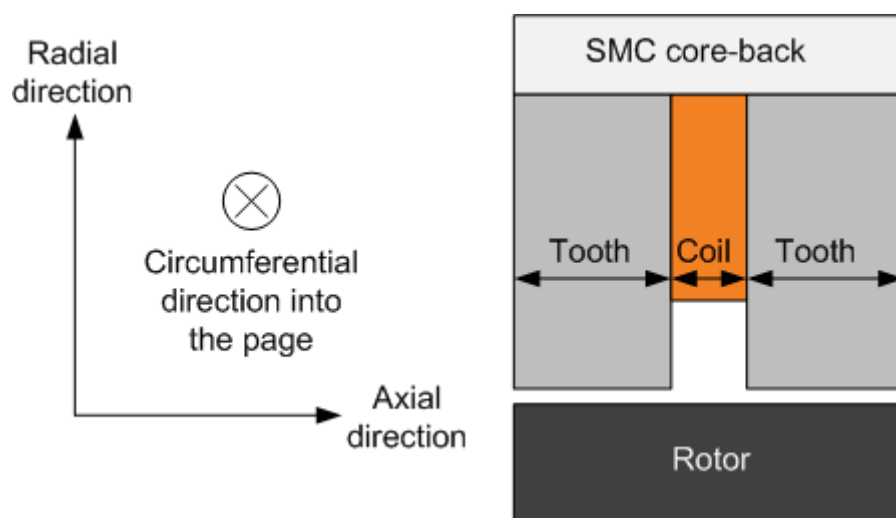


Figure 2-3 Diagram showing the axial split ratio of the stator

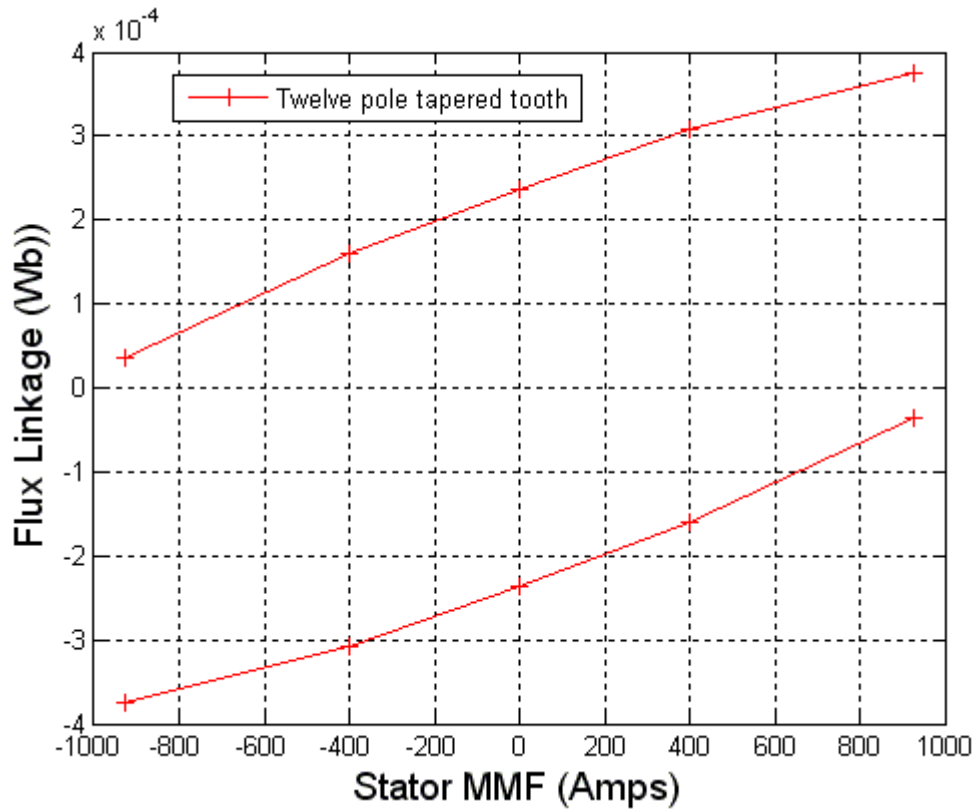


Figure 2-4 Flux linkage - MMF plot for a single pole up to an MMF of 925A

Table 2-2 Leading motor details

Parameter	Value
Stator teeth	12
Rotor Poles	12
Phases	1
Axial length	50mm
Stator OD	195mm
Stator bore	126mm
Core-back depth	16mm
Lamination stack length	20mm (two sets of)
Coil axial length	10mm

Air-gap	0.5mm
Rotor OD	125mm
Rotor (active) ID	100mm
Magnet dimensions	12.5mm x 3mm x 50mm

## 2.7.2. Design Analysis

### Torque

The flux linkage- MMF characteristic in Figure 2-4 is calculated over a range of d-axis MMF up to  $\pm 925$  Aturns. This is an electrical loading of  $5\text{A}/\text{mm}^2$  assuming a 100% copper fill. But the copper will probably fill just above 60% of the slot, so  $8\text{A}/\text{mm}^2$  is more realistic for a 925A loading, relating to a 62.5% copper fill of the slot. This value of electric loading is on the high side when compared to the machines of Dickinson [8] in which the thermal paths for dissipating the winding loss should be similar. This noted, the assessment of this initial design was made at this level of electrical loading, for reasons that will later become clear.

Using the method described in section 2.5, the mean torque capability of this machine was calculated using equation (2-3) and found to be 8.5Nm. The mass of the active components of this machine is estimated to be 5.7kg, meaning the specific torque density is 1.5Nm/kg. This compares favourably with the 24 pole claw pole machine of a similar size built by Jack et al [23], although, as already noted the electric loading is probably above the thermal limit presenting an unfair comparison. On the other hand this is substantially below the 9.3Nm/kg of Dickinson's 50 pole machine. As increasing the pole number increases the electric loading in direct proportion so it is no surprise that a 12 pole machine will not compare favourably in specific torque output with a 50 pole machine.

$$\begin{aligned}
 \text{MeanTorque} &= \frac{\text{Energy\_Converted\_One\_Pole} \times \text{Number\_Poles}}{\text{Angle\_Spanned\_By\_One\_Pole}} \\
 &= \frac{0.37 \times 12}{\pi/6} \\
 &= 8.5\text{Nm}
 \end{aligned}
 \tag{2-3}$$

### **Power Factor**

As discussed in Chapter 1, work by Harris et al [18] shows that by neglecting the resistive voltage drop across the winding, the power factor angle of these machines is  $\Phi = \arctan(IX/E)$ . Taking this a step further and neglecting saturation effects, then  $IX/E$  can be expressed as the flux ratio; (Peak flux linkage due to the armature current)/(Peak flux linkage due to the magnet).

Based on the flux ratio, the power factor for this design comes out at 0.75 for a winding  $MMF=925At$ . Interestingly, scaling the electric loading to a thermal limit more in line with previous work,  $MMF=555At$ , suggests the power factor would increase to 0.86. Whilst this is a relatively high figure for a claw pole machine it is lower than would be expected for a conventional permanent magnet machine and reflects the abundant leakage paths inherent in claw pole geometries. As noted above, increasing the pole number also increases the electric loading and this in turn can be expected to increase armature current driven flux and hence drive down the power factor (and make the VA rating of the inverter rise). One of the major design goals of any modulated pole machine is therefore to find a geometry which limits armature driven flux without loss of magnet flux.

### ***2.8. Leakage path assessment***

From the previous section it can be seen that minimising the leakage of the armature flux is very important. To try and understand the leakage paths of this design a simulation was run with the magnet switched off and only the MMF of the coil inducing flux. It was then possible to integrate the flux density over chosen areas of the teeth, to see how much flux was travelling through it and in which direction. Obviously this will not give a true representation of the leakage paths, as there will normally be an influence of saturation due to the combination of flux induced by the winding MMF and the magnet.

The different surfaces of a half tooth from the model are shown in Figure 2-5 and are annotated with the magnitude of the flux through each. The direction of the flux, in (positive) or out, is indicated by the respective polarity of the number. As the majority of the flux is flowing through the tooth between the air-gap and the SMC core-back, it is logical that the difference in the values of these two surfaces, which amounts to  $0.2131 \times 10^{-3} - 0.1562 \times 10^{-3} = 0.0569 \times 10^{-3} \text{Wb}$ , should be accountable by the values in the other surfaces. But actually the totals do not quite add up. The reason for this error is due to a combination of effects in the method of calculating the flux values. Firstly, the ANSYS model solves the model using a Scalar Potential and a source term to capture the rotational part of H with which it solves Maxwell's Equations; specifically it finds a value of H which satisfies Ampere's Law in the

form  $\nabla \times H = J_s$ . The value of flux density is then calculated over the area of volume of the element from the H values of the attached nodes using the constitutive properties of the material assigned to that element. To get flux, the value of flux density, which might be affected by nodes in a different plane, as these are 3D elements, is integrated over the required surface, resulting in errors in the value. To simplify, the integral value of H around a closed loop for the scalar potential part of the solution will be zero, but the sum of the flux will not and the error is a function of the refinement of the mesh and the tolerance set for the criteria of convergence by the solver. The secondary result of this is that the directional component of the flux densities of the element will not be correct when considered at the surface, i.e. it is not the normal component, resulting in this method suggesting that flux is leaving a surface when it has a flux tangential boundary condition posed upon it.

Having taken account of the accuracy arguments, the flux values in Figure 2-5 still give a good indication of where the main leakage path is, especially if it is considered in parallel with the surface flux density plot in Figure 2-6 which again is due solely to armature flux.

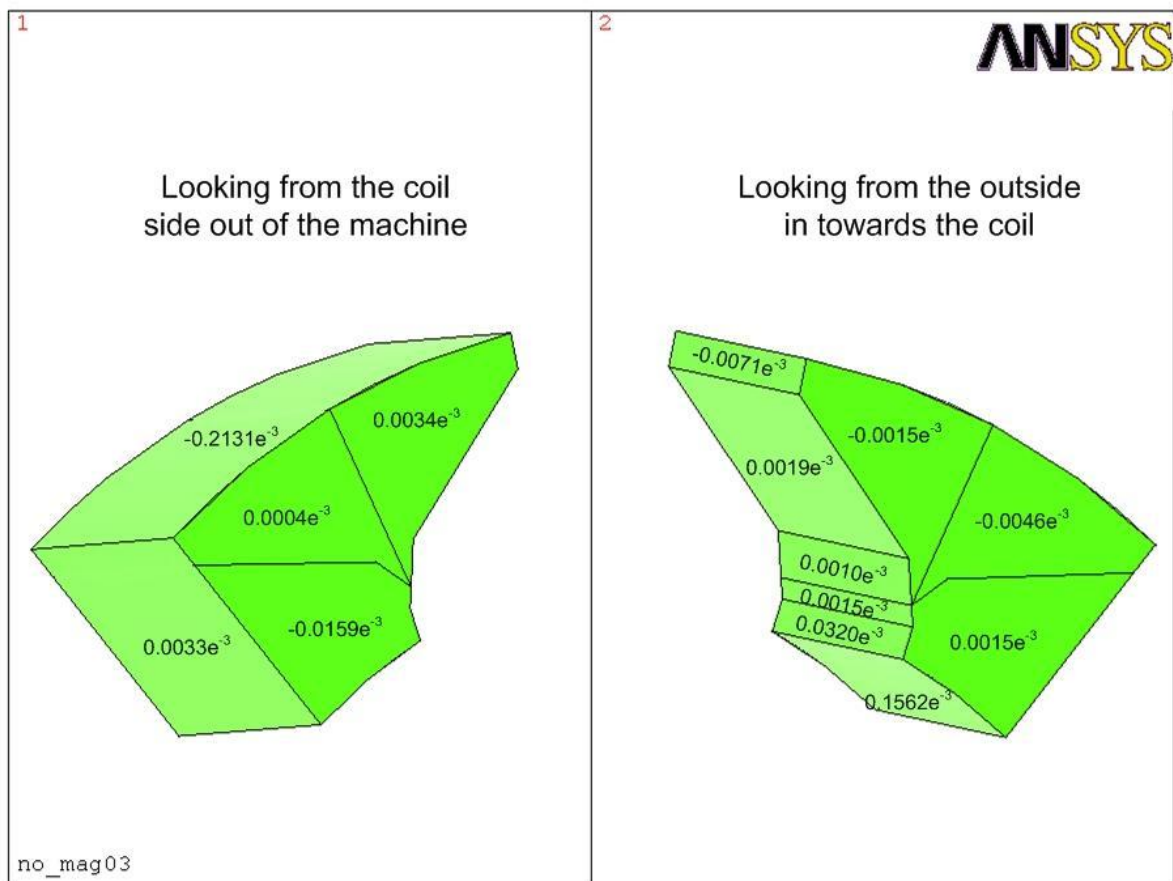
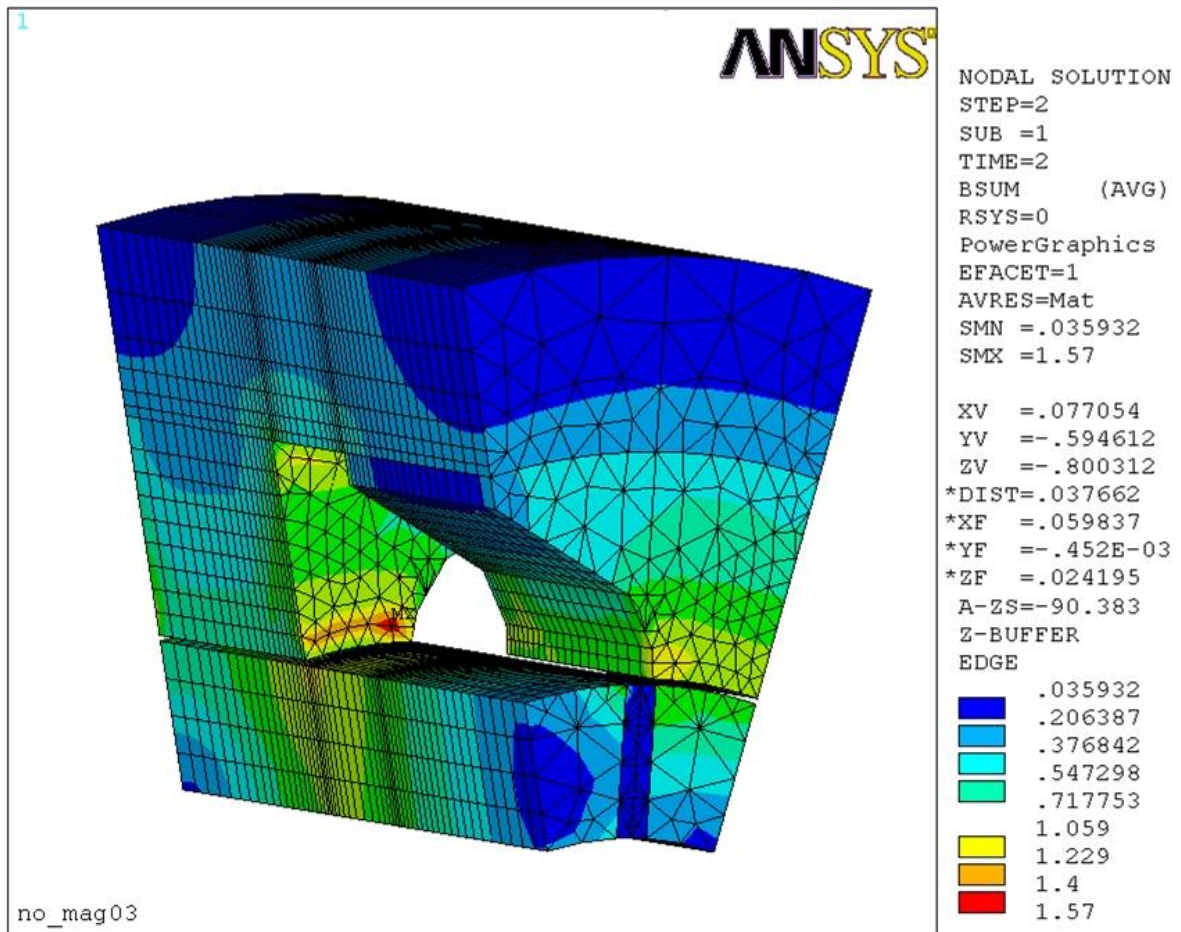


Figure 2-5 Showing the different leakage paths and their magnitudes around a lamination tooth

When viewing the data in Figure 2-5 and Figure 2-6, it is worth remembering that as this is solely due to armature flux, the flux patterns and hence flux densities in both teeth are symmetrical about the centre of the model. It can be seen that there is one main area of leakage towards the air-gap on the tooth side facing the coil. This analysis of course does not take into account any saturation effects that may occur as a result of the interaction of the field and armature flux, which could change the location and magnitude of the leakage paths.



**Figure 2-6 Flux linkage due solely to the coil MMF (magnet modelled as air)**

While this assessment shows the general area of the leakage is at the bottom of the teeth near the air gap, a more refined analysis with the model of the teeth split into several extra sections would be needed to produce firm numbers of well defined specific leakage paths.

## 2.9. Fifty pole design

It was clear from the analysis of the 12 pole design that it will not give the torque densities comparable to the similar size 50 pole machine of Dickinson; hence it was decided to alter the pole number. To produce a fair comparison, it was decided to increase the pole of this design to 50 to match Dickinson's. As the torque capability of a machine is also closely linked

with the diameter of the air-gap, this was also altered slightly to match identically that of Dickinson's machine.

### **2.9.1. First Fifty Pole Design with a 20-10-20 stator ratio**

The first design with fifty poles was a circumferentially scaled version of the 12 pole design. The active flux carrying parts of the model, over one pole pitch are shown in Figure 2-7 which is taken from the ANSYS FE model. As with the 12 pole design, the model only shows one pole pitch due to the presence of cyclic symmetry. From a comparison of the two designs (Figure 2-6 & Figure 2-7) it is clear that the span of the rotor poles and stator teeth at the air-gap have had to be reduced (circumferentially) to allow for the extra poles.

The reduced span of the poles means that the magnet surface area must be reduced to prevent saturation in the flux carrying parts. Still trying to utilise the existing source of magnets, the magnet width was reduced to 6mm in the radial direction. The existing magnets have a 12.5mm dimension in this direction, meaning that the 6mm magnets could be produced by halving these, with a 0.5mm excess to allow for the machining. What was found was that this reduction in magnet surface area is not enough and that the SMC starts to saturate due solely to the magnet flux. The saturation can clearly be seen in the flux density plot of the design in Figure 2-8, the SMC wedge is saturated from around the axial centre of the coil through to the centre of the tooth that it is supplying.

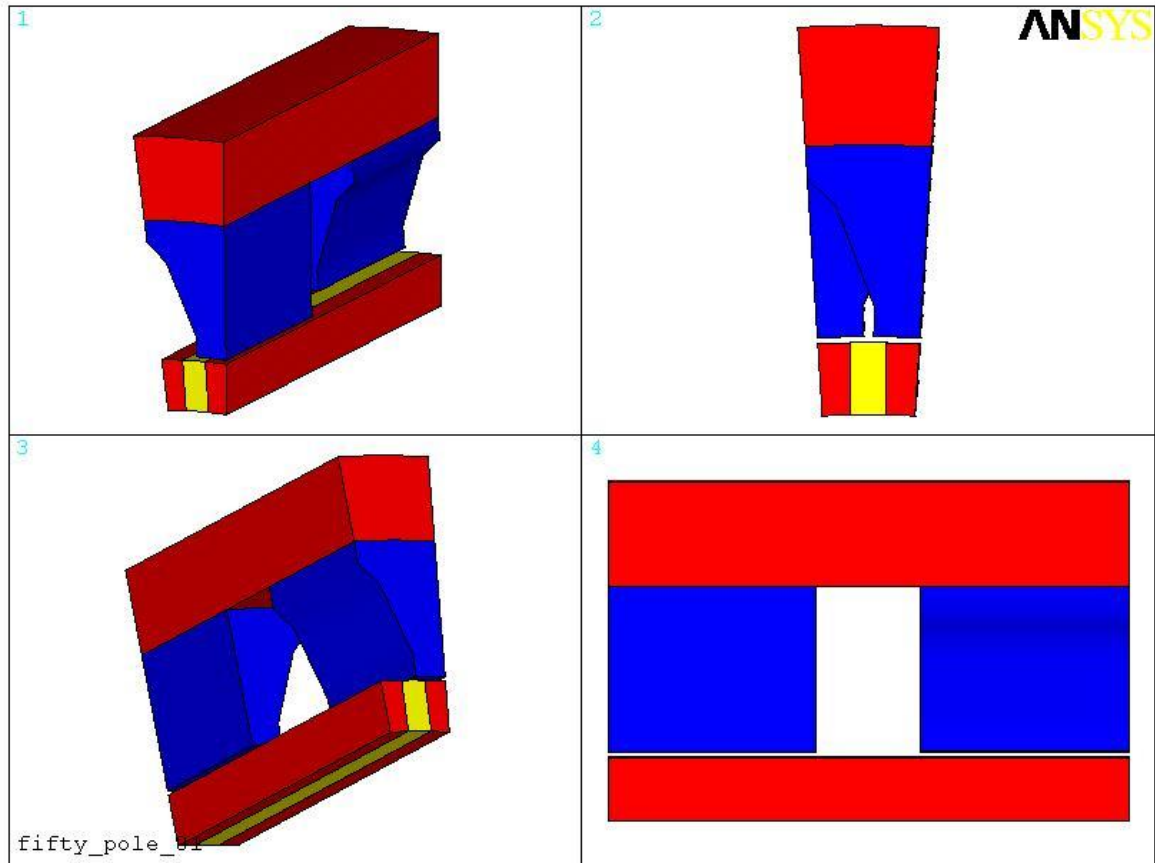


**Figure 2-7 Active parts from the ANSYS model of the 20-10-20 fifty pole design**

It is clear that simply increasing the pole number by circumferential scaling the poles, does not work with a flux concentrated rotor of this type, and the ratio of the parts in the rotor must be adjusted to get maximum performance from the magnet, i.e. maximum flux linkage. The next sections will discuss designs aimed at optimising the axial dimension ratios for a fifty pole machine.

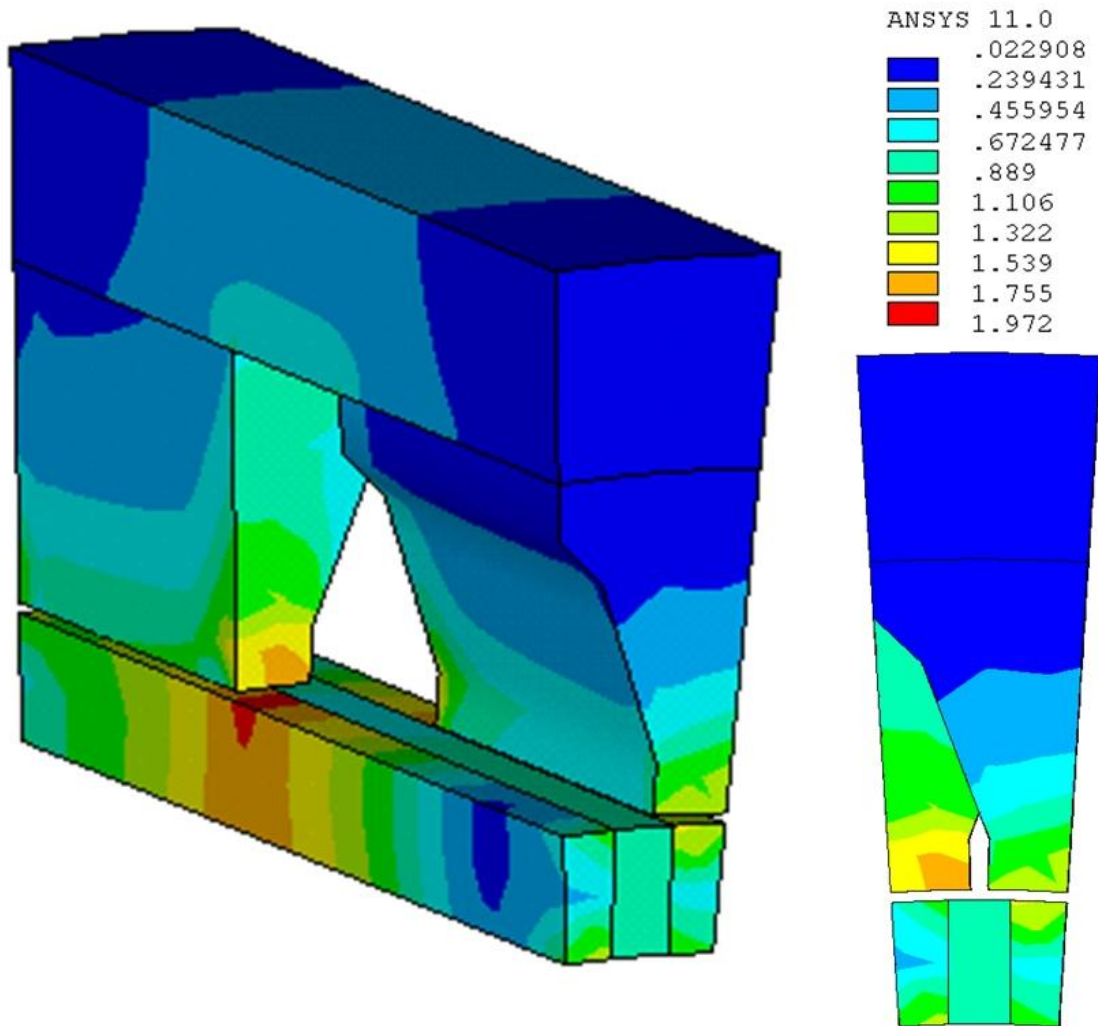


Figure 2-8 flux density plot of the 20-10-20 fifty pole design

### 2.9.2. Reducing the Axial Length

To maintain the same dimension and material of magnet and overcome the saturation in the SMC flux concentrating wedges would require increasing the diameter of the stator bore. This would allow an increase in the cross sectional area of the SMC wedge when viewed in the axial direction, allowing it to deliver the flux to the air-gap under the stator tooth, greatly improving the machines magnetic circuit. This is not an option however, as the OD of the machine was fixed to allow fair comparison of similar dimensioned machines. An alternative would be to reduce the slot opening in the radial direction, but this would greatly reduce the electric loading of the machine, counteracting the advantage of the high pole number and bring the torque density down.

So the only way to prevent the saturation in the SMC is to reduce the ratio of the working cross sectional area (radial-axial) of the magnet to the cross sectional area of the SMC in the

circumferential-radial plain. The only way to change this ratio for the same rotor outer diameter is to reduce the axial length of the machine.

### **11-6-11 stator ratio**

The first attempt at reducing the axial length brought it down from 50mm to 28mm. The ratio for the stator teeth to slot opening was altered slightly just by rounding the dimensions off to the nearest millimetre. This resulted in the lamination stacks being 11mm thick and the slot being 6mm wide.

It can be seen in Figure 2-9 that the flux density in the SMC around the centre (axially) of a tooth is only peaking at 1.2T - a little under saturation. The mean flux density of the air-gap was calculated by taking the average flux density across the surface of the tooth where it meets the air-gap. This came out at 1.16T, which is less than the saturation point of the SMC which will be the limiting factor. To try and increase the air-gap flux density, the design was altered to increase the axial length of the machine to 30mm.

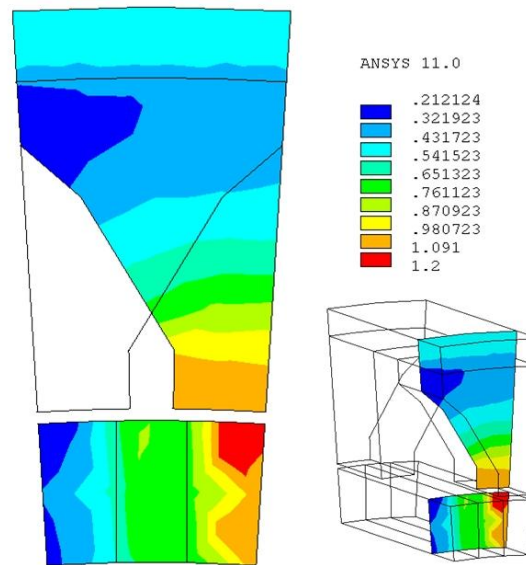


**Figure 2-9 flux density plot in the centre of a tooth of the 11-6-11 design**

### **11-8-11 Stator ratio**

By increasing the axial length to 30mm it was hoped that the extra magnet working area would help increase the air-gap flux density to the target value of 1.4T. The result was no change in the air-gap flux density despite a 7% increase in magnet area. The increased flux had started to heavily saturate the SMC, which can be seen in Figure 2-10, showing a flux density plot on a surface slice through the centre of a tooth. So all the extra magnet was wasted due to this saturation and the net result was the unchanged air-gap flux density.

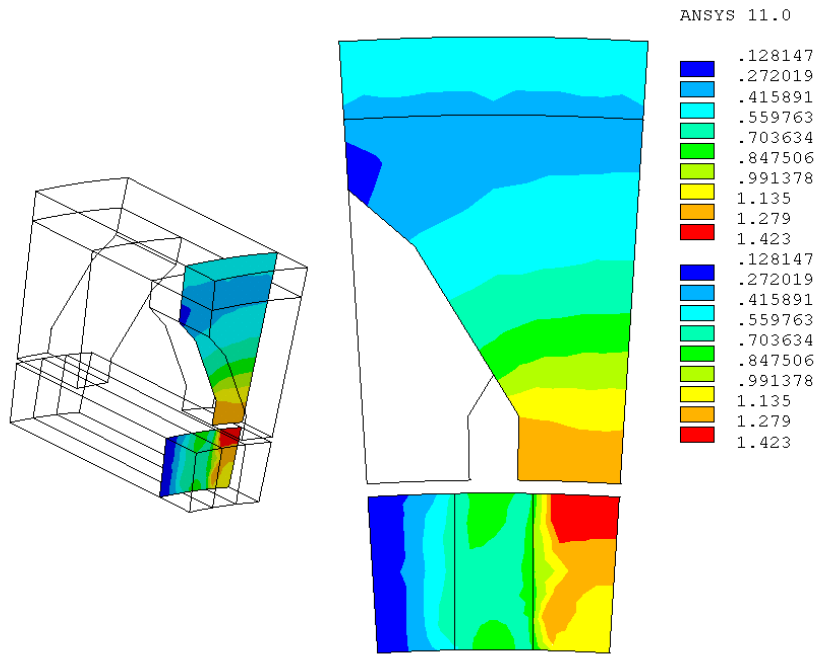


**Figure 2-10 flux density plot in the centre of a tooth of the 11-8-11 design**

#### **8.5-8.5-8.5 stator design**

With the 11-8-11 30mm design, the SMC was operating into saturation, and the air-gap flux density is lower than desired, the next step was to reduce the widths of the lamination stacks to force up the air-gap flux density. As the overall length of the machine produces too much flux for the SMC, the overall length was reduced as well.

It was found that a design with an equal ratio between the lamination stack and the slot width of 8.5mm provided a balance with an air-gap flux density of 1.28T. At this value the SMC is starting to saturate and pull the magnet field strength down with no useful outcome.

The key area regarding saturation in the SMC wedge is at the axial depth relating to the interface of the tooth and the coil, as this is the point of maximum flux concentration. It can be seen from Figure 2-11 that the flux density here ranges between 0.9T at the bottom (inner diameter) of the SMC, to 1.6T at the air-gap. The actual average flux density at this point across the SMC is 1.26T.

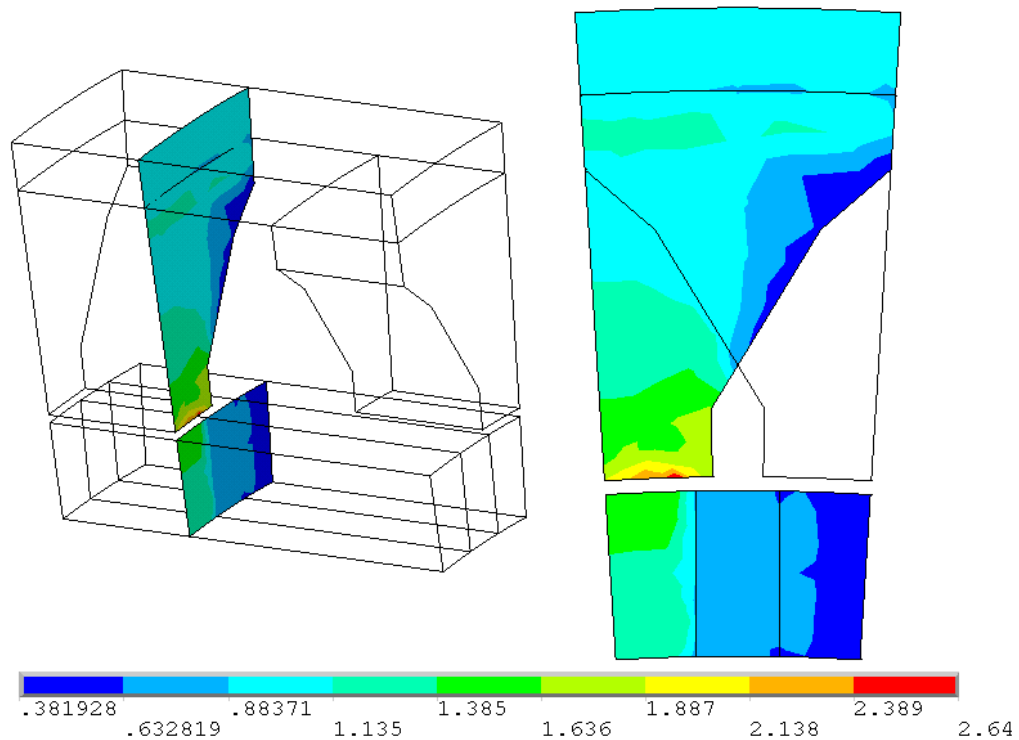
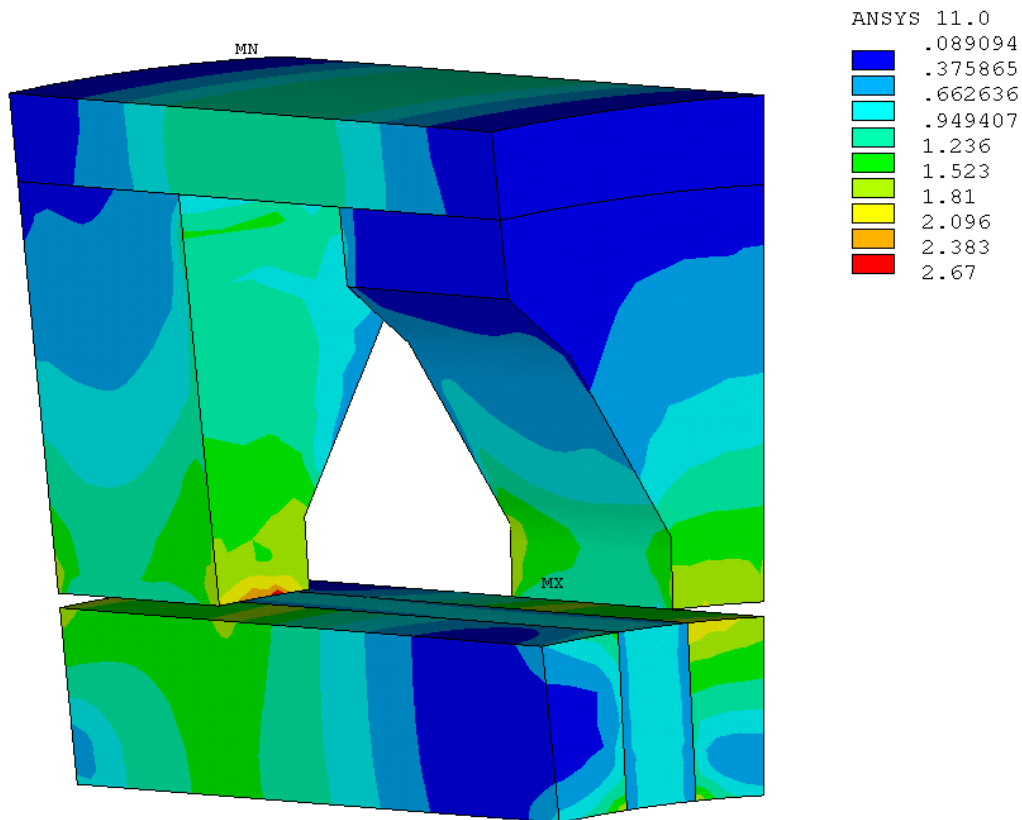


Figure 2-11 flux density plot in the coil side of a tooth of the 8.5-8.5-8.5 design

### 2.9.3. Stator ratio 8-8-8 with straight teeth

In the earlier 12 pole design, a study of leakage paths for the armature flux was performed showing a large amount of flux leaking across the slot between the teeth, these paths allow magnet flux to “leak” without coupling the winding. The slot width has been reduced by 15% in the equal 8.5mm design, and 20% in this design, compared to the 20-10-20 design for which the armature leakage paths were investigated. The reduction in slot width will have increased the leakage between the two teeth. Looking at the flux density plot of the equal 8.5mm design, Figure 2-12, the flux density in the teeth outer two thirds (radial direction) is quite low, roughly between 0.3T and 1T. It is also clear that there is a shift in flux towards the slot side of the tooth as it rises towards the SMC. This is to be expected as the flux will take the shortest path. This will be greater in this model than in reality as the effect on permeability from laminating the teeth in the axial direction has not been accounted for in the B-H characteristics in that direction. What is clear is that the flux is not spreading circumferentially into the widening tooth as much as was anticipated. So there is not the benefit for this extra material as first thought, in fact it is contributing to leakage across the slot.

By remodelling the tooth to take the shape of the tooth at the air-gap most of the way (radially) towards the SMC core-back, a large amount of redundant material can be removed, increasing the torque density of the machine. This will also reduce the crossover of the teeth in the slot, reducing the leakage flux across this path.



**Figure 2-12 Flux density plot on the surface of the 8.5-8.5-8.5 design**

Altering from the tapered tooth design with an axial length of 25.5mm to a straight tooth 24mm axial length design, it was found that the flux linking the coil due to the magnet was reduced, but the reduction in material mass meant that the torque per unit active mass of the machine increased. Figure 2-13 shows the Psi-I characteristic for two designs, both 24mm long with an 8-8-8 split between the stator teeth and slot, however, one design had tapered teeth and one had straight teeth. Comparison of the flux linkage (Psi) for the two machines at the zero MMF point (where all the flux is due to the magnet), shows that both have the same value, so the back EMF of the machines is the same. However, there is a gradient difference between the two curves; the tapered design is steeper. The symmetry of this gradient difference around the zero MMF point suggests that this is an increase in inductance. This is plausible due to the larger cross over area of teeth in the tapered design.

The reduction in tooth axial length has also increased the air-gap flux density to 1.37T. The flux density plot through the centre of a tooth and SMC wedge in the radial-axial plane is

shown in Figure 2-14 and it is clear that the SMC is working into its saturated region under most of the tooth due to the more even distribution of the flux coming from the concentration block, i.e. no heavy saturation at the edge of the tooth, reducing flux flow under the tooth.

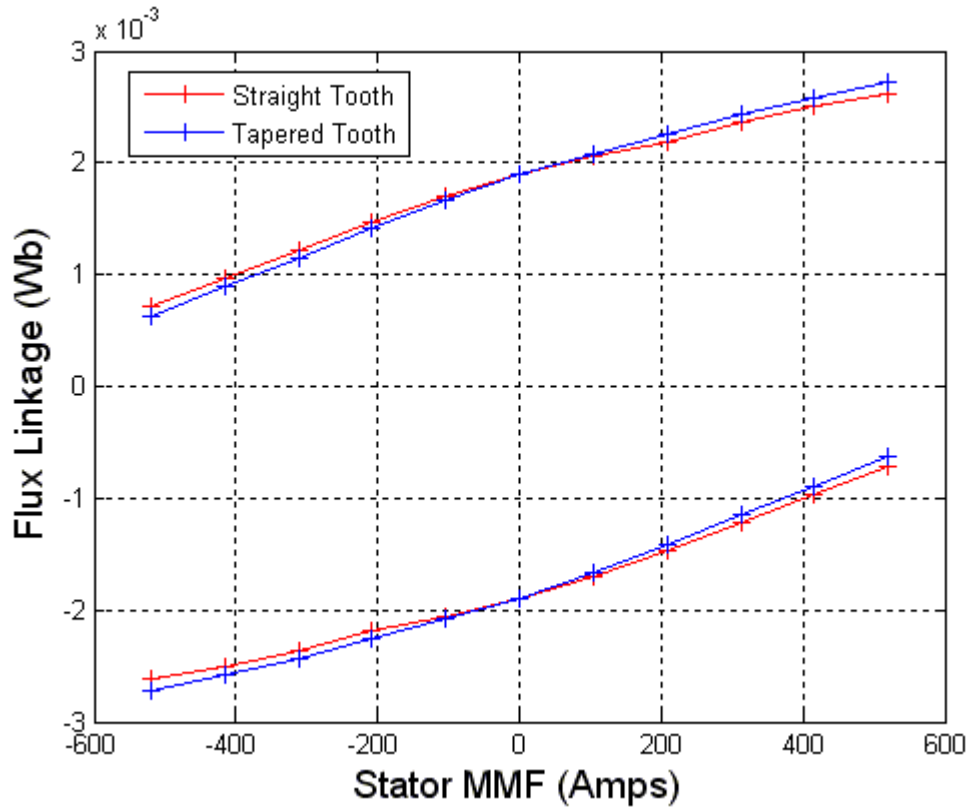
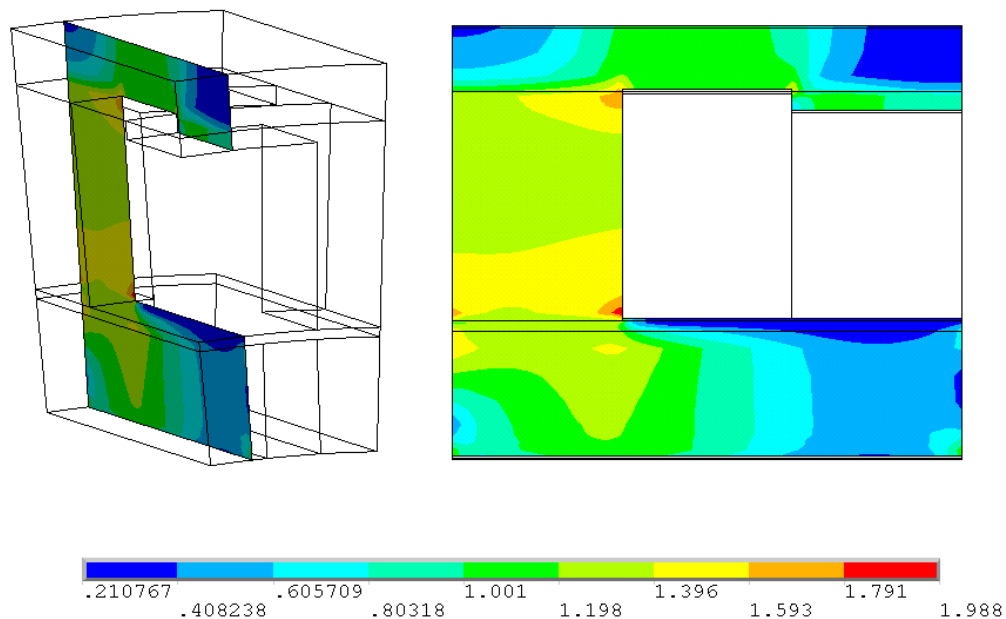


Figure 2-13 Psi - I characteristic for the same 24mm design with tapered and straight stator teeth



**Figure 2-14 stator ratio 8-8-8 design with stright teeth**

#### 2.9.4. Larger SMC cross section area

An archetypal use of SMC involves taking full advantage of its isotropic characteristics. Some of the designs have shown problems with saturation in the rotor SMC parts and this has limited the design for the given dimensions. A way of increasing the cross section of the SMC without altering the outer diameter of the machine would be to extend radially inward, while holding the magnet working area the same. This instantly raises issues with flux leaking back to the magnet as the gap between the SMC pieces would only be the depth of the magnet (three millimetres) with a large cross sectional area, only three times longer than the air-gap (which is  $2 \times 0.5$  for flux linking the stator) that has a much smaller area. But if the SMC was shaped to a point, such that when viewed in the axial direction, the extra SMC takes a triangular form, the average distance between opposite SMC poles would be greatly increased, suggesting that the leakage might be limited and out weighted by improvements of flux linking the coil.

The flux density plot in Figure 2-15 shows a design with the SMC wedges extended to a point. This is an adaptation of the 24mm 8-8-8 tapered tooth design. This design already had an acceptable level of peak flux density in the SMC, so adding the extra SMC should improve, or at a minimum maintain the flux linkage of the design. However, what is actually found is that the leakage increase due to the SMC extending radially inward beyond the

magnet is substantial and the flux linking the coil actually goes down from  $1.825 \times 10^{-3} \text{Wb}$  to  $1.625 \times 10^{-3} \text{Wb}$ , a 11% reduction and hence this modification is counterproductive.

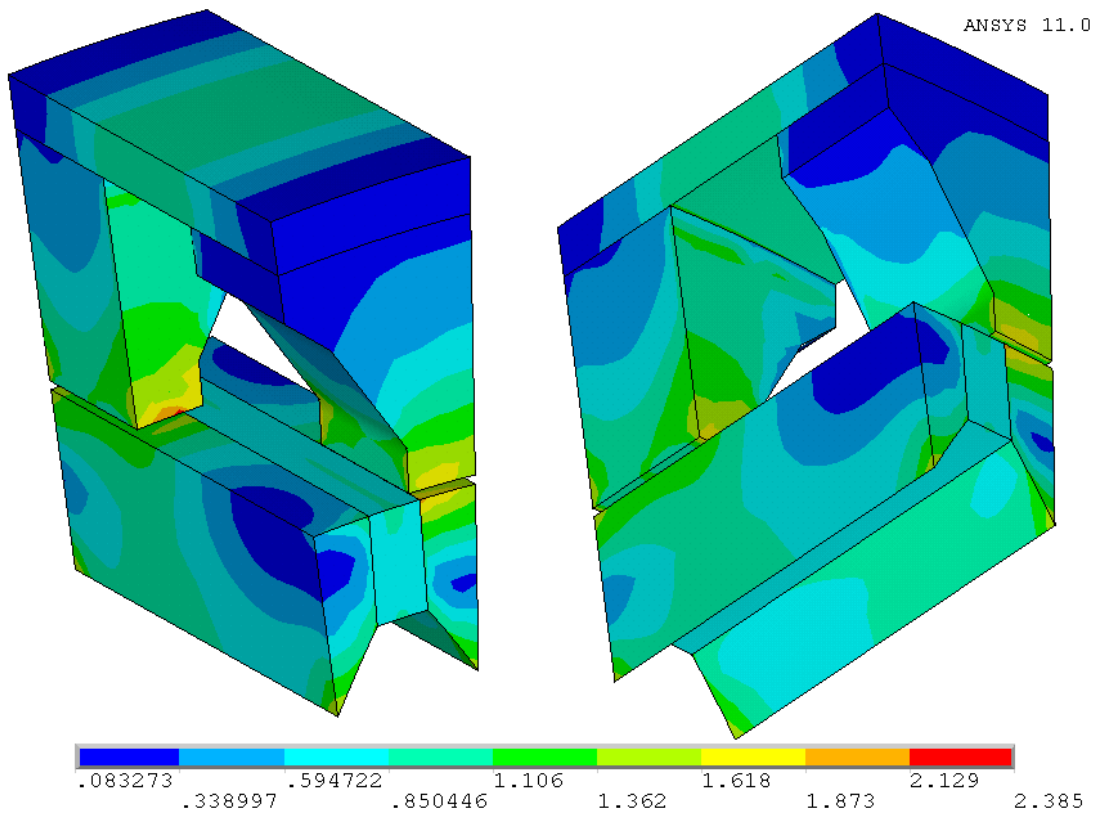


**Figure 2-15 Flux plot of a 8-8-8 design with enlarged SMC wedges**

### 2.10. Final Design summary

A prototype was built to validate this design i.e. the design which is 24mm long with an 8-8-8 ratio in the stator with straight teeth and no extra SMC in the rotor so as to minimise leakage. To finalise the details of the design and to give more accurate figures to compare against the final design, the model was refined. This refined mesh is shown in Figure 2-16, where all the active parts including the air-gap mesh are shown. The major areas of refinement are in the tooth close to the air-gap, in the tooth close to the SMC core-back (as the flux flows around the corner and into the bridging piece to the next tooth) and finally in the mesh extrusion in the axial direction.

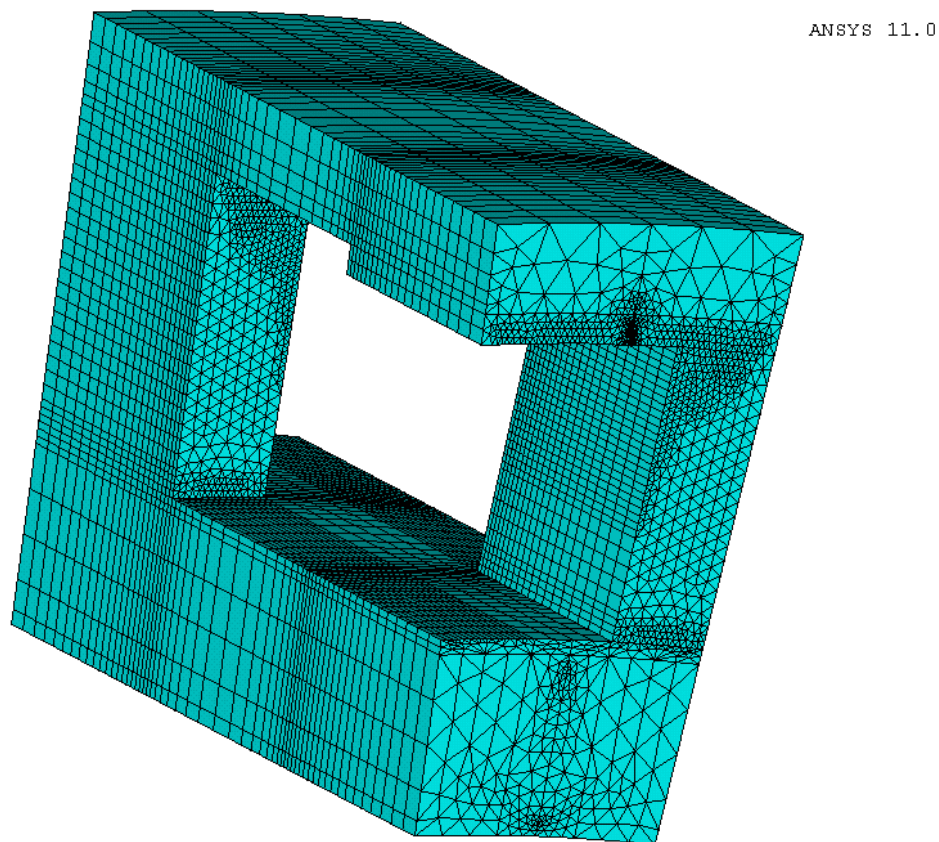


**Figure 2-16 ANSYS one pole pitch model showing the refined mesh of the final design**

The results from this mesh refinement made only small changes to the results, within 3%, but greatly increased the solution time of the model. Flux density plots from this refined mesh are shown in Figure 2-17. The top two plots are first due solely to the magnet flux and then second the armature flux. A good power factor requires limiting the size of the armature current driven flux in comparison with the magnet flux and this is apparent in the results. The bottom two plots show the result of  $\pm$  rated MMF applied in alignment with the field from the

magnet. The bottom left picture in Figure 2-17 shows that the armature flux is acting against the field flux (i.e. is a negative d axis current), limiting the overall flux linkage, so the flux densities are quite low all over the model. The bottom right picture shows the armature and field flux in the same polarity and as a result the flux carrying parts are well saturated, with the flux density in the teeth being about 0.3T higher than the SMC (by design and in line with the better magnetic performance of the laminations relative to the SMC).

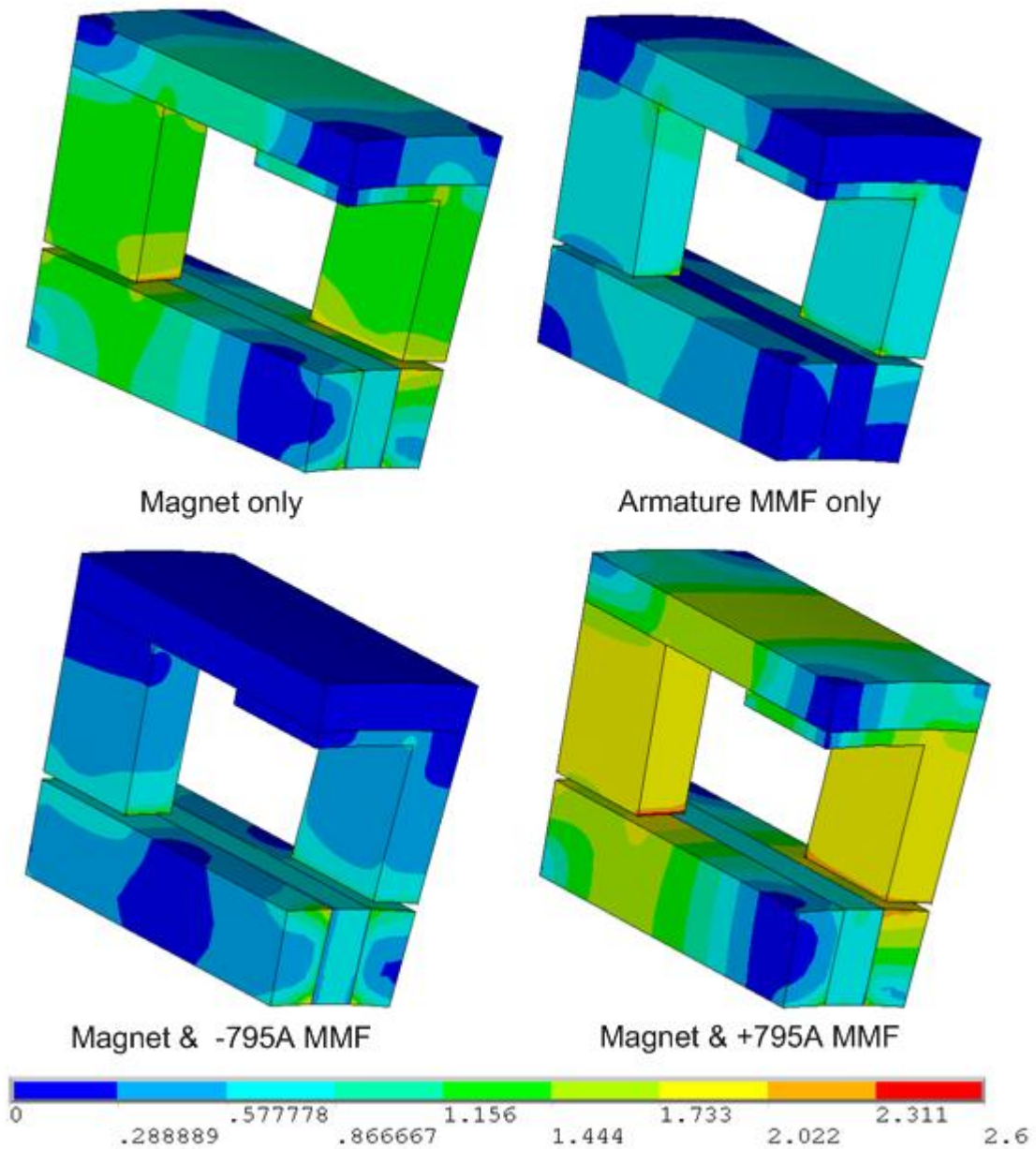


Figure 2-17 Flux density plots for the final design with different flux sources

The Psi-I characteristics in the aligned position for the final design are shown in Figure 2-18. From this it is predicted that with an MMF of 624A, which is the predicted thermal limit based on machine built by Dickinson [8], the average torque will be 17.17Nm. The leading design details are presented in Table 2-3, a key one to note is the predicted power factor of 0.82 which is a very good value for a modulated pole machine.

**Table 2-3 List of leading design details**

<b>Parameter</b>	<b>Value</b>	<b>Parameter</b>	<b>Value</b>
Armature flux	2.598e-5	Stator OD	188mm
Field Flux	3.67e-5	Stator bore	156.2
Predicted Power Factor	0.82	Core-back depth	3mm
Stator teeth	50	Lamination stack length	8mm
Rotor Poles	50	Coil axial length	8mm
Phases	1	Air-gap	0.5mm
Axial length	24mm	Rotor OD	155.2
Magnet dimensions	24mm x 6mm x 3mm	Rotor (active) ID	143.2mm

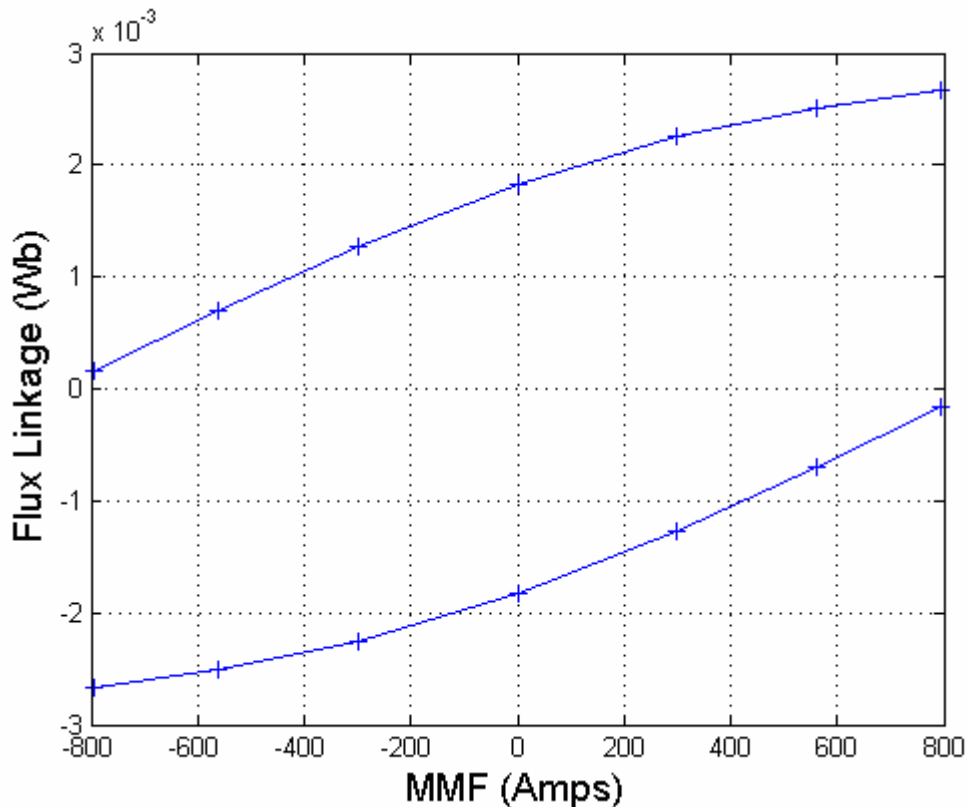


Figure 2-18 Simulated Psi-I data for the final machine design

### 2.11. Chapter summary

The start of this chapter gave an introduction into finite element analysis and applying it to MP machines. It is shown that by taking advantage of the symmetry of the MP machine the size of the simulation can be greatly reduced, diminishing the time required to attain a converged solution.

A twelve pole machine was simulated and was found not to perform well compared to known MP designs. This model was also used to assess the leakage paths in the machine. A second design using fifty poles was simulated and, as anticipated; improvement was seen in the torque density. For a fixed outer and inner diameter the machine was optimised which focused around the split in the axial direction of the stator laminations and the slot opening for the winding. A final design was reached and simulated results with greater resolution were presented, ready for comparison with a prototype.

## **Chapter 3. Construction of the Material Hybrid Prototype**

### **3.1 Stator**

#### **3.1.1 Introduction**

The reasons for the particular method of construction of this machine have been covered earlier but it may make the understanding of the construction easier if the major points are covered once more here. The concept of this machine was that the stator would be separated into two sections – an SMC core-back and laminated teeth. The core back has three dimensional alternating fields and hence it was manufactured from SMC segments. The teeth section is laminated and it carries the field radially (and to some extent circumferentially) from the air gap and onwards into the core back. The teeth section forms a (toothed) thin ring shape and in practice would be a very uneconomical (and difficult to produce) component because of the large amount of scrap. To get over this problem the toothed section was manufactured in a series of (marginally) connected tooth segments in a linear arrangement which were subsequently bent into a circle to form the final ring shape as shown in Figure 3-1.

#### **3.1.2 Laminations**

The laminations were manufactured from 600x300mm sheets of M270-35A grade electrical steel by laser cutting (outsourced to a local manufacturer). Although the laser machine was capable of cutting to a tolerance of  $\pm 0.1$ mm, the finished product did not match this tolerance due to the laminations moving on the bed plate of the laser cutter during the cutting process. The process also left a residual splatter (i.e. small “blobs” of molten material which had been transferred from the sacrificial bed plate). This was in spite of a new bed plate being used precisely with the intention of minimising the splatter. A small hand file was used to remove the splatter in the worst affected areas, applying light pressure at 45 degrees to the surface of the lamination which minimised removal of the insulation layer. More laminations were produced than were needed, allowing a selection of the best to be used in the construction of the prototype.

There were two possible sequences in the production of the circular stator shape from the long linear laminations (see Figure 3-1) either gluing before bending or bending and then gluing. Gluing all the laminations together in the linear state then bending the assembled laminations as a unit to form the stator ring gave rise to two concerns: firstly, the force needed to accurately bend the stack into the desired shape would be high and secondly,

there was the possibility that the bending action might shear the glue joint of adjacent laminations causing the whole stack to spring apart.

For these reasons a compromise was adopted. Each individual lamination was pre bent on a jig that matched the dimensions of the final ring, Figure 3-2. On release from the jig, there was some spring-back, leaving the laminations around 20mm short (circumferentially) of connecting. Although it would have been possible to compensate for the spring-back by over-bending the lamination so that the spring-back returns the lamination to the desired position, this would have introduced a significant increase in complexity to the bending jig and was considered unnecessary for this single prototype. Such methods could be envisaged being used in an automated large scale production.

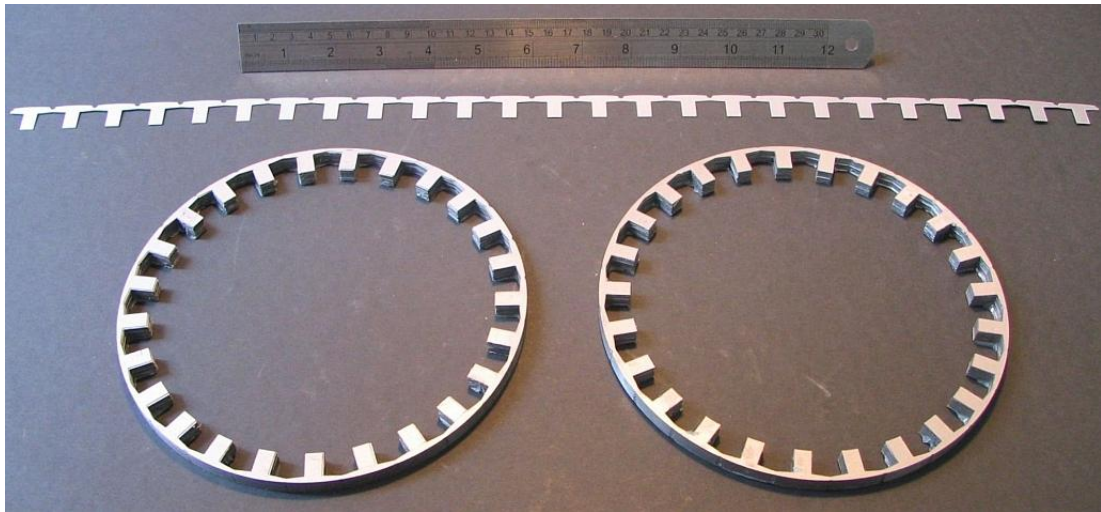


**Figure 3-1 A single strip lamination and the two halves of the stator pre final assembly**

The pre bent laminations were then assembled into a second jig, made from aluminium, see Figure 3-2. This jig is to hold the laminations during the gluing process and subsequent machining (during which parts of the jig are machined away. The jig consisted of two parts. The first had castellations circumferentially milled to align the teeth. It also had a flange for locating the outer diameter of the laminations. The assembly of the pre bent laminations into this half of the jig was performed in an uncured, “wet” epoxy state.



**Figure 3-2 picture of the sacrificial jig before assembly**

The second part of the jig consisted of a lid with a circumferential projection on it for locating with the laminations. The first part was drilled and tapped to allow bolts to pull the lid down onto the laminations compressing them to the desired thickness while the epoxy set.

Once the laminations were assembled and cured into the jig, the outer diameter of the laminations was milled to the desired size. This resulted in a good tolerance in the lamination outer profile allowing a close fit with the SMC core-back. The inner diameter also required machining to achieve the required dimension against the lower manufacture tolerances of the rotor. This was done during the assembly stage and is described later in section 3.5.1. The outer diameter was achieved using a miller and a rotary table rather than by turning on a lathe. The turning process would see the cutting piece drag across the laminations, increasing the chance of damaging the glue joint and lifting adjacent lamination making successful disassembly of the jig uncertain. As the assembly was done in a wet state most air regions were filled by epoxy, providing some further support. After the outer diameter was machined to size, the remainder of the former jig was unbolted and removed, leaving the finished laminated section. The jig had been coated in mould release agent to minimise the adhesion of the epoxy to the jig. The same process was used to produce the second laminated stator section.

### **3.1.3 SMC core-back sections**

As already discussed, prototyping in SMC is difficult and the aspect ratio of the core-back places it on the limit (if not beyond) what can be compacted. Producing a complete core back

would require that it be compacted in an axial sense. This means that component is much longer (in the direction of pressing) than its thickness. In powder metallurgy this is described as the “aspect ratio” - the length in the pressing direction divided by the minimal dimension at right angles to the pressing direction. If the ratio is too high (6:1 is often quoted) the friction with the die walls prevents proper compaction in the centre of the section (i.e. remote from the punches). The result is lower densities and probable cracks and this would be the position for a core back which was pressed complete. In any event a punch and die for the part is not justifiable for the prototype on cost grounds and hence recourse was taken to machining the core back from a standard rectangular blank. Notwithstanding the aspect ratio argument, ideally the core back would be manufactured as a single ring but this ring would need to be cut in at least one position to prevent circumferential eddy currents being induced. Clearly the part would then be very weak. The obvious way forward is to split the core back into short arc sections. These could then be pressed (in a production process) in a radial direction. In the prototype the ring to make the core back was manufactured as a series of ten arcs, each arc section being machined from one of the standard rectangular SMC blanks.

The outer radius and radial edges were milled first by clamping the blank of SMC axially. A jig was then built to house the partially machined SMC sections at the correct diameter, with an adjustable clamp pressing each section in place from the inner radius (see the left-hand photograph in Figure 3-3). An aluminium plate was then bolted over the partially machined sections to clamp them in place axially and the radial clamps removed. The inner radius of the arcs was then milled out as a complete ring, guaranteeing concentricity, as can be seen on the right of Figure 3-3 and in detail in the centre of Figure 3-3. The key feature in this method is that the edges of the SMC are supported, reducing corner damage because the SMC is sandwiched axially between two sacrificial aluminium plates.

All parts were machined from virgin material in the green (pre-heat treated) state. As already discussed in earlier chapters, the SMC in this state is softer and more amenable to machining and produces a part whose properties are closer to those found in a pressed part. Heat treatment was performed post machining by Höganäs AB in their research laboratories. One of the reasons for heat treatment is to release stresses built up in the part during the pressing process. In parts machined from blanks, these stresses can take unwanted patterns; depending on the position within the blank from which it was removed. It is this mechanism that resulted in the arcs deforming slightly in the heat treatment process. The deformation was such that the arcs straightened marginally, resulting in a larger radius and also losing some of their concentricity. This was not ideal, but was small enough not to cause major problems in the construction.



**Figure 3-3 SMC core back sections being machined**

## **3.2 Rotor**

### **3.2.1 SMC Flux Concentration Blocks**

The most challenging aspect in the manufacture of these rotor parts is in assuring that the angles between the sides of the parts, which join with the magnets, are accurate enough so that, on assembly, the rotor is cylindrical of the correct diameter and with the air-gaps between the magnets and wedges minimised. In production, these wedges would be manufactured by pressing and the high tolerance requirement would be easier to meet. In prototyping, it is more difficult, for as with the core back, the wedges were machined from SMC blanks in the green state.

First, the rectangular blanks (120x30x25mm) were milled with slots creating a castellation that formed the basis for several of the wedges. These blocks (i.e. each individual castellation) were then detached manually from the blank by carefully using a hacksaw to separate the remaining connection. The use of a hand tool rather than a miller was to try and minimise damage to both the edge and the interior of the small sections. The blocks were then placed in jigs for milling out the angled edges and the outer radius. These jigs were designed to support the edge where the milling cut would exit the piece - to try and minimise tarring of the edge. The success of the finish quality can be seen in the picture of Figure 3-4. As with the core-back arcs, this machining was undertaken with the material in the green state. Heat treatment was again performed by Högånäs AB. Due to the substantially more rigid body form of these parts when compared to the core back arcs, no visible or easily measured deformation resulted from the heat treatment.

### 3.2.2 Magnets

The magnets were rectangular blocks of Neodymium Iron Boron (NeFeB) grade NE38H with a Nickel coating. The dimension of each magnet is 24x6x3mm. The magnetisation is parallel with the axis of the 3mm dimension which was performed by the supplier Precision Magnetics Ltd.

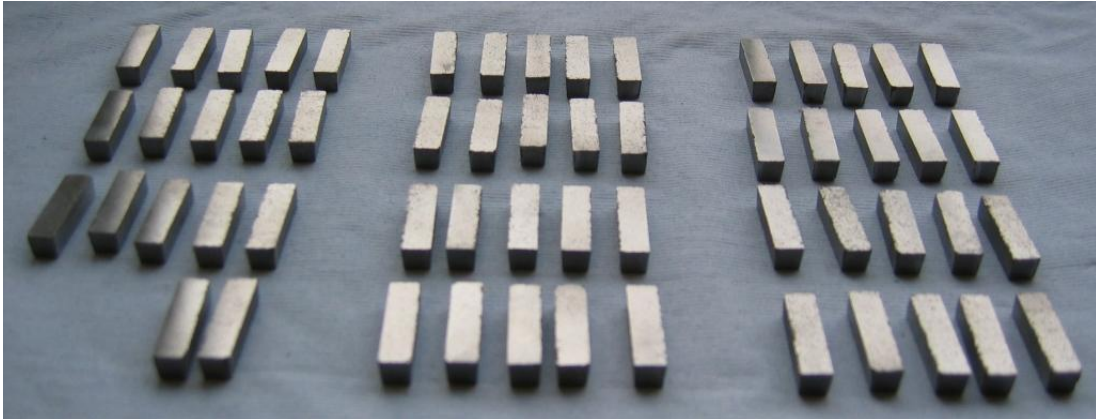


Figure 3-4 SMC flux concentration blocks

### 3.2.3 Shaft and Rotor Mount

The diameter at the air-gap of this machine is much larger than that of the shaft, by the order of 7:1. To achieve concentricity it is desirable to manufacture the shaft from a single piece of material. The choice of material was a non-magnetic stainless steel, which is strong enough to produce a stiff, thin shaft, reducing material and weight. However, stainless steel is not required to form all of the structure to the diameter upon which the active parts would be mounted, so an aluminium section was also used. This significantly brings down the outer diameter of the stainless steel shaft; resulting in a simplified yet still heavily featured (see Figure 3-12) shaft that could be manufactured from a smaller blank, with the advantage of reducing the machining resources required to produce the shaft, by limiting the waste material from the roughing cuts and hence the rest time between cutting stages.

As briefly mentioned already, an aluminium section was used to span the large difference in shaft and air-gap diameters. It is upon this section that the active parts for the rotor were assembled. When viewed from an axial-radial cross section, as shown in Figure 3-5, this section forms a T shape. The vertical section is a 5mm wide plate which increases the diameter to 131mm, more than doubling the outer diameter of the shaft flange to which the aluminium mount is bolted. At this diameter the section width increases to 24mm to form a 6mm thick (radial direction) support upon which the magnets and SMC flux concentration

blocks are mounted. To assist with the location of the active sections (magnets and SMC blocks) on assembly, a series of 0.1mm deep keyways were milled into the outer surface of the aluminium section into which the SMC blocks can locate. The depth of these keyways was constrained by the electromagnetics of the motor. From the FE it was determined that at this level, the resultant magnetic flux leakage path would increase the flux leaking by a level that was within the error of the model. More depth would have been preferable from an assembly perspective, especially when the rounded edges of the SMC wedges are taken into account, but this would introduce a more noticeable magnet flux leakage because the SMC pieces protrude inwards from the magnet edges.

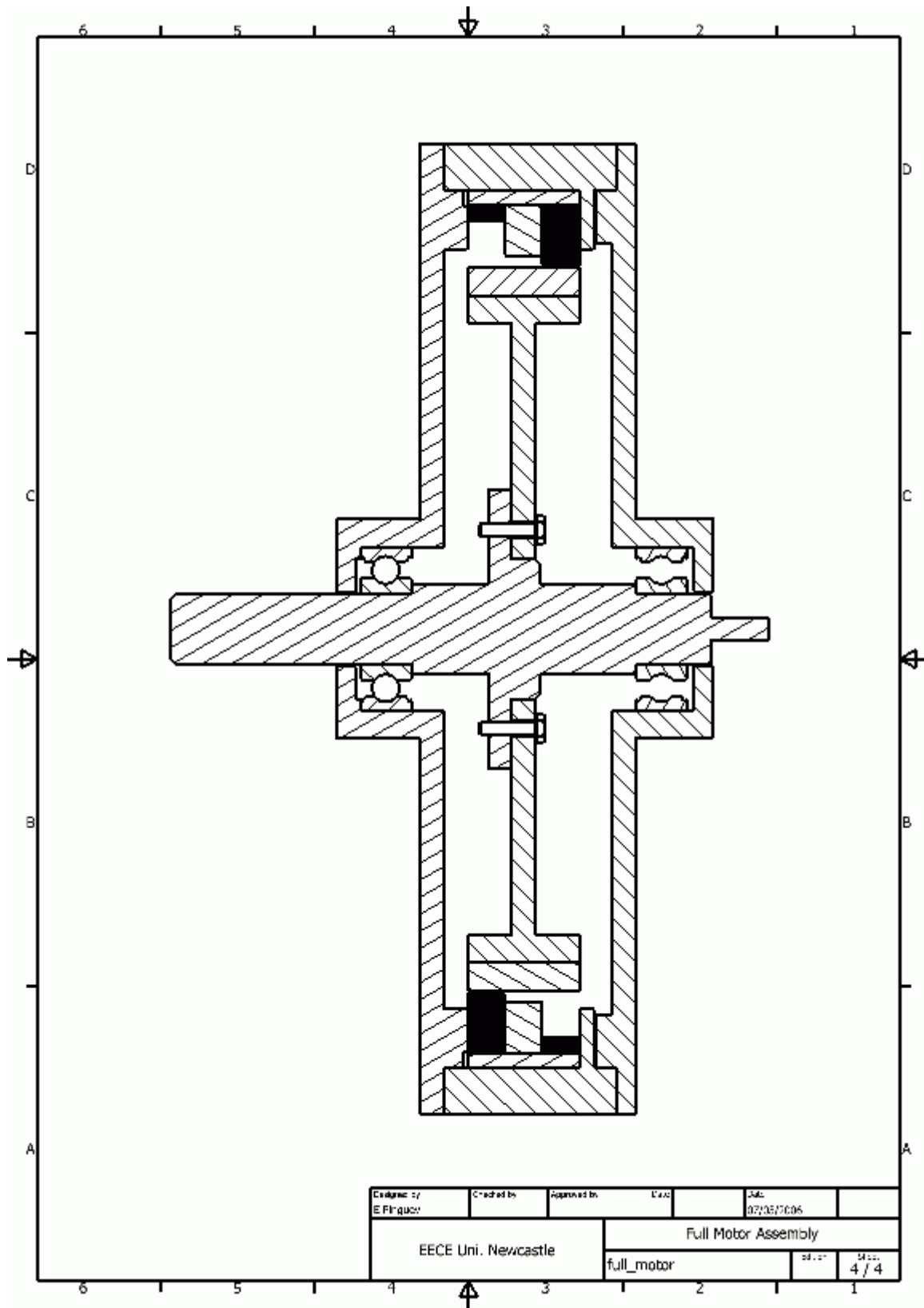


Figure 3-5 Cross section view from engineering drawing of the full assembly

### **3.3 Coil**

As noted earlier, the coil is a simple hoop shape that sits sandwiched between the two lamination stacks when the stator is assembled. This gives a rectangular slot profile for the winding. It is a design objective to fill this slot with as much copper as possible and limit the air gaps between the coil and the surrounding stator iron (laminations and SMC), this improves the heat transfer from the coil and it is the thermal limit of the coil that will govern the power rating of the machine.

It was decided to construct the coil from round enamel coated copper conductor. The geometry of the stator, makes winding the coil in situ difficult (i.e. using the stator iron as a former) as the core back is outwards from the outer diameter of the coil. However, the sectional stator assembly and the simple rectangular cross section of the coil, coupled with the relatively low turn count (roughly twice the number of poles), facilitates well a preformed bobbin wound coil with ordered and structured turns and layers, resulting in a high copper fill factor. The coil was pre-made using a winding machine. To allow the coil to be handled after removal from the winding bobbin, the conductor was coated with epoxy resin as it was fed into the bobbin.

There were two versions of the bobbin winding jig, the first was made from medium density fibreboard (MDF). MDF was an appealing material as it would not scratch the enamel insulation of the conductor as it was guided into the slot. The jig consisted of three sections: A central disc 8mm thick (the width of the coil) that formed the central diameter of the bobbin. Either side of this disc, were two more discs matching the outer diameter of the winding. This was all clamped together with four bolts and mounted on a mandrel for fitting into the winding machine. The sides of the jig were lined with a thin plastic to assist in disassembly once the epoxy had cured. After the production of two coils from this jig, two things had become apparent.

- 1) The MDF former was not stiff enough, and the high tension applied to the wire to keep it in the desired location during winding had deformed the jig, giving poor tolerances on the sides of the coil.
- 2) There was a tolerance stack problem - each time the winding came to a new layer, the conductor would gently rise up to the new level over several times the thickness of the wire leaving a void, reducing the length of that turn by a few degrees. This could be minimised by forcing the wire into the void for longer at this point but then the wire would take a sharper bend to the next level, the radius of this bend is limited by the diameter of the wire, and generally results in a bump being created in the layer

which, over the several layers, built up to a large asymmetry in the coil ruining the overall fill factor of the coil.

In an attempt to minimise the asymmetry, radial force was applied directly to it following the winding process. On inspection of the coil, when removed from the jig, it was found that although the radial force had reduced the bump notably, the MDF jig had allowed the coil to deform sideways.

To try to eliminate tolerance problems on the sides of the coil, the MDF bobbin jig was replaced with an aluminium one. This meant that the dimensions of the wire and the liner were much more critical as the aluminium jig would not deform to accommodate differences as the MDF jig had in the previous coils. During winding of the coils on this new jig, good copper fill and a reduction in asymmetry was achieved by the use of hard plastic punches which were used to force the wire to the required position. This method was found to greatly reduce the bump, while the stiffer former jig maintained a good edge tolerance.

The initial idea for the winding pattern is shown in the left diagram of Figure 3-6. The turns of each layer line up exactly with the previous and preceding layer, there is no interlocking between the layers. It was found that achieving this consistently through whole of the coil was very difficult, particularly with the MDF jig in the later layers as it warped under the force of the coil. The tension required to hold the wire in place was quite high and became counterproductive, the epoxy acted as a lubricant between turns and the wire was found to slip out of alignment into the groove between two turns of the previous layer. This small misalignment may only be noticed when winding the final turn of the layer (due to lack of space); the previous turns would then be very reluctant, due to the tension, to move back into the desired alignment. The solution was to go for a winding that had interlocking between layers but with the same number of turns in each layer, as shown in the right of Figure 3-6.

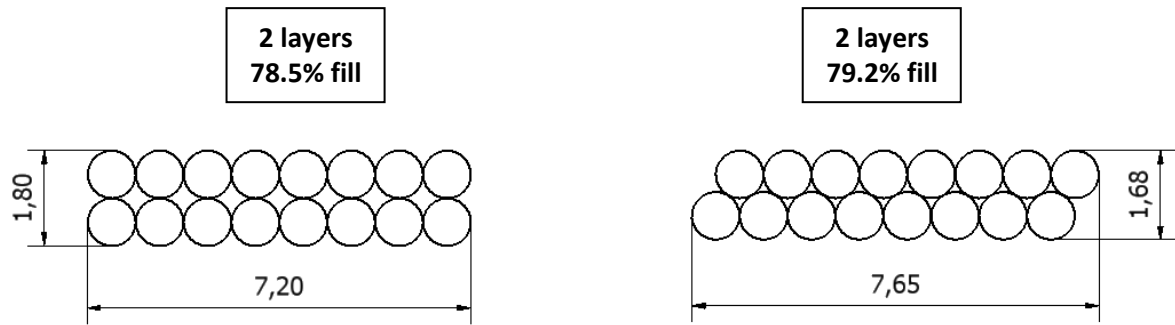


**Figure 3-6 Winding patterns considering just two layers**

When considering the two patterns for winding over just a couple of layers as in Figure 3-6, the difference in theoretical maximum fill factor is only 0.7%. This gap would change with respect to the wire size, as the greater the wire diameter, the greater the side gap due to the offset in layers in the interlocking pattern (right diagram of Figure 3-6). When considering the cases with the same wire size, the number of layers highly influences the fill of the interlocking design (right diagram Figure 3-7). Maintaining an 8 turn layer, but increasing to 13 layers from 2 layers increases the maximum theoretical fill factor from 79.2% to 84.3% when considering a rectangular slot profile of the outer dimensions of the coil. This compares favourably to the aligned pattern, which maintains its 78.5% theoretical fill factor, independent of the number of layers.

To assist with understanding the layer structure and causes of asymmetry, a practice coil was cut through in two points. Figure 3-8 and Figure 3-9 show photographs of the sides (axial direction) of the coil displayed either side of a photograph of a cross-section view. The cross-section in Figure 3-8 is the point in the coil where the layers start and stop. The voids left by the conductor as it rises from one layer to the next are easy to see in the side views. It is also clear in the cross-section that at this point in the coil, the first layer is not correct and as such influences the preceding seven layers. The disturbance and apparent missing turn is a result of the way that the terminal of the coil was fed out of the jig. In this coil, it was fed out of the side of the jig at a near 90degree angle. Obviously the conductor could not form a perfect right angle and had to take a small radius, reducing the width of the jig for the eight turns. This is why it appears that there are only seven turns in this layer, in actual fact the eighth turn has been forced to rise to the new layer before it has completed a full revolution. In future coils, the angle of entry of the wire in to the bottom of the jig was reduced minimising the radius of the wire and allowing a much better structure of the first layer to be formed.

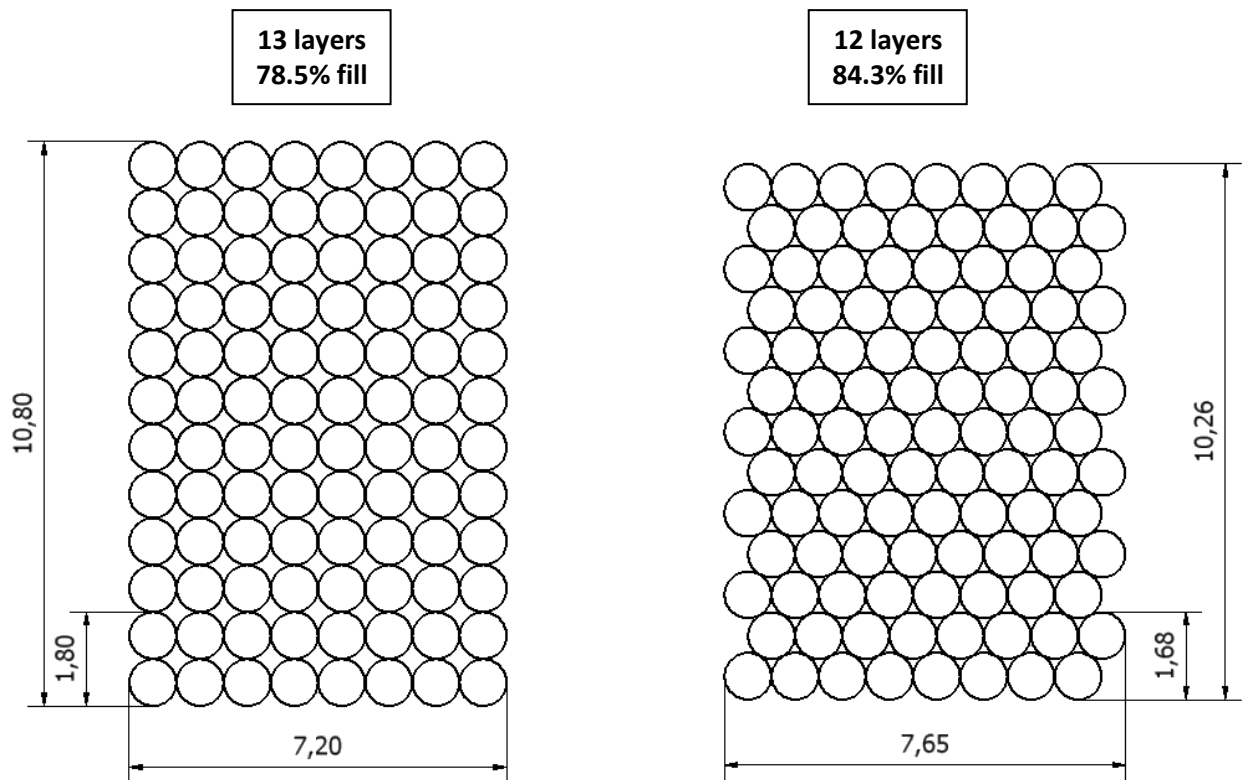


**Figure 3-7 Winding Patterns considered over the whole slot**

Extreme deformation of the conductor has occurred as a result of tension in the wire and also because tapping by the winder has been used to force the required eight turns into the layer. By the eighth layer, the initial misalignment has been resolved, and these layers look much more structured. The top layer does have a slight horseshoe shape, which is seen in all coils made. The increase in height at the outer edges of the coil result from the bend in the wire as it rises to the next layer and is what causes some asymmetry to the outer diameter of the coil. It is clear that minimising this is the key to getting the best fill factor for the coil in terms of how much space it occupies in the final machine.

Figure 3-9 is roughly 45degrees round from Figure 3-8. It is evident that the problems caused by the wire entering the jig have not affected the coil here and a well structured eight turns per layer structure is clearly visible with interlocking between layers. It is also clear that the tension in the wire on turning has been enough to deform the wire from round to near hexagonal, which improves the fill factor even more.

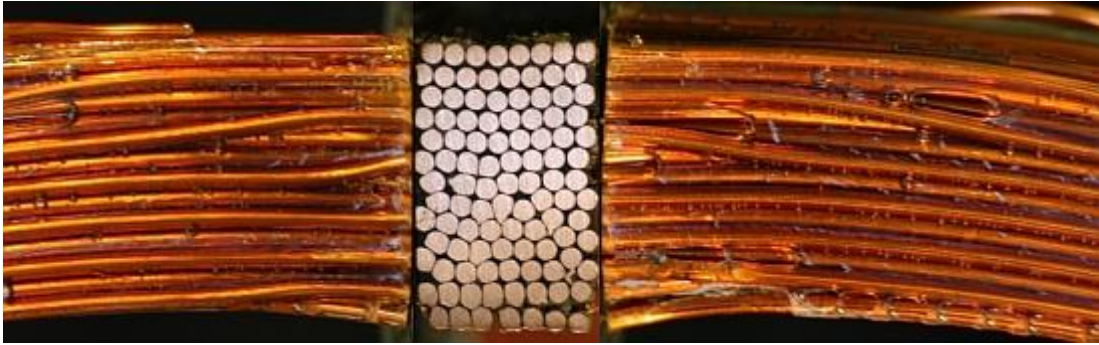


**Figure 3-8** view of the layer intersection

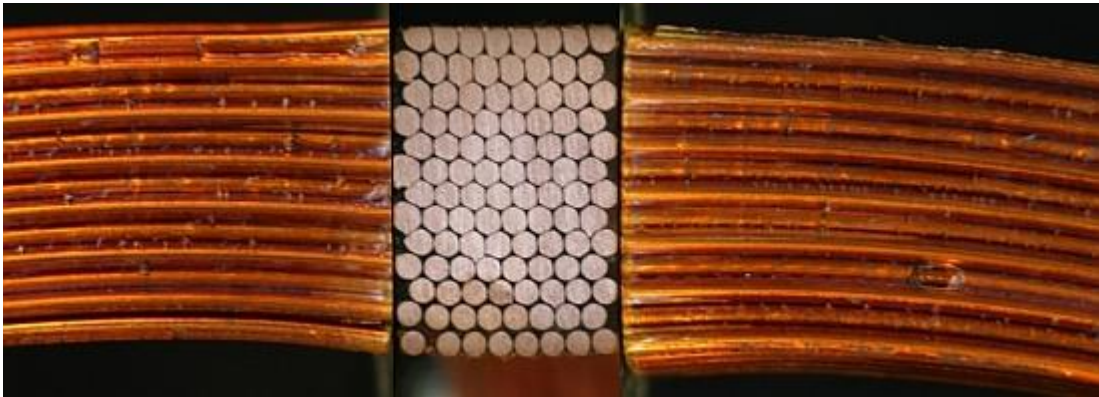


**Figure 3-9** view away from the layer intersection

### **3.4 Casing and Shaft**

This section describes the non active parts of the motor that are required to make up the mechanical structure of the machine.

#### **3.4.1 Outer Casing**

The outer casing was manufactured from Aluminium. It is a cylinder with a flange on the inside diameter for the stator components to locate on when assembled. Around the edges the outer casing it is tapped to take bolts for holding the end caps. These details can be seen in the photograph, Figure 3-10, which shows the outer casing with the SMC arcs already mounted in place against the flange.

#### **3.4.2 End Caps**

Both end caps are of the same design and as with the outer casing are manufactured from aluminium. They comprise of a circular disc (cross section shown in Figure 3-5) with a projecting bearing housing and a central hole for the shaft to protrude. On the other side of the disc is a flange to locate on the outer casing to maintain concentricity. One bearing housing is slightly longer to accommodate a spring for bearing axial preload. The cap that fits on the casing side, where the stator parts will be assembled has a flange such that it is a

mating fit to the stator parts to apply a compression load and hold them in place, this can clearly be seen in the drawing in Figure 3-11



Figure 3-10 SMC arcs in the outer casing

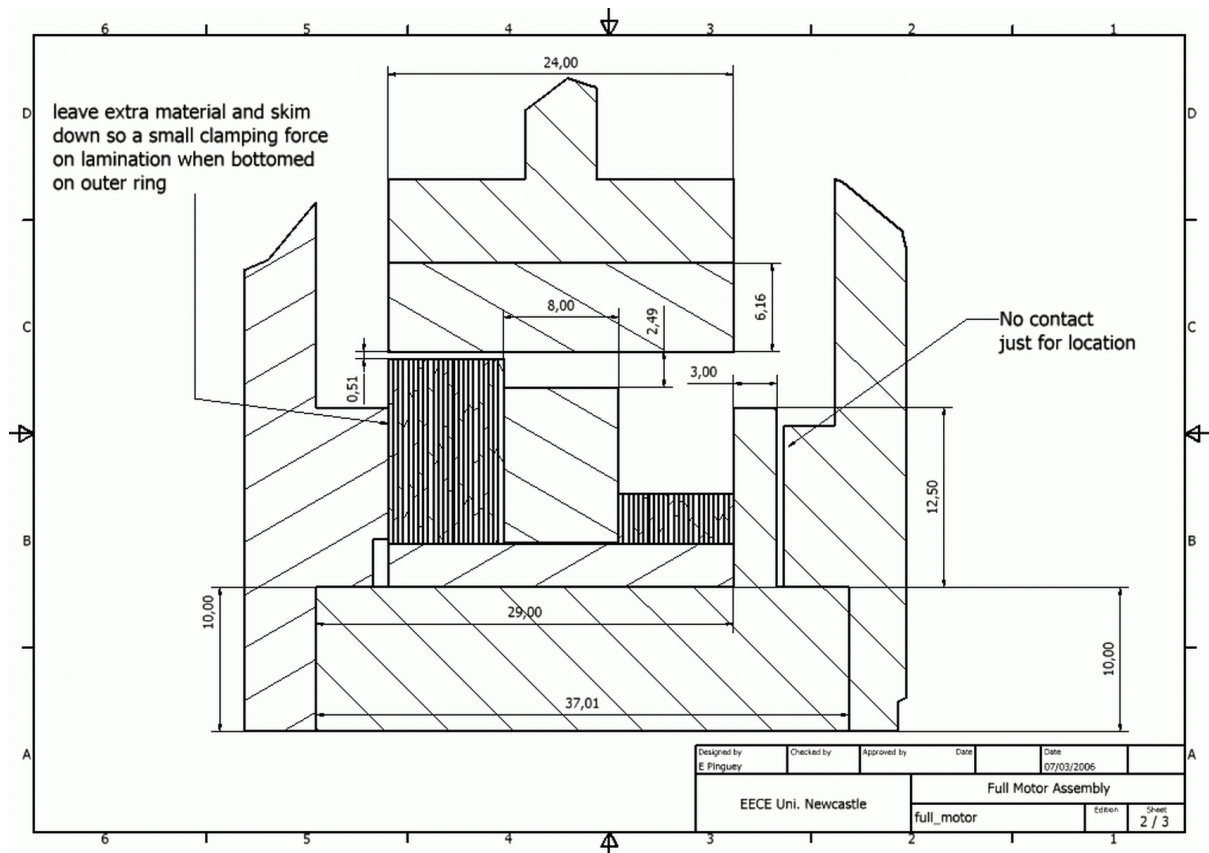


Figure 3-11 engineering drawing showing a view cutting through (circumferential into the page) the main active area of the machine

### 3.4.3 Shaft

The shaft has a lot of detail built into it, see Figure 3-12. The main feature is the flange for bolting onto the rotor aluminium hub section and the seat to locate it on to maintain concentricity. Either side of that are seats for the bearings. On one side the bearing inner diameter is continued right to the end of the shaft, this section will appear outside the bearing housing of the end cap for coupling to a load. On the other end, the shaft is stepped down to 5mm after the bearing seat, to facilitate any light couplings such as an encoder.

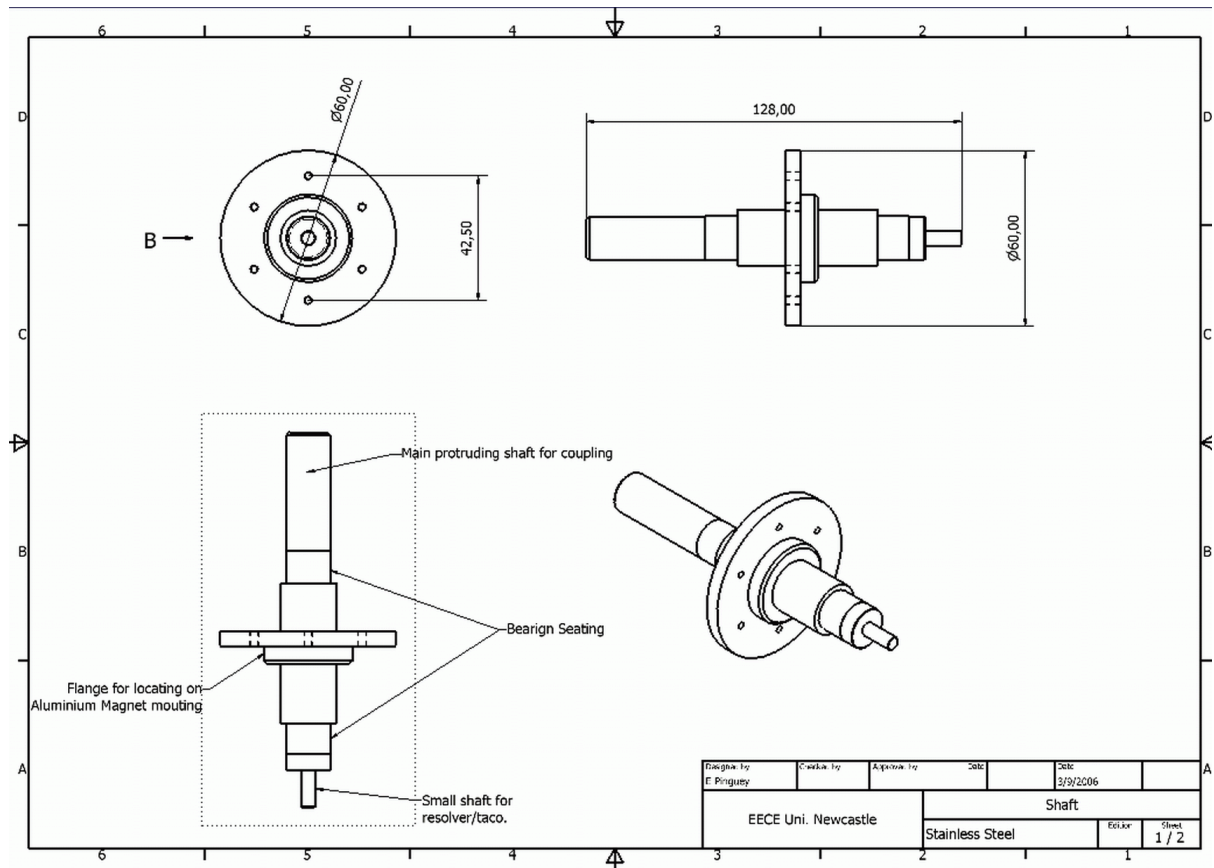


Figure 3-12 Engineering drawing of the shaft.

## 3.5 Assembly

### 3.5.1 Stator Assembly

Location of the SMC arcs to form the stator core back in the outer casing was made as a good sliding fit against the inner diameter of the casing with the advantage that the shape of the pieces naturally lock together to form a solid ring once assembled. As well as this they were glued in place to ensure no circumferential or axial movement as no axial force could be applied to the core back arcs in case it cracked the SMC material. Secondly epoxy was used to take up any spaces left between the arcs and the casing due to the arc's deformation in heat treatment, reducing stress points which again could have led to cracking of the SMC.

With the SMC sections in place, (shown in Figure 3-10), the sandwich of the two lamination stacks and the coil was put in place, again with epoxy, to ensure no circumferential movement, the layout of which is shown in Figure 3-11 the result is shown in Figure 3-13 and Figure 3-14. The outer wire of the coil was fed out through the gap that naturally occurred in the bending region of the stator laminations, the inner coil wire was fed out between two adjacent teeth.

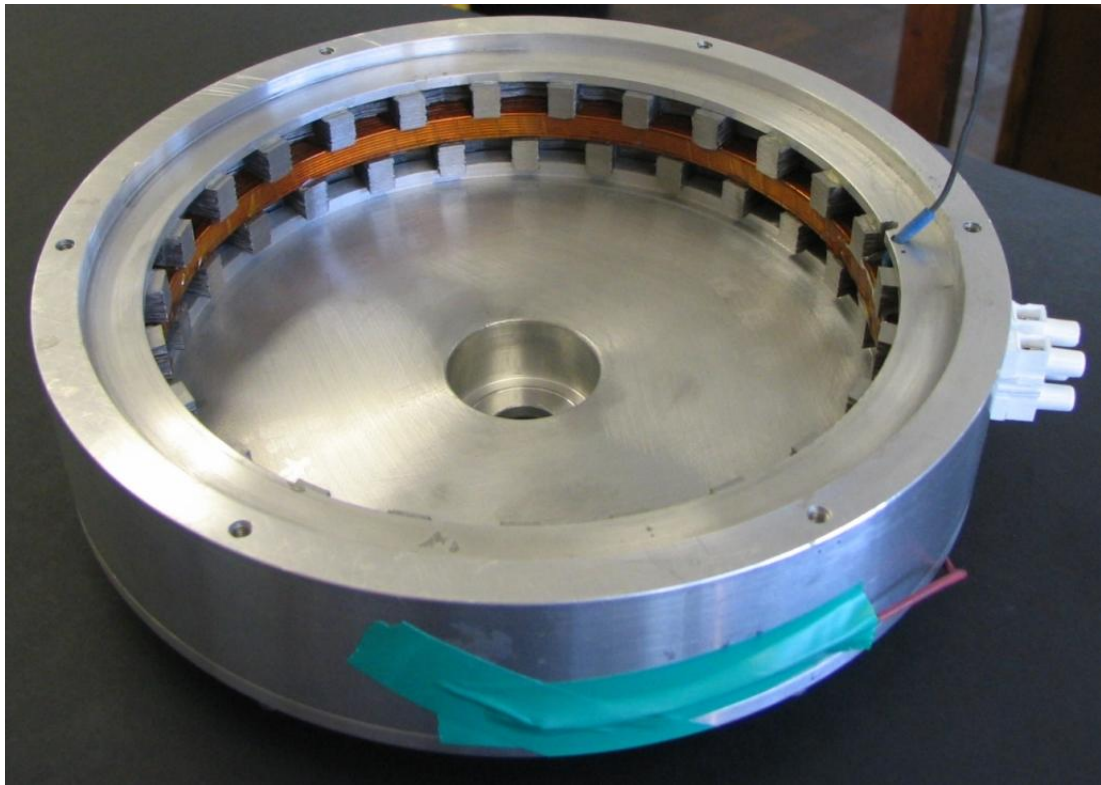


**Figure 3-13 Full stator assembled in case with one end cap**

With an angle of only 7.2 degrees between the two lamination packs, a high tolerance on this dimension was critical to ensure the correct operation of the machine. This was achieved by a set of steel dowels placed in both the flange of the outer casing and the end cap. When the first lamination stack was placed in the casing, it was positioned so that a tooth mated against the dowel, giving it the correct alignment. When the second lamination pack was placed on top of the coil, it was positioned visually in line with the first. The end cap was then put in place and rotated to a pre marked position. The dowel in the cap engaged with the top lamination stack and located it correctly. The end cap was then fastened to the outer case with six M3 bolts. The interference fit of the end cap and the lamination meant that when the bolts were tightened, the axial alignment of the parts was held in the correct position while the epoxy cured.

Concentricity of the lamination stack's inner diameter to the casing was guaranteed by turning off excess material of the tooth tips once assembled in the casing. This also guaranteed a 0.5mm air-gap in reference to the average outer diameter of the rotor (see Rotor Assembly). The machined finish of the tooth tips can be seen in Figure 3-14.

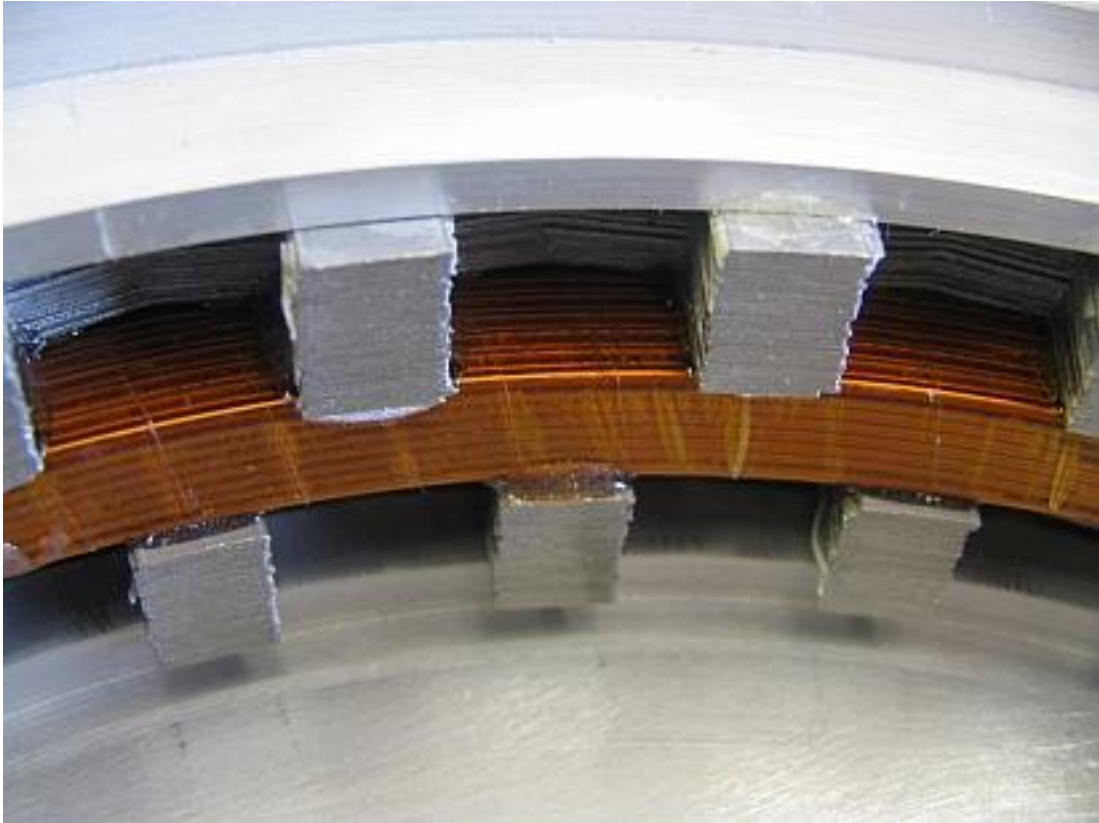


**Figure 3-14 Close up of the stator teeth and winding**

### **3.5.2 Rotor Assembly**

The SMC blocks and magnets were assembled onto the rotor aluminium mount in two stages. A dish shaped jig within which the mount could be centrally located was used. Around the edge of the jig were a series of tapped holes housing nylon bolts. These bolts allowed a radial direction force to be applied to the parts while the epoxy used to bond them to the mount cured.

The larger footprint of the SMC blocks on the surface of the rotor mount made them the logical choice to bond in place first and created a good framework for mounting the more problematic magnets. The previously described recess on the surface of the rotor mount helped to locate the wedges to some extent, but the machining of the SMC did not leave a good sharp square corner to mate with the slot. It was therefore necessary to ensure that the correct spacing and clearance was achieved for the second phase of assembly by using plastic spacers to temporarily replace the magnets.

Once the epoxy had set and the spacers were removed, the magnets were glued in place using the same jig to hold them in place (imprints of the bolts can be seen in the residual epoxy of the rotor surface Figure 3-15). It was found that the local fields of the magnets interacted with the SMC sections to hold the magnets naturally in place. This greatly assisted in the second phase of the assembly.

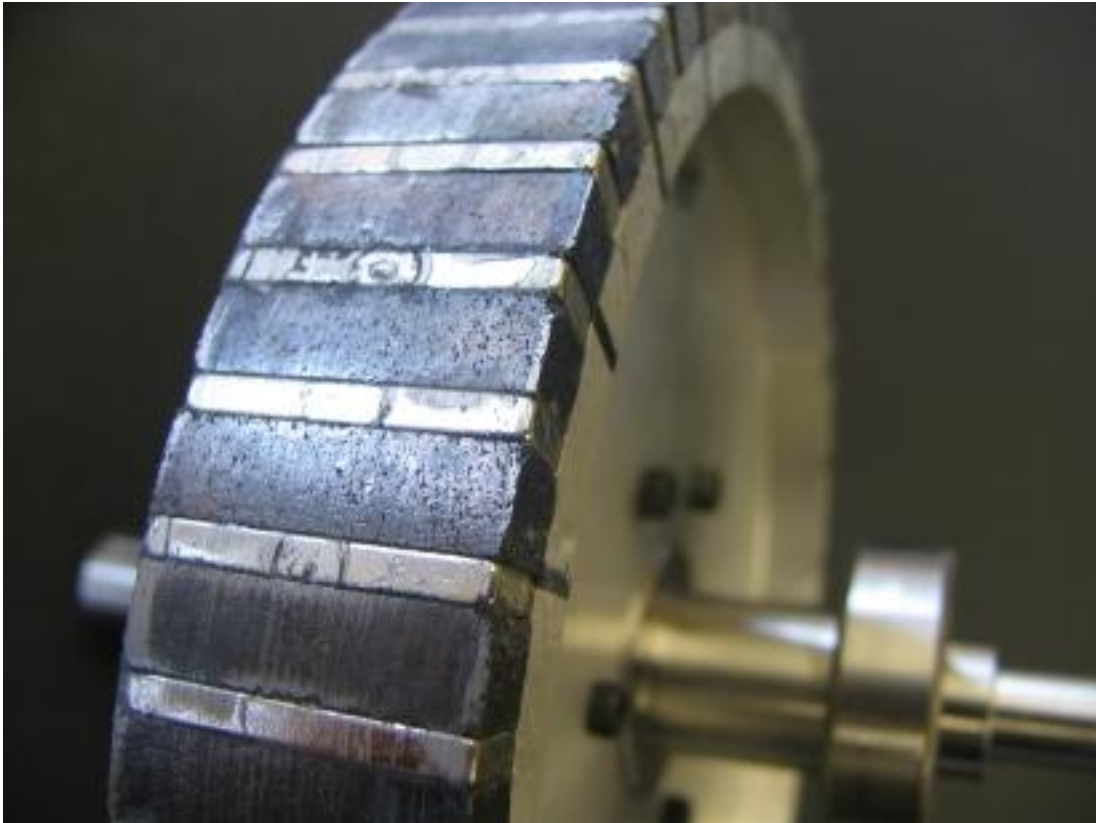


**Figure 3-15 Close up photograph of the finished rotor before assembly**

Once everything had set, the assembled rotor mount was then bolted onto the shaft. Excess glue was removed with emery paper and the mount was clocked for centricity on a lathe. Most parts of the rotor were found to be within  $\pm 0.05\text{mm}$  of the specified radial dimensions. Three locations where the SMC blocks were slightly outside this tolerance were identified. These were turned down on the lathe, to match the aforementioned tolerance. One of these points can be seen after turning in the second from the bottom SMC wedge in Figure 3-15, which shows the finished rotor on the shaft.

### **3.5.3 Final Assembly**

The rotor and stator ready for assembly are shown in Figure 3-16. The shaft with the rotor, bearings and end cap mounted on it was held in the jaw of a milling machine. This end cap was the one which housed the pre-load spring which was compressed before assembly. The stator parts assembled in the outer housing ring were held on the bed plate. This allowed the

two parts to be aligned and then slowly moved together. The shaft was long enough so that the bearing engaged the housing before the end of the magnets started to enter the stator. This meant that the shaft was not subjected to a high force while only supported from one end.

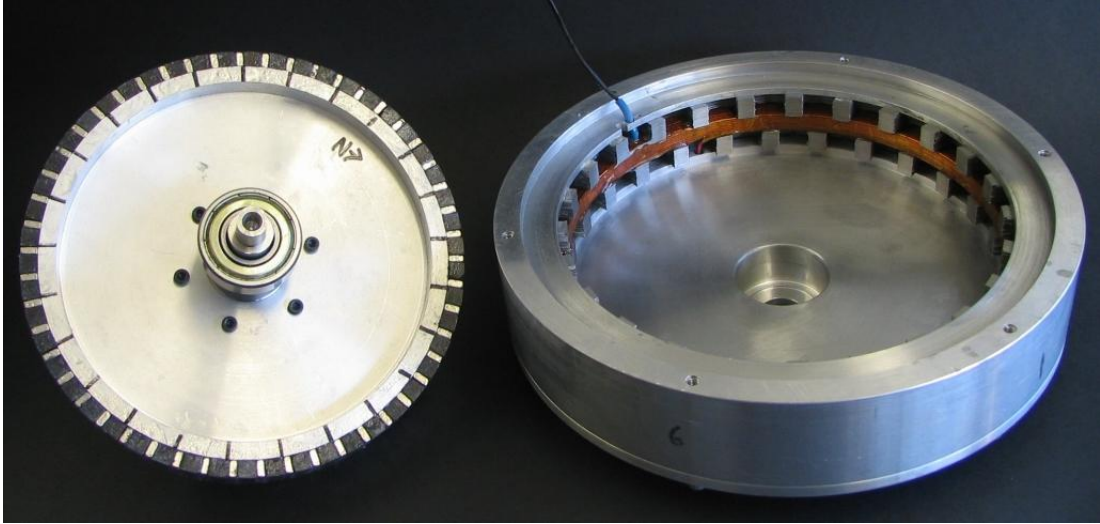


**Figure 3-16 Rotor and Stator ready for assembly**

## **Chapter 4. Testing and Comparison with Calculations for the Material Hybrid Prototype**

This chapter discusses the testing of the machine using a mix of laminations and SMC for the stator and compares the test results with the design and subsequent calculations. The design and construction of this machine has been presented and discussed in chapters 2 and 3. The tests are limited to static situations mostly because the running torque is pulsing in nature (this being a single phase) which causes excessive vibration. In the first test dc current is applied and the average temperature of the winding is measured using the rate of change of resistance with temperature. This allows an indication of the thermal limit for the current. The second test once more applies dc current at various levels and the rotor is moved to various chosen angles and the torque is measured using an in-line torque transducer. This can be directly compared to values predicted using FE. As will be shown a sizeable difference between torque measurement and the original design calculation is present and hence some retrospective FE work to explain this is also discussed. Finally a value for power factor at a “rated” operating point is presented.

### **4.1 Thermal Testing**

It is usually the ability of the machine to dissipate heat that limits the maximum torque capability of most machines. There are also electromagnetic limits formed by issues such as magnetic saturation, magnet demagnetisation and insulation breakdown but they usually fall outside of the thermal limit. The resistive loss due to current in the winding is a major source of heat in this machine and is equal to the product of the resistance and the square of the current passing through it. By measuring the machine’s ability to dissipate the resistive loss as heat to the surrounding air of the casing, a thermally limited current can be found, beyond which the winding insulation is under too much thermal stress. When the machine is running iron losses are significant. These losses are proportional partly to speed and partly to speed squared. However the weakest link in the machine’s thermal withstand is the winding insulation and the winding temperature tends to be dominated by the winding’s ohmic losses.

The winding is the source of the heat and the majority of the heat flow to the air surrounding the motor is via the sides of the coil in contact with the laminations and then through the SMC core-back. From this arrangement it is a reasonable assumption that the hottest part of the machine will be in a central section of the winding. The coil’s thermal limit is governed by the enamel (usually polyimide) insulation coating of the wire, which degrades thermally at an unacceptable rate if the temperature is greater than 150°C. As there is no application specification for this machine, a typical design rule is adopted which allows a 100°C rise in

the average temperature of the winding above ambient. The following section gives details of experimental calculation of the current which will result in such a rise.

To ensure that the heat dissipation is solely due to convection from the surface of the machine casing into the surrounding air, the motor was placed on a wooden surface (relatively low thermal conductivity) so that it rested on the corner of the casing and the shaft providing minimal contact and a poor thermal conductive path to the table. The test area was situated in a large laboratory and care was taken to make sure that large air circulation from windows and fan heating systems was not present and hence did not result in significant fluctuations of the ambient temperature or extra cooling flow other than the natural convection. Also, the motor was not enclosed in any way to avoid the heat dissipated raising the ambient air temperature. The thermal mass of the motor meant that the thermal time constant is measured in hours. To account for any small long term changes in the ambient temperature during the test, a thermocouple was used to record the temperature of a metal block near the motor. The thermal mass of this block allowed the readings to be used as a control and filter out any thermal noise, such as air movement from human activity in the area.

The winding of the motor was fed with a constant direct current (DC) of 5.5Amps and the voltage and current values were recorded every 15 seconds for the duration of the experiment. Using Ohm's law, the value of resistance for the winding can be calculated. The resistance is proportional to the temperature of the coil by the relationship of the thermal coefficient of resistance, which for enamelled copper wire is  $3.9 \times 10^{-3} \Omega/^{\circ}\text{C}$  at around  $20^{\circ}\text{C}$ . Using this value in equation (4-1) the average change in temperature in the winding was calculated from the change in resistance between measurements. The winding temperature changes exponentially with time. There are several major components in the motor and each has its own thermal time constant. A common simplified model is to assume that there are only two time constants: one short term that is essentially the winding and a far longer time constant that relates to the core and frame. The simplified thermal time constant model is shown in equation (4-2), where the subscript **w** relates to the "winding" and **c** relates to the "core and frame" elements of the temperature rise

$$\Delta T = \frac{1}{\alpha} \left( \frac{R}{R_o} - 1 \right) \quad (4-1)$$

$$T = T_w \left( 1 - e^{-\frac{t}{\tau_w}} \right) + T_c \left( 1 - e^{-\frac{t}{\tau_c}} \right) \quad (4-2)$$

The results for this test, which ran over a period of 5½ hours, are graphed in Figure 4-1. The solid blue line shows the rise in temperature derived from the resistance measurements. It can be seen that, while close, the system did not reach thermal equilibrium.

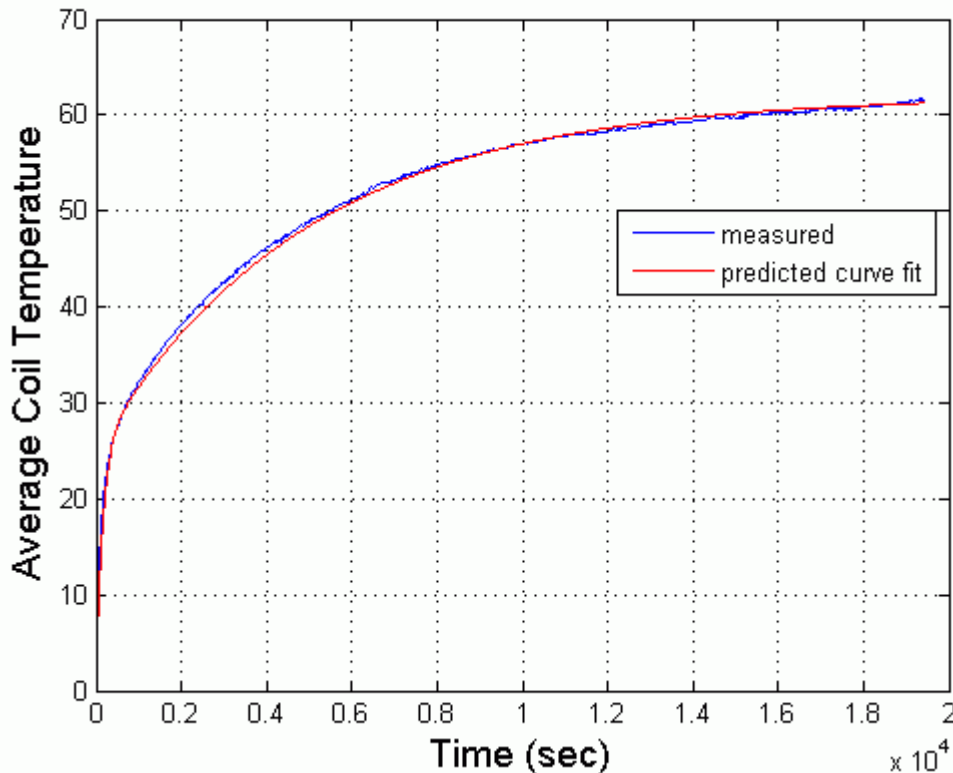


**Figure 4-1 Graph showing rise in coil temperature for 5.5A**

The red line in Figure 4-1 was predicted using equation (4-2) and represents the two (assumed) thermal masses within the system using the following values,  $T_w=25^\circ\text{C}$ ,  $\tau_w=150\text{s}$ ,  $T_c=37^\circ\text{C}$ ,  $\tau_c=5000\text{s}$ . It can be seen that the fit to the measured curve is quite good. The summation of the two temperature rises gives the final predicted steady state temperature to be  $62^\circ\text{C}$ .

In terms of operating current, the above thermal data (Figure 4-1) can be used to predict the rated current of the machine, neglecting other forms of thermal loss. Taking a  $100^\circ\text{C}$  rise in the winding as representing the (static) thermal limit. The average power loss in the coil is proportional to the square of the average current passing through it, equation (4-3). So by comparison with the  $62^\circ\text{C}$  rise for 5.53amps measured, the thermal rated current is  $I_r =$

7amps, as calculated in equation (4-4). The resistance of the winding at room temperature was 1.87 ohms, meaning that the motor is capable of dissipating 91.6W of winding loss for a 100°C rise in the average temperature of the winding.

$$P_{resistive} = I^2 R \quad (4-3)$$

$$I_r = 5.53 \times \sqrt{\frac{100}{62}} = 7 \text{ amps} \quad (4-4)$$

## 4.2 Static Torque Measurements

### 4.2.1 Rig set-up

To allow static torques to be measured, the prototype was mounted onto a bed plate with the shaft coupled to a torque transducer. The other end of the torque transducer shaft was coupled to a rotary table to allow the rotor angle to be controlled. A schematic of the set-up is shown below in Figure 4-2.

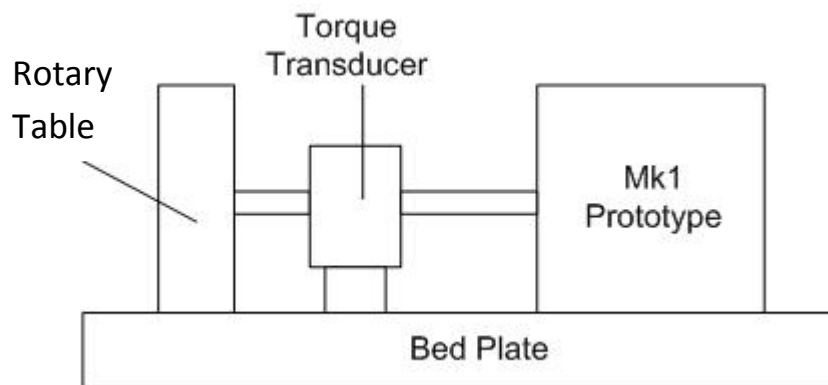


Figure 4-2 Schematic drawing of the torque measuring setup

### 4.2.2 Cogging Torque

The term 'cogging torque' refers to any torque which is due solely to rotor magnet flux and its interaction with the stator at different rotational alignments. A graph showing the results over 72 mechanical degrees (which is equivalent to 10 pole pitches of the fifty pole machine) is shown in Figure 4-3 and in more detail for one half of an electrical cycle in Fig. 4.4. The data in the graph is a sample from a full rotation of measured cogging torque. Only a fifth of the total results are shown to give clarity of details with respect to rotor angle. The small angle spanned by one pole pitch, 7.2 mechanical degrees, means that to get a reasonable resolution of measured results, the ability to move and control small changes of rotor position is required. The rotary table (Figure 4-1) had a built in vernier that allowed measurement

down to a sixth of a degree. However, it was noted that backlash in the mechanism of the rotary table allowed a third of a degree of uncontrolled movement. This resulted in the dividing head moving (within the backlash) as the magnitude of the cogging torque changed with position, resulting in abnormalities in the results such as the uncharacteristic change shown around 120 degrees in Figure 4-4.

The first point to note about the cogging is that there are no significant effects at sub pole frequency. The lack of these types of effect means that the machine is rather similar pole to pole and hence that the rotor and stator are closely round. Given the construction of the stator and rotor this is a pleasing result. There are two clear features of the cogging torque visible in Figure 4-3; it oscillates at four times the electrical frequency of the machine (one electrical period =  $14.4^\circ$  mechanical = two pole pitches), and there are two distinctive peaks in the cogging waveform which are not alternate, but create a waveform that repeats every  $7.2^\circ$  mechanical (one pole pitch). This effect was expected and is evident in the cogging torque measurements of the machine incorporating a flux concentrated rotor of similar design built by Maddison [24, 31].

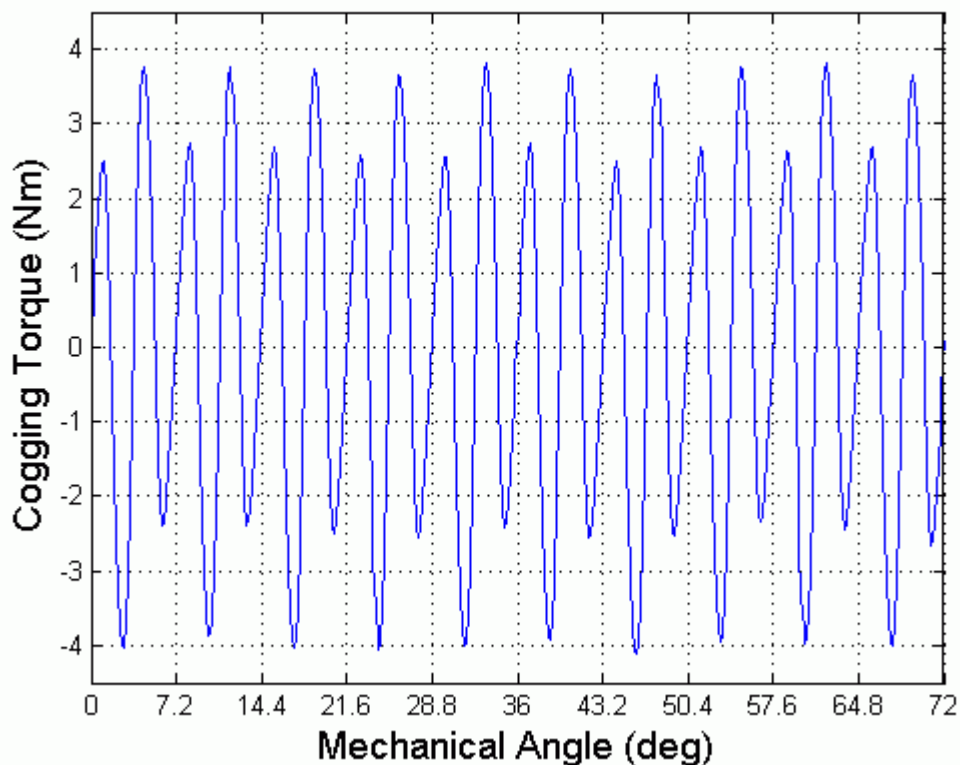
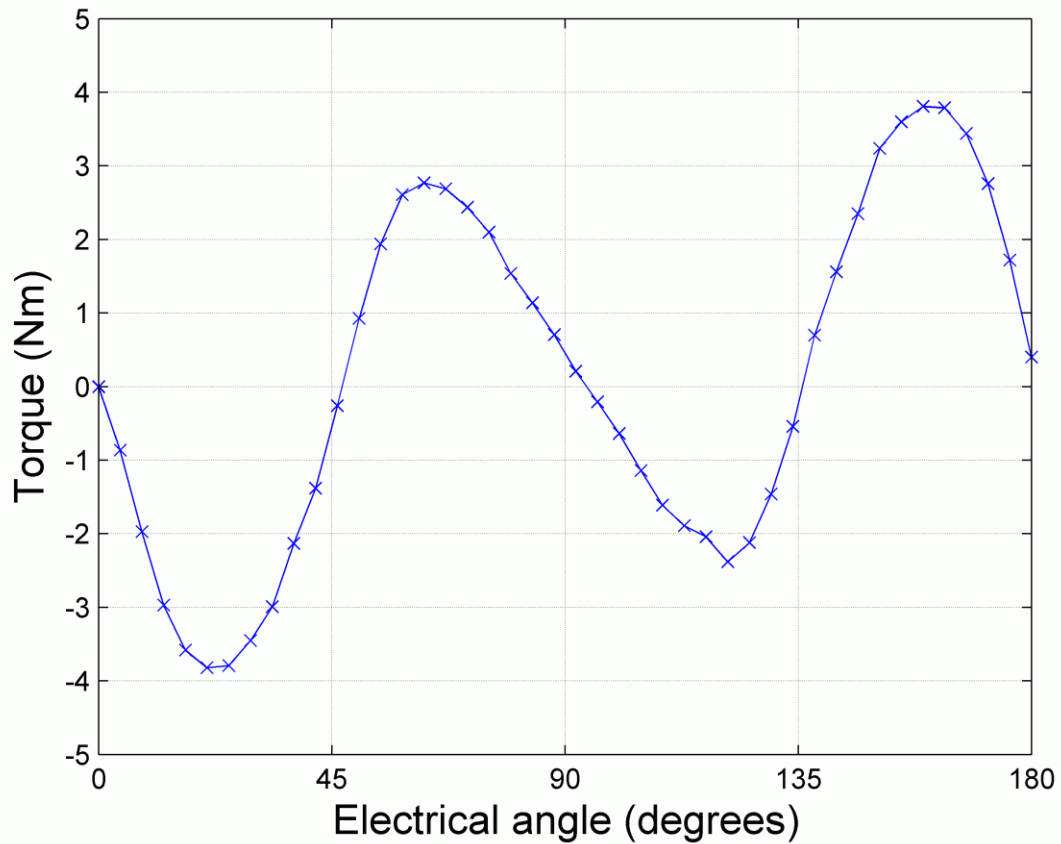


Figure 4-3 Graph showing cogging torque measured over ten pole pitches



**Figure 4-4 Graph showing cogging torque over one pole pitch, measured from prototype [note that the angle shown here is electrical degrees = mechanical degrees\*25].**

The cogging torque has a period half that of the fundamental torque but with a harmonic content resulting in a waveform that oscillates at four times the fundamental torque. This is a direct result of the magnetic structure of the rotor, created by the alternate arrangement of SMC and magnet material. The cogging torque is the result of two mechanisms superimposed together. The first relates to flux which traverses the core back which has its maximum at the aligned position, the second relates to flux which returns back to the magnet without flowing through the core back which has its maximum at the unaligned position. The following sections describe these two mechanisms individually and the consequent explanation of the resulting waveform.

### 4.2.3 Aligned Cogging Torque

This torque is a result of the difference in reluctance of the path the magnet sees in different rotor positions. In the aligned position the flux goes straight across (radial direction) the air-gap from the flux concentration SMC wedge to the stator tooth, flows around the stator core-back and back down an opposite tooth, across the air-gap again returning to the magnet

through the SMC wedge. Moving away from the aligned position, the air-gap surface area of alignment between the stator teeth and the rotor SMC reduces, increasing the reluctance of the path across the air-gap. In Figure 4-5, the rotor has moved  $0.8^\circ$  mechanical in the clockwise direction from the aligned position and this relates to the first peak of the reluctance torque in Figure 4-4. The torque at this point is negative, showing that the rotor wants to move in an anticlockwise direction, back to the aligned minimum reluctance position. In the final peak of Figure 4-4, the situation is identical to that shown in Figure 4-5, with the exception that the alignment has the rotor advanced  $5.6^\circ$  mechanical so the torque is positive, trying to pull the rotor forward to the next aligned position. This mechanism results in a cogging torque period of half the fundamental torque with peaks in torque between the aligned and unaligned positions, a stable zero torque at the aligned position and an unstable zero at the unaligned position.

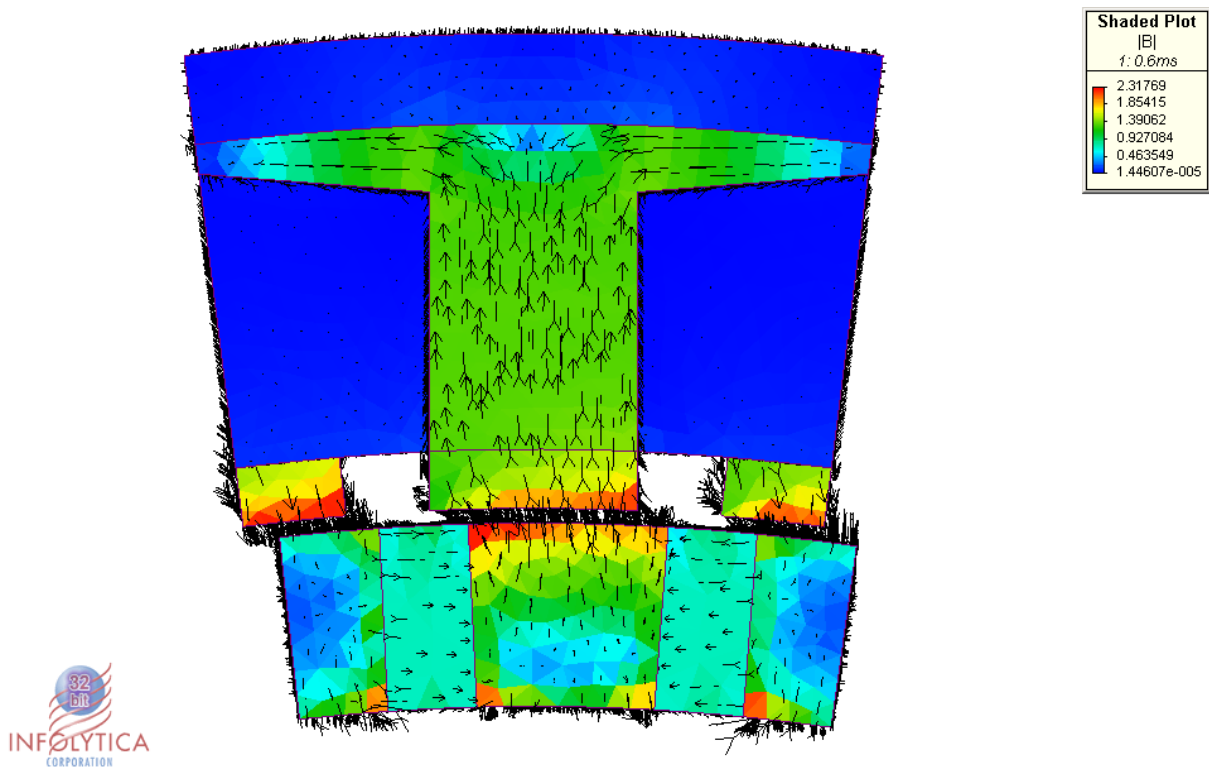


Figure 4-5 FE flux density plot at a position of peak (negative) aligned cogging torque

#### 4.2.4 Unaligned Cogging Torque

As the rotor moves from the aligned to the unaligned position, the centre line of the magnet moves towards the centre line of the stator tooth. As this happens, the flux starts to take a path that does not pass around the stator as in the aligned position, but instead uses the stator tooth to traverse the width of the magnet and back to the opposite side of the magnet. This flux is maximised when the magnet centre line coincides with the tooth centre line i.e. the unaligned position. A movement away from this position will thus produce a component

of force from this mechanism which attempts to align the rotor with the unaligned position. This can be seen in the flux density plot in Figure 4-6, (which relates to the second peak of torque in Figure 4-4). Here the torque is positive and tries to drive the rotor forward so the magnet sits centrally with the stator tooth i.e. in the unaligned position.

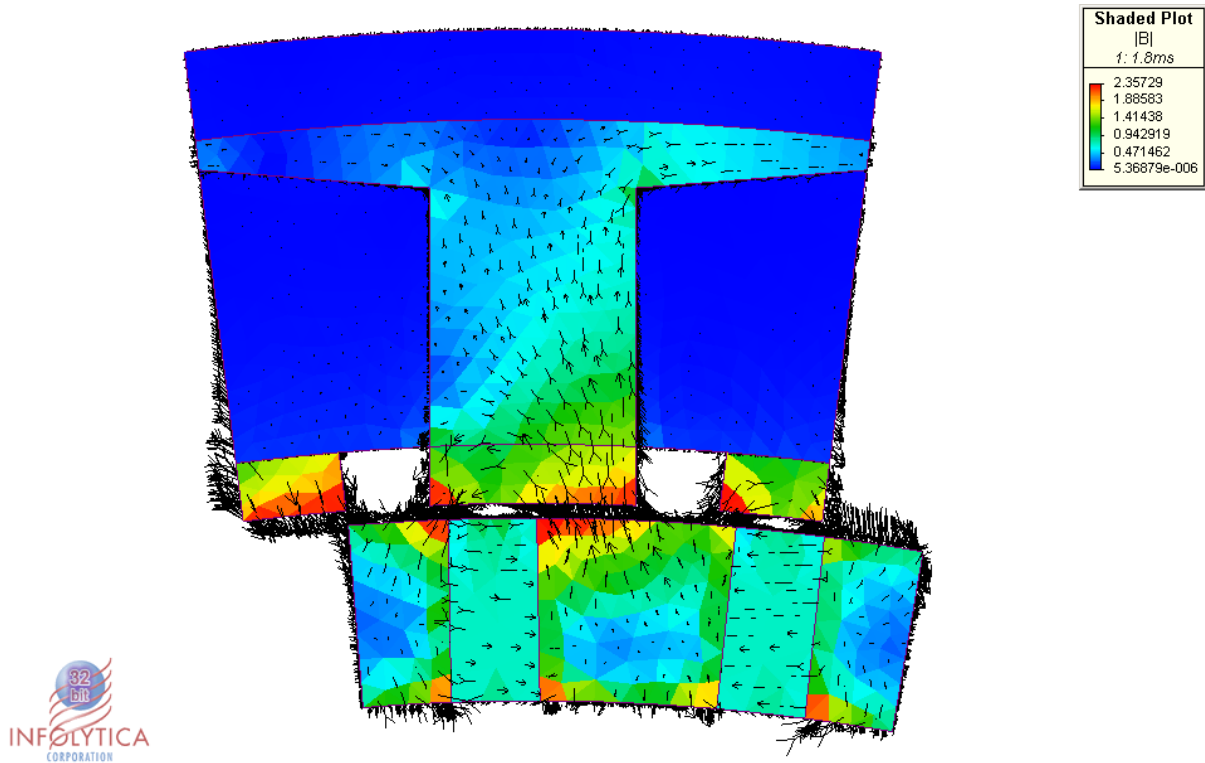


Figure 4-6 FE flux density plot at a position of peak (positive) unaligned cogging torque

#### 4.2.5 Combined Aligned and Unaligned Cogging Torque Effects

In order to try to help an explanation of the summation of the two effects described in the previous two sections the FE model of the machine has been simplified by making all the iron sections have a fixed permeability. The permeability of the stator core can then be reduced to more or less remove the flux which traverses magnet to magnet via the core back and hence to remove the aligned cogging torque effect. From these results the magnetic co-energy is plotted in Figure 4-7 for three cases. Considering first the case with the core back removed (i.e. the relative permeability is set to 1), it can be seen that the co-energy shows a single maximum at the unaligned position where the flux is best able to cross and then re-cross the air gap back to magnet. The resulting force (which is the differential of the co-energy with position) will have a full cycle in 180deg electrical (i.e. is a second harmonic in relation to the torque from the interaction between the magnet and the coil current). The second two cases have a core with a high permeability (a relative permeability of 1000 is greater than the unsaturated value for SMC) and a more realistic (partially saturated) value of 200 for the relative permeability. Now for both these cases the largest co-energy occurs in

the aligned position when the flux traversing the core back is a maximum. This is a higher value than occurs in the unaligned position because in that latter position the magnets occupy a significant part of the width of the teeth and hence cut down on the width of the available air-gap. In between the aligned and unaligned positions there are local minima where the flux traversing the core back builds up more slowly than the rate the flux returning to the magnet via just the tooth falls. The net result of the double peak is that the resultant cogging has two stable positions, one in the aligned the other in the unaligned position and the basic shape is at four times the spatial frequency of that of the torque of interaction.

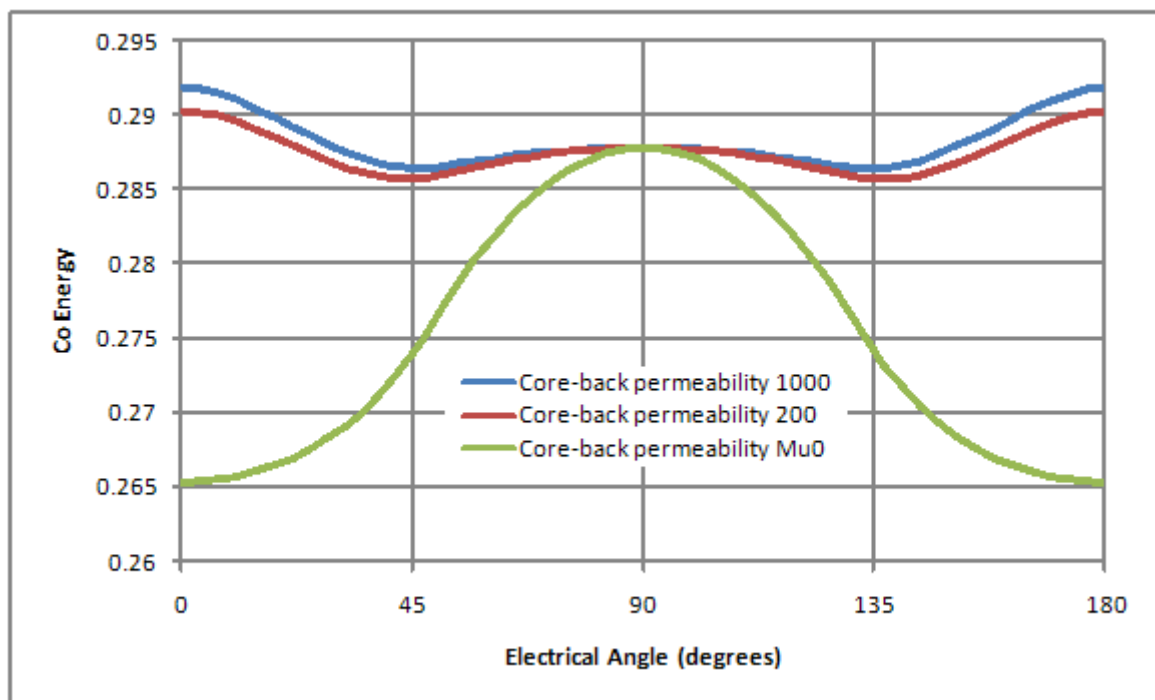


Figure 4-7 Co-Energy against position for the linear model

#### 4.2.6 Retrospective FE investigation of Construction Issues

This section might seem out of order as it appears before the measured torques with current applied are presented. However, it seems appropriate to tackle some of the construction issues found first to help appreciation of the meaning of the measurements. As will be clear from the measurements of the torque when current is applied the mean torque actually measured from the prototype machine is only 84.3% of the predicted value from the ANSYS FE model. To try and ascertain the reason for this difference, retrospective simulation of the prototype machine was performed using INFOLYTICA's MAGNET [53], an electromagnetic specific FE software package that became available after the finalisation of the prototype design using ANSYS. The advancement in computer processing power coupled with the suitability of the MAGNET software in modelling electrical machines allowed a two pole pitch model with even periodic boundary conditions to be simulated. This has an advantage over

the single pole pitch model developed in ANSYS with which the design was developed, as it allows the modelling of intermittent points between the aligned and unaligned positions of the rotor. From this model, torque profiles can be generated, greatly increasing the ability to probe the design to try and account for the differences in simulated and measured data.

The first MAGNET simulation used the same dimensions as the ANSYS model; this included the amount of surrounding air that was modelled, but obviously spanning two pole pitches. The mesh densities in the active parts were the same or finer than in the ANSYS model. However, the element count was preserved at a reasonable level, despite the increase in size, by grading the element size in surrounding air such that it increased along with the distance from an active part.

The MAGNET model gave a torque profile with respect to rotor position. The measured torque is plotted with the calculated over one pole pitch for a DC current of 6amps in the stator in Figure 4-8, along with the mean value of this profile, which is then analogous to the average torque calculated from the ANSYS FE based on D-axis flux with square wave excitation. Comparison of the mean torque with 6 amps, Figure 4-8, reveals that the MAGNET results predict a mean torque of 18.7Nm, which is 8.7% more than the 17.2Nm ANSYS predicted. What is more important to note in this result is that both are substantially greater (29.0% and 18.6% respectively) than the mean torque of 14.5Nm measured from the prototype with 6amps DC armature excitation.

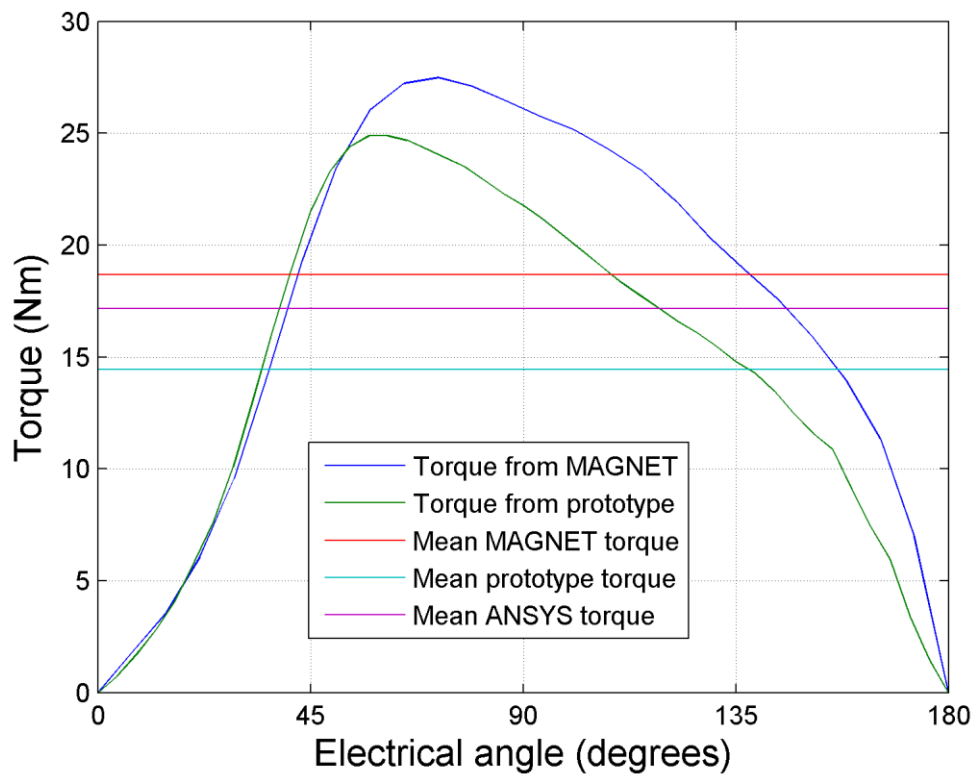


**Figure 4-8 Comparison of measured and simulated torque at 6 amps**

As both FE models largely over-predicted the torque, an apparent difference exists between the model and the actual prototype. The construction method of the prototype means that gaps between components are likely to occur and may be significant in comparison to the air-gap between the rotor and stator and these gaps are likely to reduce performance in the same way as the measured versus simulated results are indicating. The rotor assembly involving 100 small pieces being assembled onto a hub with a diameter several orders of magnitude larger than the individual pieces is bound to present an accumulated tolerance problem. This effect is magnified by the need to assemble the SMC and magnets in two separate stages, resulting in air-gaps between the SMC poles and magnets of the same order of magnitude as the active air-gap between rotor and stator. In the stator, the sintering process of the SMC core-back arcs resulted in some deformation specifically affecting the concentric tolerance of the outer and inner radius. Although the outer diameter of the lamination rings were machined to be a good sliding fit with the SMC core-back, the lack of concentricity could not be accounted for, resulting in air-gaps at intermittent points between the two.

Noting that the probable cause of difference in the torque results is related to the magnetic circuit, a study of the cogging torque, which is a sensitive measure of the magnetic circuit, was performed to quantify the effect of the size of the air-gaps between the core back and

teeth sections in the stator and between the SMC pole pieces and magnets in the rotor. In the original ANSYS model and the subsequent first MAGNET model, no account for construction air-gaps was made and boundaries between adjoining active parts were modelled as a perfect fit. The ANSYS model did not facilitate the modelling of the cogging torque profile. However, comparison of the MAGNET predicted cogging torque and that actually measured on the machine is presented in Figure 4-9. Differences between the two profiles can be clearly observed, with the actual machine showing a similar order of magnitude for both the aligned and unaligned components of the cogging torque. However, the FE predicts that the aligned component is much higher than the measured value, while the peak unaligned component is lower than that measured.

Considering first the introduction of a 0.1mm air-gap (in the radial direction) between the stator lamination and the SMC core-back and modelled in the MAGNET software. The result, plotted in Figure 4-9, shows that this increases the peak unaligned reluctance torque (the peaks either side of 90 and 270 deg) to about three times that modelled with no gaps. At the same time it reduces the peak aligned reluctance component by about a sixth. This is as expected from the simple linear material calculations shown in Figure 4-7. If the flux path through the core back is impaired the variation in co-energy about the unaligned position is increased (consider the change from a core back relative permeability of 1000 through a value of 200 to a value of 1). It is clear that the cogging torque near the unaligned position is modelled quite well by the introduction of this gap but the aligned cogging effect is less well matched.

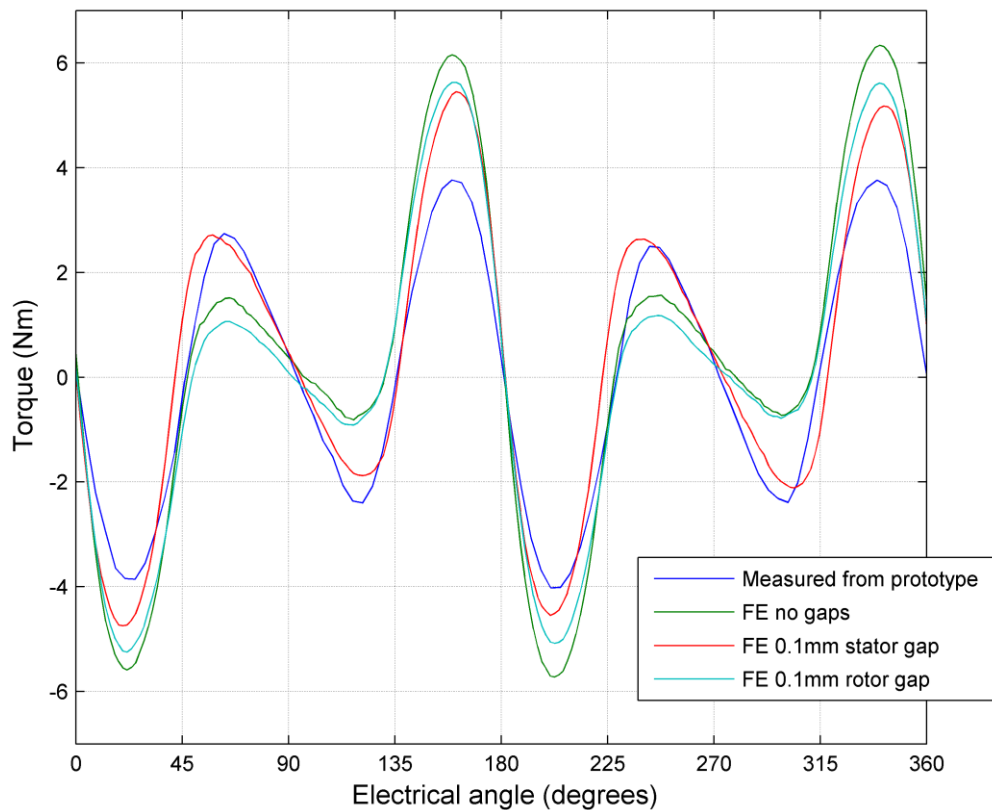


**Figure 4-9 FE cogging torque showing effects of construction air-gaps**

The introduction of a 0.1mm air-gap (circumferential direction), between all the magnets and SMC wedges in the rotor results in only a small reduction in all peak cogging torques compared to a model with no gaps.

Individually, neither of the air-gaps account for the cogging profile of the actual machine, although it is known from the construction that both exist, leading to the question what happens if the two effects are combined? A very coarse study found that a 0.2mm air-gap between the stator laminations and the SMC core-back, coupled with a 0.1mm air-gap between all magnets and SMC wedges in the rotor gave quite a good correlation between simulated and measured results. This is shown in Figure 4-10 and as can be seen the correlation is reasonable. This combination of gaps is carried forward to the comparison with measured results across a range of currents in the next section. The major differences now are more related to the position of the peaks rather than their size. This may be due simply to measurement error or it could be caused by the tolerance in the angular placement of the stator teeth section in the prototype.

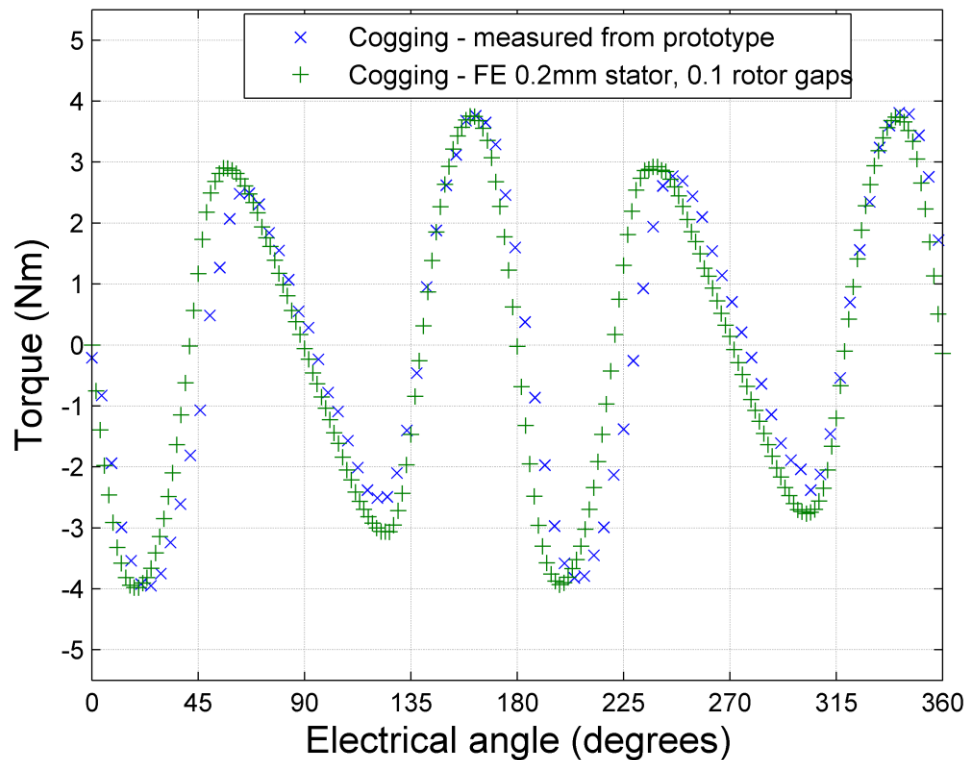


**Figure 4-10 Measured cogging compared to simulated with a 0.2mm stator core/teeth gap and 0.1mm rotor pole/magnet gap**

#### 4.2.7 Armature excited torques

The torque profiles in this section are measured, as with the cogging torque in the previous section, using the rig described in 4.2.1. The data was measured as a series of tests, each one relating to a different DC current excitation of the armature winding. Each test was performed over the same pole pair to give a comparison at different levels of excitation. The measurements were taken in both directions so that any hysteresis in the system (mechanical or magnetic) could be seen. In practice the hysteresis in the measurements was about 0.8Nm and quite constant with position and current. Some of this will be stiction in the bearing system and the rest is the drag torque that comes from magnetic hysteresis (particularly in parts of the machine using SMC which has a rather high hysteresis loss). There is no method by which the magnetic and mechanical drag torques can be separated and so no attempt is made to analyse the drag torque further. All torque results therefore show the average of the forward and backward torques. Another effect in the measurements is an overall offset in the torque results. This has been removed in the results shown by averaging the torque over one complete revolution and using this to remove the offset. The results processed in this way are shown graphed in Figure 4-11. The two pole pitch span,

coupled with the DC excitation, leads to the torque being negative over the first pole and positive over the second (taking as a convention that torque in the positive direction of the angle is considered as positive), according to the change in polarity of the rotor flux alignment with the stator MMF.

The results in Figure 4-11 show an asymmetric torque profile. This is due to the cogging torque, combined with the torque of interaction with the armature current. As can be seen the agreement between the measured data and the calculated data is quite good across all angles and current. It should be remembered that the calculated data uses the gaps between teeth and core back (0.2mm) in the stator and magnets and SMC pieces in the rotor (0.1mm) derived earlier. The differences are mostly between the phase of the waveforms rather than peak values in much the same way as the differences found in the cogging only results. In considering this problem it is useful to examine the results at 180deg. This is an aligned position at which all torques should be zero. The finite element results obey this rule but the measured results show a rather random spread perhaps by about 5deg electrical. This is a clear indication that the measured angle is only accurate to that level. As mentioned earlier the likeliest source of this error is the backlash in the rotary table which is used to set the angle. In the tests the backlash tended to be taken up with a sudden “clunk” as the torque reversed in direction. Perhaps this can be observed in the measured results with the measured torque tending to have a different phase on either side of a torque reversal.

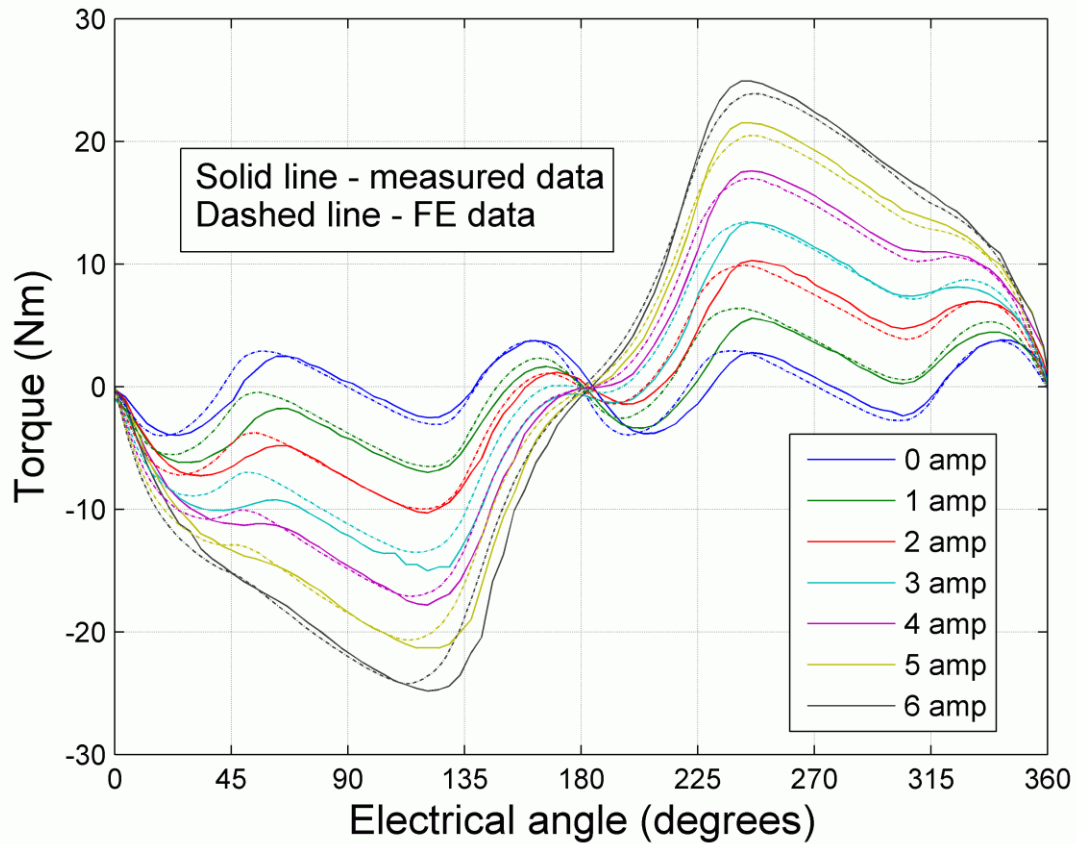


Figure 4-11 Static torques for a range of stator currents measured from prototype and MAGNET FE analysis

#### 4.2.8 Average torque

The average torque comparison has already been mentioned in a previous section; this section gives more detail on the resulting values and a discussion around them. The initial 3D FE modelling for this design was performed using ANSYS and did not have a readily available method for modelling multi rotor positions. So the results were a prediction of average torques from a co-energy calculation using the extreme limits of the magnets aligned in the plus and minus D-axis.

The ANSYS model predicted an average torque of 17.17Nm at 6 amps which is 16.3% above the actual measured average torque of 14.77Nm. The MAGNET FE model, with refinement to include the effects of extra air-gaps on the cogging torque (0.2mm between core back and teeth in the stator and 0,1mm between the magnets and SMC pieces in the rotor – the “gapped “ model), predicts the average torque at 6 amps to be 14.68Nm which is within one percent of the measured value.

Using the “gapped” model the computed average torque against current is plotted in comparison with the average torque measured from the prototype in Figure 4-12. The two sets of results show a good comparison and the same trend. There are two results, at 1amp and 3amps that show a larger difference, these are probably erroneous points as the final values show a consistent growth of the torque and the predicted value is within 2% of these values.

This similarity of the simulated and measured results allows predicting the 7amp average torque from the FE which was not measured in the prototype due to a failure of the rotor, which will be discussed later in the thesis. From the FE the mean 7amp torque is 16.78Nm.

It is clear that these gaps between components are inevitable in a production machine – one could not envisage practical tolerances that would allow assembly without a gap of this sort of order. The reduction in torque due to gaps (16% or so in this machine) must therefore be considered as a design feature of this form of construction.

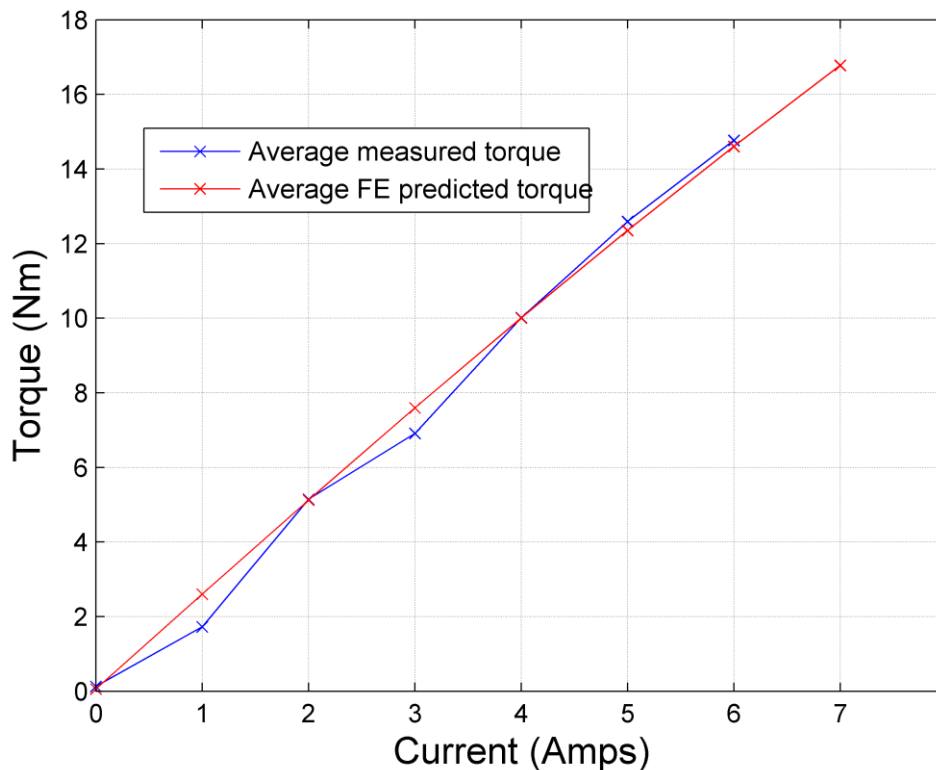


Figure 4-12 Comparison of measured average torque and that predicted from the MAGNET model over a range of armature currents

### 4.3 Torque per unit mass

The maximum average torque a machine produces does not facilitate a good means of comparison with the other machines. The torque per unit mass tells how well the machine

utilises the active components of the machine and becomes a more accurate way to compare machines with similar dimensions and cooling systems.

Table 4 lists the masses of different active parts of the prototype and the total mass of the active components, which is 1.6Kg. For the average torque with 6 amps armature current (which was the maximum current for which torque measurements were made), the torque per unit mass is 9.23Nm/kg but the thermal limited armature current of the machine is actually 7 amps. Using the predicted average torque at this value, the torque per unit mass is 10.49Nm/kg.

**Table 4 shows the masses of the different active components in the machine**

<b>Component</b>	<b>Mass (kg)</b>
Lamination steel	0.456
Core-back SMC	0.332
Winding copper	0.308
Rotor SMC	0.342
Magnet	0.166
<b>Total</b>	<b>1.604</b>

#### ***4.4 Inductance Measurements and Computed Power factor***

Due to the assembled structure of the rotor from SMC and Magnets, which have very different permeability values (assuming that the SMC is not saturating), the inductance with respect to angle relative to the stator might well be expected to display saliency. The inductance has been measured in the prototype by applying a 50Hz voltage to the winding, with the rotor stationary and measuring in-phase and reactive components using a power analyser. The applied voltage was chosen to be mid-range – large enough to avoid measuring mostly hysteretic effects and small enough to avoid saturation. The measured inductance with respect to rotor angle over one pole pitch is shown in Figure 4-13. The mean value of inductance is 19.7mH. While the exact alignment position within the assembled machine was not known, it is assumed from general understanding of electrical machines that the maxima coincide with the rotor in the unaligned position i.e. the quadrature axis. This

“inverse” saliency ( $L_q > L_d$ ) is as expected for buried magnet machines into which category this machine falls.

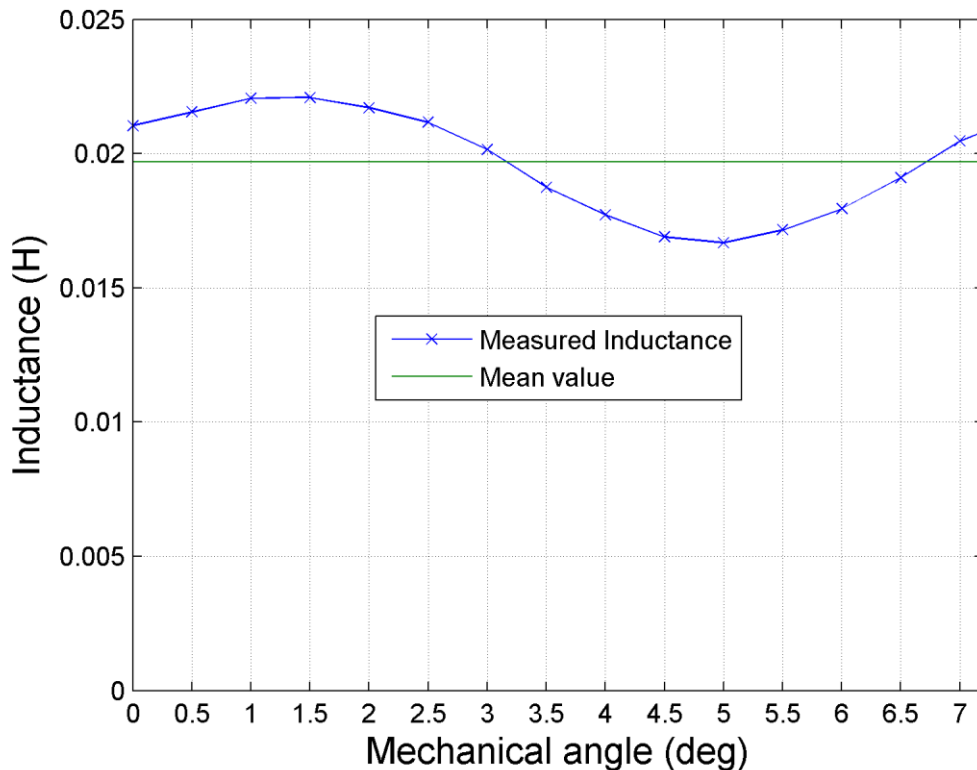


**Figure 4-13 Inductance measured over one pole pitch**

The power factor of the machine is very important as it heavily influences the volt-ampere rating of the power electronics needed for a converter for the machine. Figure 4-14 shows a phasor diagram for the machine for rated current operating with a supply voltage of 50Hz, which corresponds to a rotational speed of 120rpm. Here it has been assumed that the power electronics is operating with a control scheme that applies only q-axis current so it is in phase with the back EMF, producing maximum torque with rated current neglecting saliency effects. The back EMF value measured from the machine at 120rpm is shown in Figure 4-15. The resulting power factor angle (that between the supply voltage and current) is  $\phi=44.6\text{deg}$ . This results in a power factor of 0.71. This value means that the converter power electronics supplying the machine need to be VA rated to 141% that of the real power of the machine.

In a modulated machine with fifty poles and a torque density above 10Nm/kg when naturally cooled, a power factor of 0.71 is a good figure and probably reflects an advance on what has been achieved previously. However, in comparison to a conventional permanent magnet machine, where power factors of 0.9 and greater are common, this value is rather low. This is a well known attribute of modulated pole machines which is a natural result mostly of the

high electric loadings possible if the pole number is high and partially of the tortuous magnetic path necessary to produce the modulation of the flux from a single coil into a high pole number field. In this machine the stator teeth do not overlap at all; in contrast to the machines of Madison [24, 31] and Dickinson [8, 25] which used partial or full claws which helps to cut down on leakage flux. In addition the use of laminations for the teeth help to keep the reluctance of the main flux path down and hence maximise the ratio between leakage and main flux paths. More magnet flux means less armature MMF for the same torque and reduced leakage flux also leads to a lower reactance.

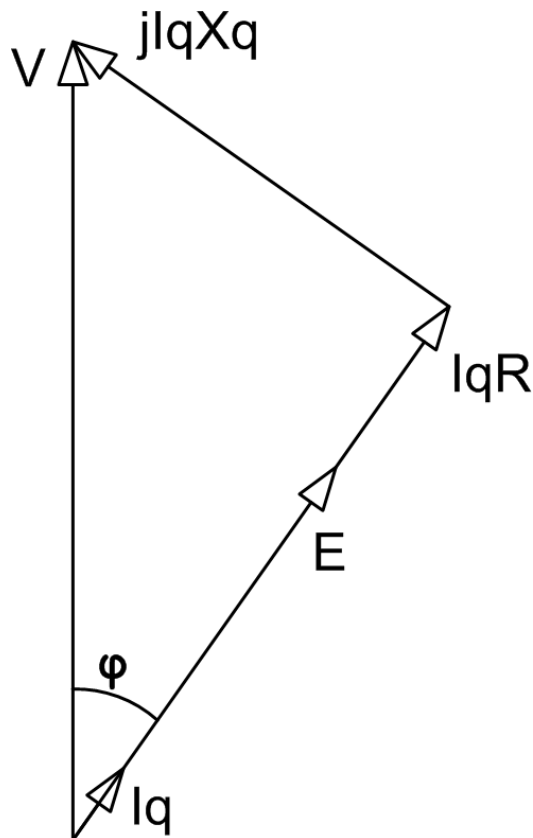


Figure 4-14 Phasor diagram showing maximum torque situation

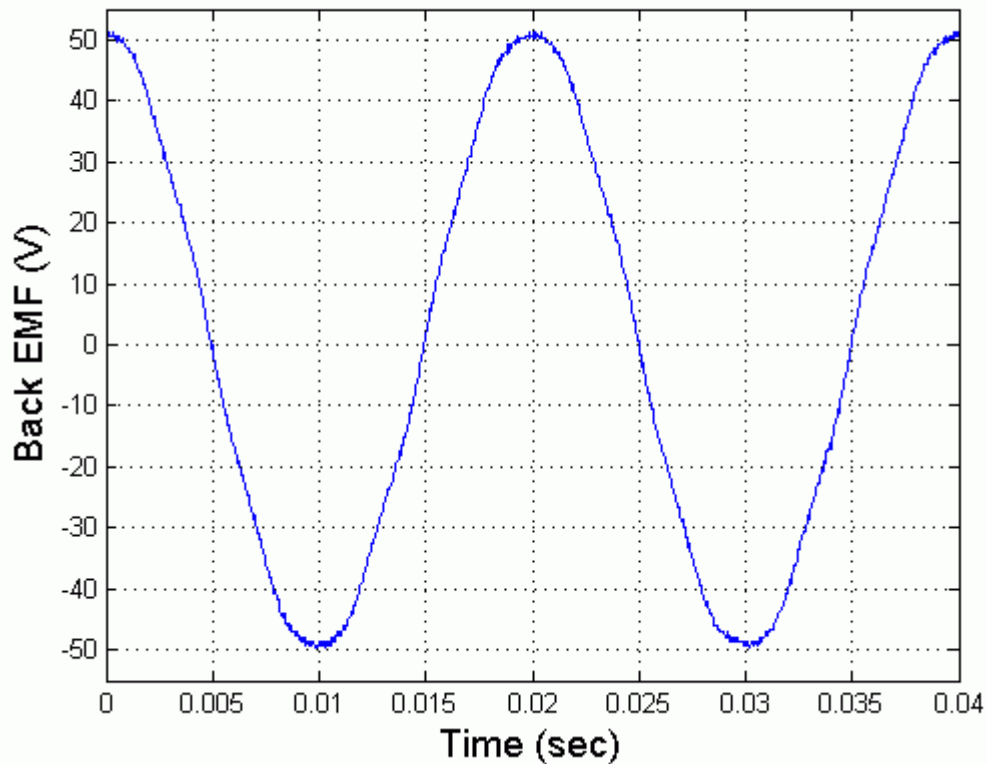


Figure 4-15 Back EMF measured results at 50Hz, 120rpm

#### 4.5 Rotor Failure

The first test to be performed on the prototype was the torque measurements, followed by the thermal measurement. The results from the thermal testing showed that the original torque measurements were not taken up to the thermally rated current, so the static torque measurements were repeated. During this test the rotor became wedged. Removal of an end-cap and the rotor from the stator revealed that a glue failure had allowed three sections of rotor, made up of multiple SMC pieces and magnets, to come away from the rotor mount and stick magnetically to the stator laminations. It is thought that the increase in temperature in the thermal testing softened the glue, allowing some movement and weakening of the joint to the rotor mount. When the static torque test was repeated, and the armature current approached the thermal limit, the resulting force fractured the remaining glue joint.

The broken sections were split into the individual components using a releasing agent and the rotor was reassembled, using the same techniques as the original construction. It was clear that there was a risk of further fractures. To prevent this problem in the future, a containing band was required for the rotor. Initially a thin stainless steel band was considered. The loss in this band was calculated and deemed to be an acceptable compromise. However, it would need to be 0.2mm thick to leave a sensible 0.3mm air-gap and would require being heat shrunk on to provide an interference fit such that it counteracted the magnetic forces. Such a thin loop would be infeasible as it would not have enough thermal mass to allow a heat shrink method of assembly. Instead, epoxy impregnated glass fibre tape was wound round the rotor under tension. The torque measurements were then successfully retaken.

## **Chapter 5. Development of the Formed Lamination Machine**

The Material Hybrid (MH) prototype discussed in the previous chapters had two undesirable features, both stemming from the material hybrid construction of the stator. These were the part count and air-gaps between the laminated stator teeth sections and the SMC core back. The part count is undesirable as it increases the cost of manufacture. The air-gaps resulting between the laminations and the SMC core-back were undesirable as they reduced the machines magnetic performance. In addition, the design of the machine was such that the SMC core-back thickness was limited by mechanical properties rather than magnetic saturation, resulting in a thicker core back than was necessary and a below optimum flux density.

This and the following two chapters will cover the development and construction of an alternative stator which addresses the problems of the MH prototype. To allow a fair comparison and to minimise the manufacture time, the new stator was designed to use the rotor of the MH prototype.

### ***5.1 The Approach***

Simplification of the stator construction could be achieved by reducing the part count. The material hybrid prototype consisted of thirteen parts, which were assembled to form the active stator. This figure did not include the winding or the twenty-two laminations, necessary to minimise eddy currents, which made up each of the lamination stacks. The reason for the high part count was the ten arcs making up the SMC core-back. By replacing the SMC core-back with a lamination bridge that is an extension of the two stator laminations stacks, the active part count could be reduced to three. This led to the following stator lamination designs and construction ideas.

### ***5.2 Design Development***

#### **5.2.1 Solid Core-back with projecting teeth**

If the stator of the constructed MH machine were to be cast from solid steel rather than laminations and SMC, the problem of consequent construction air-gaps is addressed, ignoring the resulting eddy current problems. This solid stator shape can be unfolded to form a 2D footprint, assuming for the moment that the axial thickness of the teeth and the radial thickness of core-back are the same. This requires the teeth of the stator to be bent outwards 90° to be axially aligned with the core back, and the result is a ring. Unrolling this ring would form a flat sheet with a footprint such as that represented in Figure 5-1 (which shows only three teeth of the stator - the rest can be imagined by repeating this pattern). The resulting

2D footprint is realisable as a lamination stack, with the stack direction into the page of Figure 5-1. A construction process to form the lamination stack into a machine would be as follows-

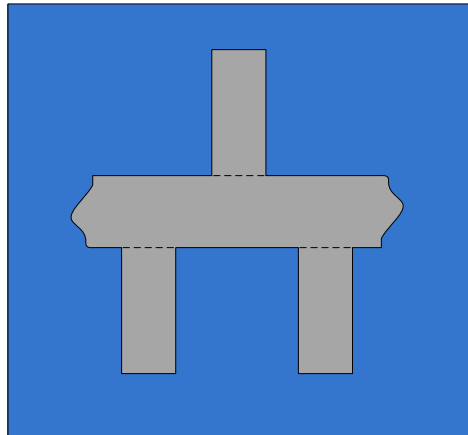


**Figure 5-1 Footprint of the material Hybrid unrolled.**

1. The strip would be rolled up to form a ring.
2. A pre-made toroidal coil would be inserted inside the ring.
3. The teeth would be bent round to encase the winding and form the final stator shape.

The resultant machine would be over-engineered electromagnetically in the core-back and require a high force to bend the teeth because the bend would have to extend into the core back section. This basic idea forms the starting point for a simpler construction method, which will be discussed in the subsequent sections.

The construction process discussed above will need to address material deformation and misalignment resulting from the bending of the material. To help understand the effects which cause this, it is a good idea to take a step back and consider the bends if the machine was not laminated, but constructed from a single solid piece. When a bend is formed, the material is be taken beyond its plastic limit resulting in deformation; the inner radius under compression and the outer radius under tension with a neutral axis centred between the two. This deformation would be more established in the right angle bends of the teeth, than in the gentler bend in the core-back as it forms the outer diameter of the machine. The deformation due to such a right angled bend can clearly be seen in the right-hand side of Figure 5-2, which is a trial tooth bend using aluminium bar.

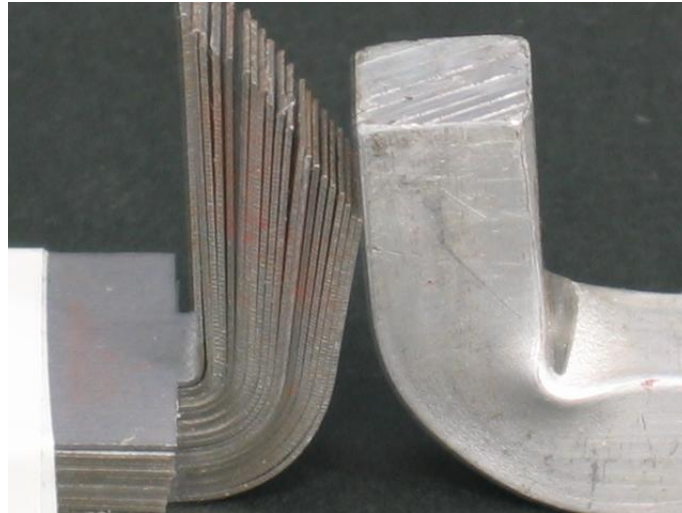


**Figure 5-2 A comparison of a bending solid bar and laminated stack**

Consider the same tooth bending process with the stator constructed from a stack of laminations. A test bend for such a case can be seen in the left of Figure 5-2 and shows clearly that there has been slip between adjacent laminations, resulting in an undesired tapered face at the tooth end. Even if a bond is formed between adjacent laminations prior to the bending process, it is very difficult to imagine any bond that would have a shear strength great enough for the steel to plastically deform enough to avoid this tapered end. From this it is clear that any bend in the laminations in their plane (as in the test bend in Figure 5-2) will always result in slip and staggering of the end faces.

Accepting that the slip will happen, the following two characteristics will result. Firstly, the resultant geometry will not be the same for each sheet. This is clearly visible in the test bend in Figure 5-2. The inner sheet of the bend was formed with a very small radius, whilst the outer sheets take a progressively larger radius and, because the material was not being stretched (i.e. succeeding laminations slipped with respect to each other) this longer path resulted in a tapered edge at the tooth tip. Secondly, that although the slip between laminations results in a different overall shape compared to the bend in the solid material, each individual lamination is deforming in the same way as the solid bar in Figure 5-2. However, the ratio of the width of the material in the plane of the bend to the thickness of a lamination across the bend means that the deformation is relatively small and is not clearly visible to the naked eye. At the same time, the increasing radius of the bend from one lamination to the next, moving outward, means that the deformation will be greatest on the inner lamination.

It is widely known that mechanical stress in laminations reduces magnetic performance, specifically increasing hysteresis and hence reducing magnetisation for a given applied field and increasing loss when subjected to an alternating magnetic field. This raises questions about the reduction in performance when these bent laminations are used in the main flux path of the machine. While at this stage, no figures exist to prove this either way, the slip in the bending process reduces the overall stress in the steel, which should assist in minimising the loss of magnetic performance due to bending stress.

### **5.2.1.1 Multiple individual laminations**

In the above example, the staggered end was a result of each lamination having a different bend radius, which was proportional to its position in the stack. By altering the length of the teeth of each lamination to account for their position in the stack, a core could be formed without the requirement for post assembly machining. In a replacement for the MH machine stator, twenty-three laminations, each one individual in design, would be needed. Unlike the laminations of the hybrid prototype, each individual lamination would be a separate part, resulting in a higher overall part count.

### **5.2.1.2 Single rolled up lamination**

To reduce the part count, the individual laminations of the above example could be combined into a single strip lamination, long enough to contain all the stator layers and features. The complete core could then be formed by spirally winding the lamination strip. The teeth could be bent (around the winding) or folded over after the spiral winding. This idea would require a very long strip to be punched and some very tight manufacturing tolerances regarding the dimensions of the lamination (which would be approximately 12.5m long). The spacing between adjacent teeth must be such that, as the lamination is wound up and the diameter increases, the teeth line up when viewed in the radial direction. The teeth would need to be of increasing axial length as the bend radius needed to form the tooth increases from the inside to the outside of the bend. This idea is probably impracticable due to the large length of the lamination.

## **5.2.2 Replace SMC arcs with lamination links**

Figure 5-3 shows an alternative for a laminated core. A saving in material could be made by linking the two sets of laminations that form the side of the stator with pole width pieces of lamination. Note that the two circumferential pieces are designed to be on the sides of the folded structure rather than in the core back section. The notches in these circumferential pieces are provided to allow the bend to form the circumference. The drawing is diagrammatic: in real life the bridges where the notches are would need to be very thin (as

will become obvious in the prototype described later in this chapter). A template of Figure 5-3 was produced in cardboard to help visualise the concept. This quickly highlighted the same problem as the above designs - due to the slip between layers in the bending process an increase in the joining link length was required as the stack layers increased. As the layers of the laminations stacked up, the length of the joining piece increased, therefore this idea would also require an individual lamination shape for each layer.

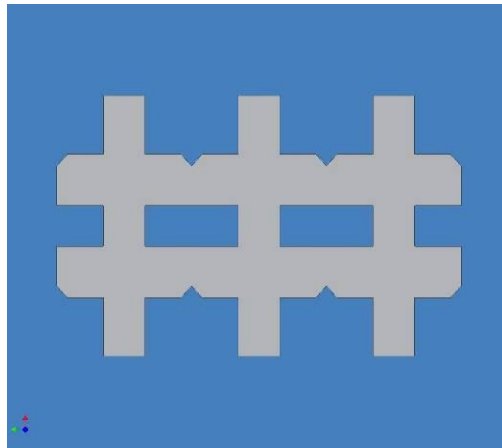
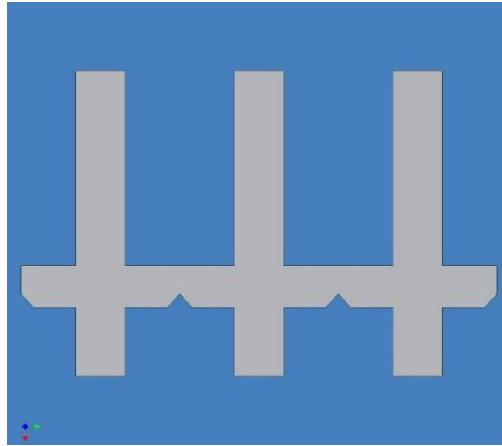


Figure 5-3 Second design small link

### 5.2.3 Overcoming the Increased Length Due to Bending

Lamination misalignment, resulting from slip between laminations in the bending process, is unavoidable. It is necessary to account for it rather than prevent it. A possible solution to the problem of differences in length due to the circumferential bend could be reached from the idea that the laminations need not be connected between the teeth on both axial sides of the stator. The connection is only there in the material hybrid prototype for construction purposes. The link gives rise to an undesired path for the flux - it was designed to be as thin as possible with the assumption being made that it would saturate and appear as air in the magnetic circuit. Omitting it completely would be considered an improvement. The design shown in Figure 5-4 is developed from the previous idea by removing the link between the teeth on one side. It is clear to that, as the layers build up in the stack, the teeth ends will taper as the bend (to form the “U” shape rather than to form the circumference) radius increases. If it is assumed that the starting length of the tooth to be bent over is great enough, the tooth will be formed with excess length, greatest on the inner layer, which could be machined away, at a later point in the assembly, to form the desired uniform air-gap. The bending to form the lamination stack into a ring would not result in a tapered joint, as the bend would be orthogonal to the stack direction (because in turn the bend is being made in the thin ligaments at the notches with the lamination in this region lying in a radial-

circumferential plane). This was a key feature that enabled a reduction in complexity for this design compared to previous ones.



**Figure 5-4 Lamination with one link removed**

#### **5.2.4 Introduction of Skew**

The ideas put forward in the previous sections would produce designs that have teeth, of opposite polarity (separated by the coil), that are in line when viewed from the axial direction. To use these designs would require a one pole pitch skew in the rotor poles – not easy to do! A target for the prototype using folded laminations was to use the original rotor. A side benefit is that this also permits a good design comparison with the material hybrid prototype.

It was recognised that the skew must be introduced into the folded lamination rather than the rotor. The first idea was to introduce it in the section that bends over the coil to form the core back, shown in Figure 5-5. This idea was flawed, as the length of the core back changes as the layers increase. Where the teeth were angled to produce the skew, they needed to be thicker as the flux would take the most direct route through the steel. As the layers increase, the point of the bends would change and the thicker section would move away from the second bend. To prevent the tooth formed by the bend having a staggered form in the circumferential direction, the bend would have to be made in the narrow part of the lamination, possibly causing a bottleneck electromagnetically.

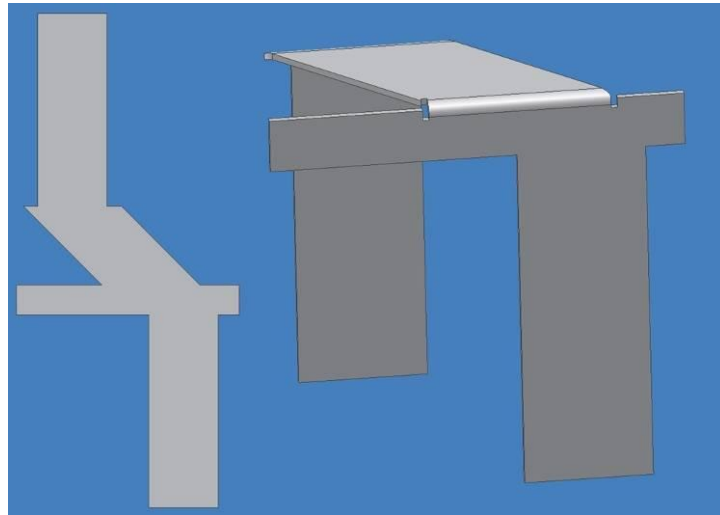


**Figure 5-5 Lamination with skew introduced in core back**

### **5.2.5 A Better Skew Position**

This idea moved the location of the skew, placing it in an area of the lamination that was not involved in the bending. By placing the skew in the teeth on the side that still had the link attached for construction, (as shown in Figure 5-6), the skew would only be affected by the bending of the lamination to form a ring, which would be the same for all the laminations as the bend would be orthogonal to the lamination stack direction. This would reduce the complexity of getting the alignment of parts correct during bending, allowing the focus to be on the methodology for bending the laminations, which is the topic of the next section.

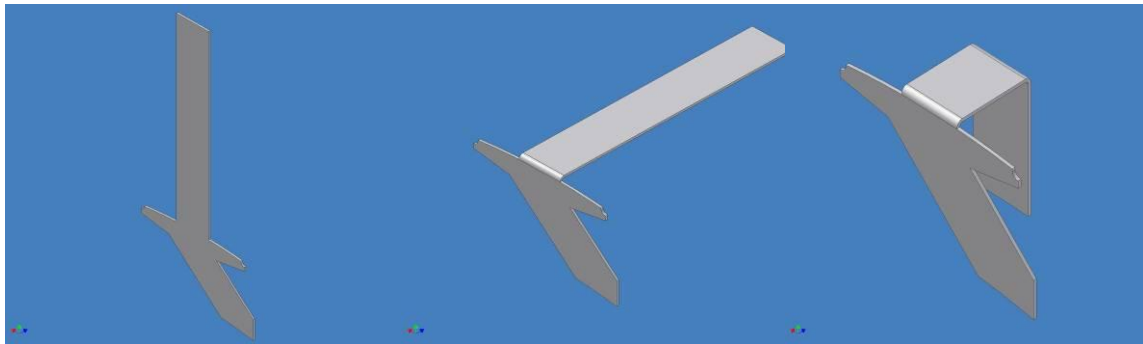


**Figure 5-6 The required process of bending to produce the second half of the stator stack**

Having chosen what appeared to be a viable lamination footprint, attention now was given to creating a method to carry out the bending. This required some knowledge of methods for folding sheet metal. The following sections describe the issues that were investigated before bending the new prototype.

### 5.2.6 Bending order

The MH prototype was produced with only one type of bending process. This bend occurred in the link between individual teeth to transform the straight long laminations into the circular shape that eventually formed the stator stack. This bend would be necessary in a prototype using the new lamination design and will be referred to as bend A. A second type of bend would also be required, which would take the long teeth over the coil to produce the second side of the stator stack. This will be referred to as bend B. The order in which the bends need to be performed, is influenced by whether the laminations are bent as a stack or individually. To bend each lamination individually would be impractical, requiring individual jigs to account for the different bend radius of bend B dependant upon where the lamination fell in the stack. Bending the laminations as a stack means that the force required to perform bend B is much greater than that for bend A. From the nature of the design, the bend that is performed last is the one which encloses the coil. As this operation has the greatest risk of puncturing the insulation of the coil and creating a short, it is logical that bend A, which takes the least force to perform is performed last and hence it is the one that encases the coil.

### 5.2.7 Creating Bend B

Figure 5-6 shows the idealised bending of a single pole, one lamination thick. Achieving this in reality with a stack of 23 laminations and 25 teeth, which need to be bent so that every tooth is equal looked to be difficult to achieve and hence it was thought necessary to investigate bending techniques.

To control the bend of the stack of teeth, it was necessary that they were clamped so that the material was held in alignment. To test this out, a single tooth trial was performed. The stack can be seen on the left of Figure 5-7 which was held in the clamp in the centre of the figure. The jig was then held in a sheet metal bending press, designed for making 90deg bends. The machine itself was capable of going past 90deg to allow for spring back in the design. When the stack was being held in a purpose built jig, the bending press was limited to 90deg due to interference with the jig. While the clamp of the bending machine comfortably held the jig in place for the bending process, it did not supply enough clamping force to prevent movement between adjacent laminations which spoil alignment and hence the need for the separate jig became clear. Bend B is actually made up of two right angle bends, which required two stages in the press. As a result there was a cumulative spring back, clearly visible in the resulting bent laminations on the right in Figure 5-7. To try to reduce the spring back, the jig was machined with a taper on one side (the right side of the jig in Figure 5-7). This allowed the machine to go beyond 90degrees in the second bend. It was not possible to do this for the first bend as the jig also had to form a right angled edge

for the second bend. Unfortunately it was found that the tapered edge made it difficult to hold the jig in the clamp of the bending machine.

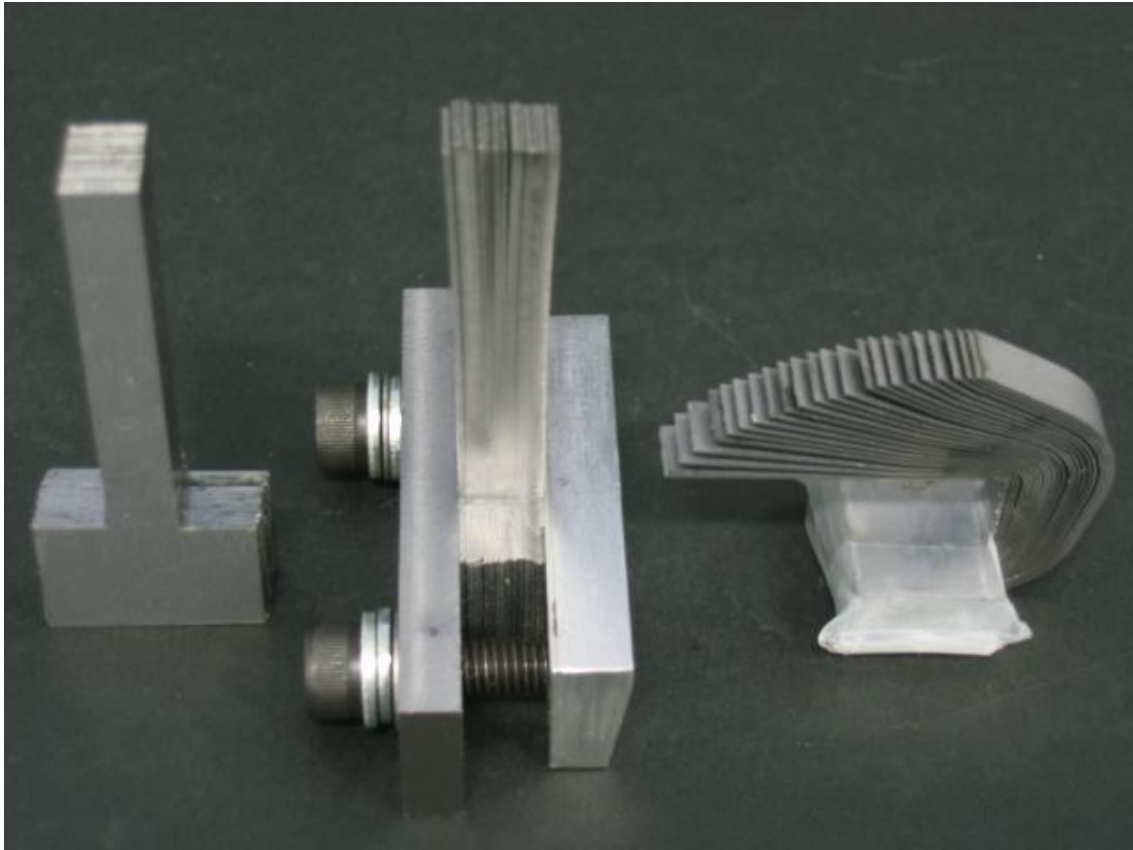


**Figure 5-7 Single tooth U-shape test bend**

### **5.3 Creating Bend A**

Bend A forms the circular structure of the stator. The coil in the prototype was wrapped in polyimide tape which acts as a slot liner. This gives protection from an electrical ground short to the core. The ground wall insulation needs to be as thin as possible because it reduces the space for copper and forms a thermal barrier. In a production machine tape wrapping is likely to be a slow and hence expensive option. In production the ground-wall insulation might for instance be formed using plastic injection moulding. The bend in the core was done by hand, using the tape wrapped coil as the forming jig. The ligatures on the circumferential sections of the core are thin and hence only a small force is required to shape the core into a ring around the coil. It was found that using the coil as the former to make this bend worked well and did not pose any threat to the coil insulation. It should be noted that the coil had been pre-wound and epoxy impregnated and hence it formed a rigid structure with good dimensional tolerance.

### **5.4 Three section test**

In order to test out the bending concepts and to calibrate the predicted post-bending dimensions, a trial of three teeth, using the profile shown in Figure 5-6, was undertaken. Figure 5-8 shows the assembled laminations in the bending jig. The jig has pins which are there to ensure the location and correct alignment of the laminations in the jig. It also has studs to clamp the laminations. The studs are not in contact with the laminations.

The laminations were formed around the jig in the bending machine as was done with the single tooth test bend. During this procedure the bending machine could only move through 90 degrees, restricted by the jig (as noted above). Figure 5-9 shows the trial after each of the two bends. The spring back can be clearly seen to be a cumulative effect, increasing as the radius of the bend increases, from the inside lamination outward. The second bend tends to close up the spring back of the first bend. It does not take much force to remove the spring back to achieve a consolidated stack but on removal of the force the spring back reappears.

A careful inspection of Figure 5-9 after the second bend shows that the spring back is slightly different for each tooth. This was a result of applying compression to the laminations post bending, to try to reduce the effect of spring back. As is clear from Fig 5.9 neither method met with much success - all three teeth are near identical, post pressing or not. The two methods will be described, if only for the purpose of saving time for anyone repeating the work. Two variations of applying compression were used. The compression was applied to the laminations using a hydraulic press, which applied a force much greater than could be applied in the bending machine. The far tooth in Figure 5-9 had no post bending compression, while the two teeth closest had this extra compression applied after the initial bends were made in the bending machine. The hydraulic ram applied 4 Tonnes in the first method and 4.9 Tonnes in the second - both very large forces.

In the first method the central tooth had a tool makers clamp applied, so that the exposed teeth formed by the second bend were clamped against the jig (i.e. in an axial sense using the geometry of the machine as a reference). With this clamp in place, compression was applied to the core back (i.e. in a radial sense). The intention was to try to close up the bends so that the lamination stack consolidated. As can be seen (in Figure 5-9) this method did not meet with much success. The near tooth in Figure 5-9 was compressed on top of the tooth (i.e. in an axial sense) as shown in Figure 5-10. This press produced no significant change. The method of clamping and pressing, as performed on the central tooth, was subsequently applied however, no visible advantage was seen from this second compression.

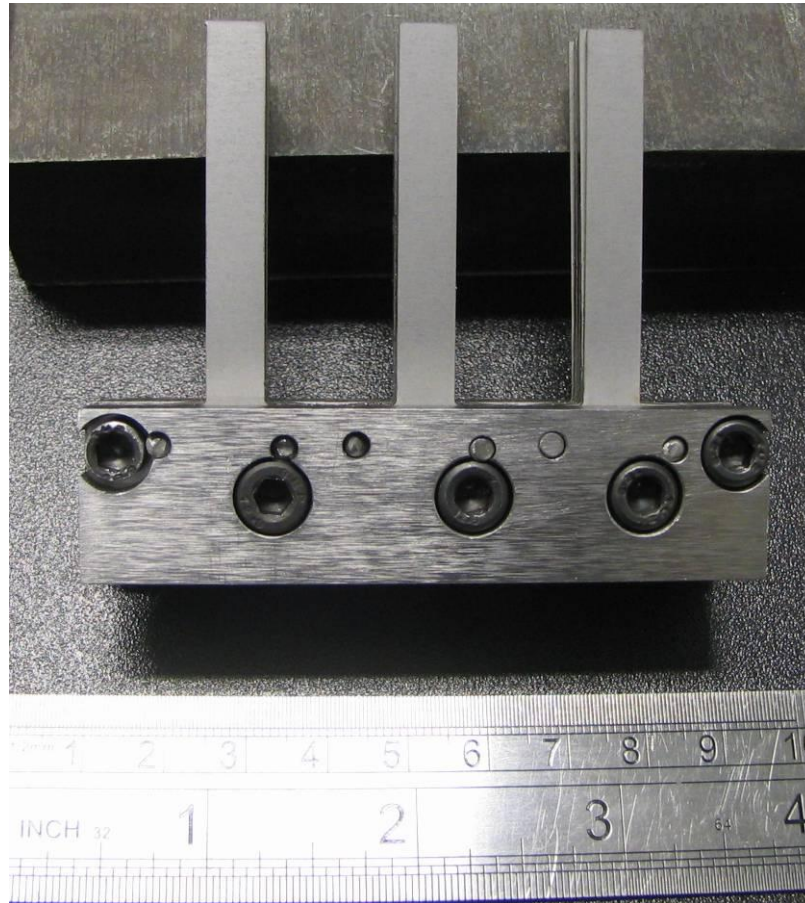


**Figure 5-8 the trial lamination stack in the jig**

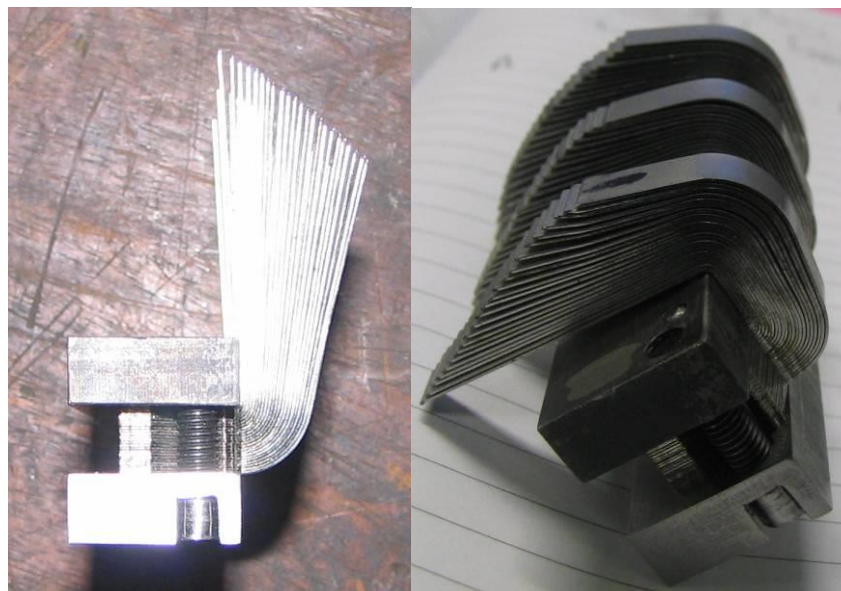


**Figure 5-9 the trial after each of the two bends**

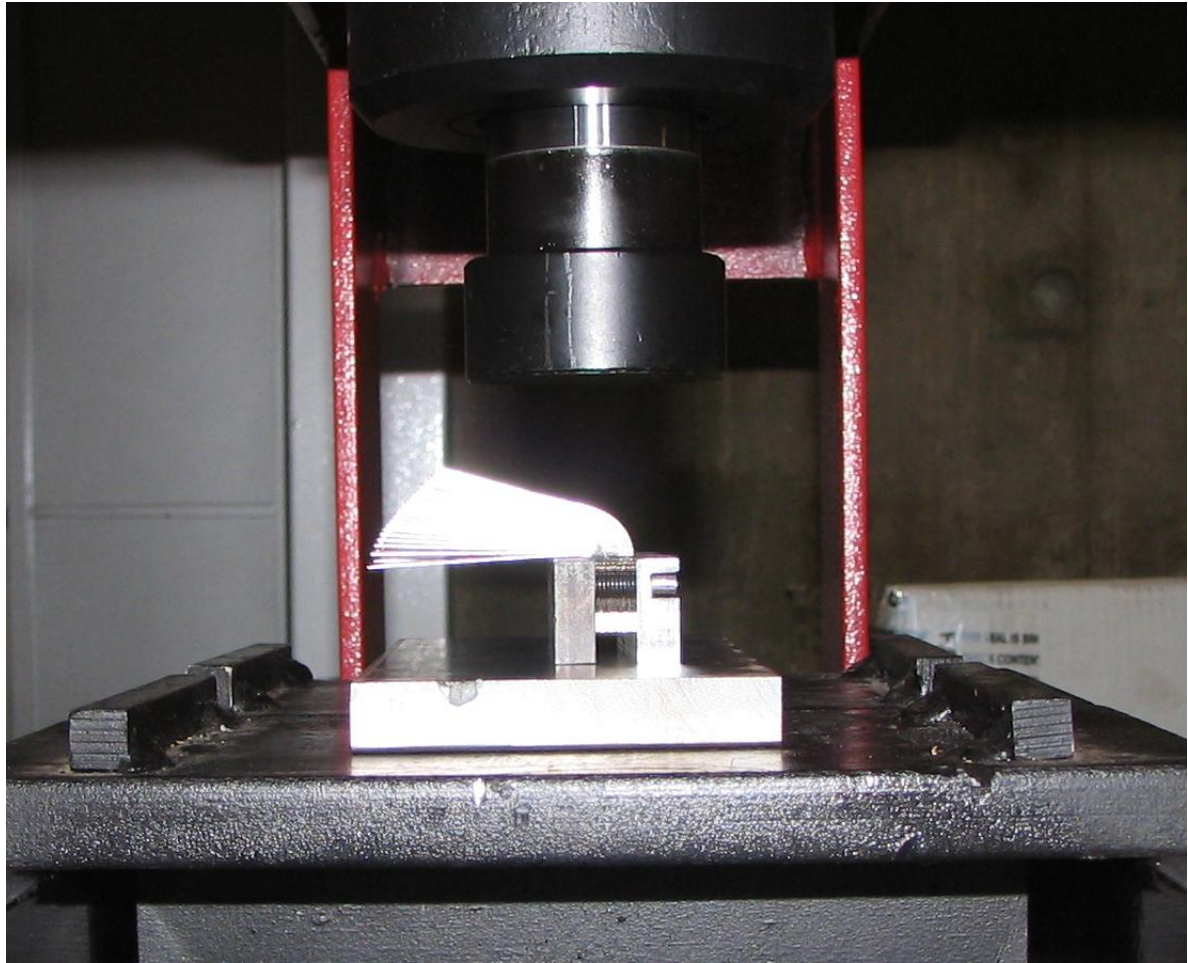


**Figure 5-10 Compression being applied after the bending process**

Cyanoacrylate glue (“Superglue”) was applied across the grain of the laminations where they were accessible around the jig. This supplied a weak bond between adjacent laminations, allowing them to be removed from the jig and handled. The bond was found to be stronger than expected and was maintained while the laminations were formed round the coil by bending the ligature in the joining pieces on one flank. All 23 laminations were bent together utilising the coil as a former. As can be seen in Figure 5-11, the method worked well, the force required was easily attainable manually and there was very little force transferred to the coil insulation meaning that there is little risk of shorts between the coil and the laminations when this method is used in the full machine.

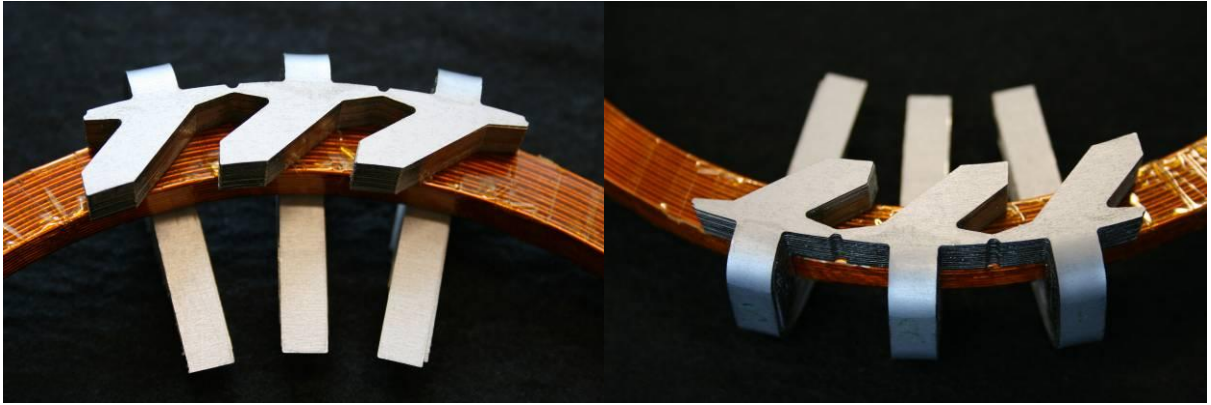


**Figure 5-11 the three tooth test formed round a coil**

## **Chapter 6. Construction of the Formed Lamination Machine**

This chapter describes the construction of a prototype using the methods developed and trialled in Chapter 5. The prototype is designed to use the rotor from the first (material hybrid, MH) prototype. This saves time in construction and allows a fair comparison of the two machines.

The principle design advancement of this prototype over the MH machine is minimising the part count by constructing the stator from a single lamination pack. This also has the advantage that the undesirable air-gaps which resulted from the construction process of the MH prototype do not occur. The previous chapter covered the development from the concept and construction of a three tooth-pair section trial of a method for bending the laminations to form the desired stator shape. This chapter discusses the implementation of this method to build a full size 50 pole prototype.

### **6.1 Lamination Production**

The laminations of the previous MH prototype were laser cut from large sheets of the steel in one pass, relying on the contact of the lamination with the bedplate under their own weight, to hold them in place. This was not particularly successful and the variation of quality in the finished cut was largely due to the laminations moving during the cutting process.

The laminations for this prototype were again laser cut from large sheets but modifications to the process were made resulting from the previous experience. The first change was the company to which the cutting process was outsourced. A visit to the production site to discuss the requirements with both the people that write the cutting program and those that operate the machines was invaluable. It allowed a much better understanding of the requirements of the final product to be developed and quickly resulted in ways to improve the tolerances and surface finish of the cut laminations. To improve the cutting tolerances, the laminations were left connected to the blank sheet with tabs of uncut material. On completion of the main cutting loop, secondary cuts were made to narrow the remaining tabs. The laminations are shown still attached to the blank sheets in Figure 6-1. A close up of a tab is shown Figure 6-2. The second cut to narrow the tab can clearly be seen as its direction is normal to the main cut, reducing the risk of cutting final part if it has moved. This two cut process allowed the tab to have strength during the first cutting loop, minimising movement of the cut part and produced a really high level of repeatability in shape from one part cut to the next. At the same time the second cut meant that the tabs are sufficiently thin (less than 0.5mm) to facilitate easy removal of the laminations from the blank sheets.

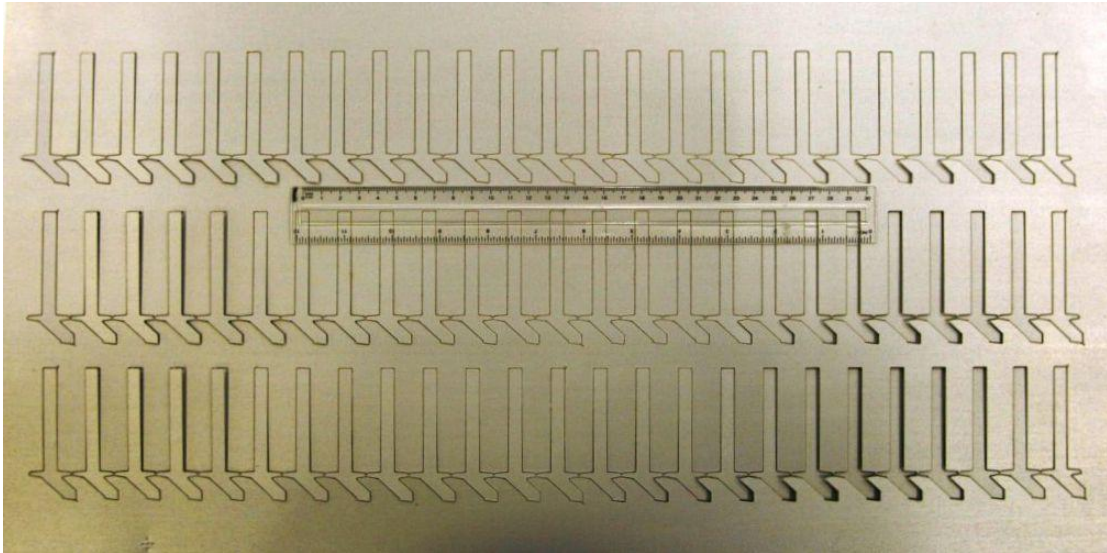


**Figure 6-1** the laminations profiles after laser cutting, still held in place by tabs.

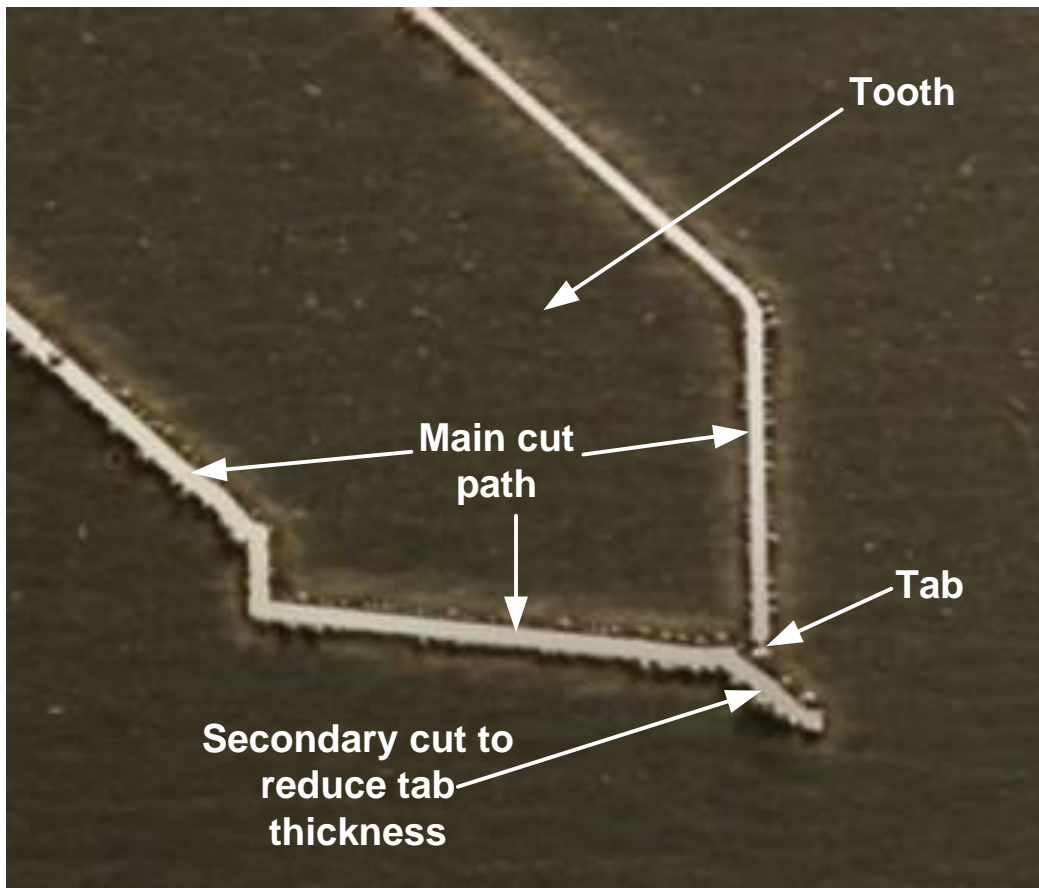


**Figure 6-2** A close up of the tab clearly showing the second cut.

As with the laminations for the MH prototype, the parts were cut with a new bed plate in the machine, which is sacrificial in the cutting process. The tabs helped to minimise movement of the cut feature normal to the bed plate during cutting. This greatly reduces the occurrence of

the lamination being welded to the bed plate with residual splatter, which was another major cause of poor tolerances in the laminations for the MH prototype.

## **6.2 *Bending the laminations***

The removal of the laminations from the large sheets requires severing the thin tabs that remain from the laser cutting process (as described above). This leaves extra material on the lamination, but the locations of the tabs on the tooth tips mean that this will not interfere with the construction process and they will be removed when machining the stator air-gap surface to its finished dimensions. It requires twenty-three laminations to build the stack to a total axial length of 8.05mm. The stack was assembled and mounted into the forming jig, which is a longer version of the one used in the three tooth trial (described in the previous chapter). The two sides of the clamping jig are constructed from tool steel (high carbon content). Two silver steel pins per tooth were used to locate the laminations in the correct place within the jig, and one bolt per tooth was used to provide compression of the laminations and also to help keep the alignment of the two sides of the jig. The laminations are shown mounted in the forming jig prior to any bending in Figure 6-3.

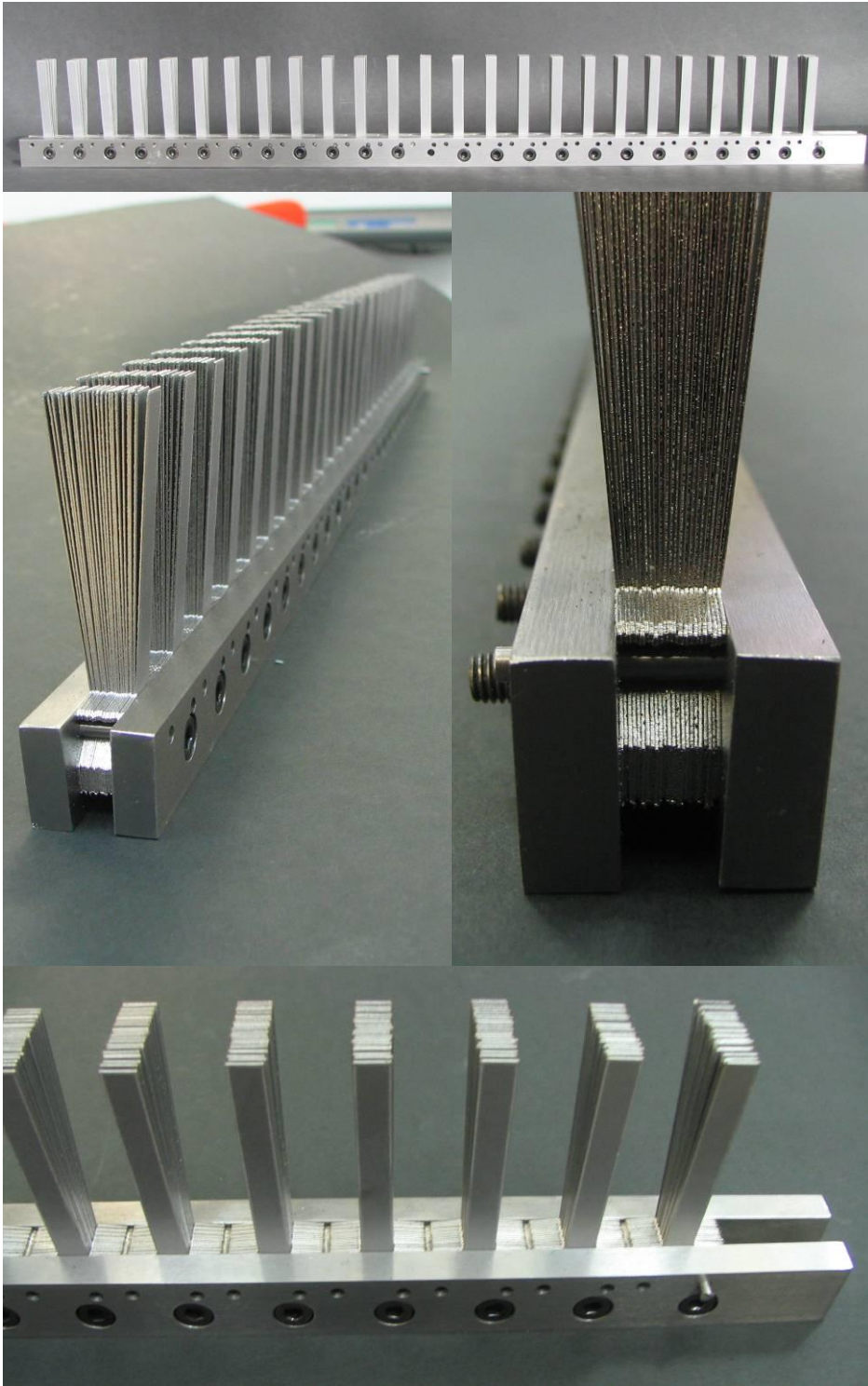


**Figure 6-3 the laminations mounted in the forming jig prior to bending**

It may be noted from Figure 6-3 that the clamping bolts need to be placed below the circumferential section (i.e. towards the lower side of the bottom picture). This means that the axial clamp is not centrally forced and the laminations, acting like an axial spring, tend to fan out in the longer tooth sections and the plates of the jig are not parallel in the plane of the laminations (which is visible from close inspection of the middle right picture of Figure 6-3).

The location of the bolts is governed by the space available between the shorter (skewed) teeth. One solution to resolve this effect would be to put dummy lamination stacks in the gaps between the plates, however this would limit the compression applied to the real stack and possibly allow movement while bending. All other solutions considered were unfeasible as they prevented the forming jig from being held in the clamping mechanism of the bending press. For these reasons, the setup in Figure 6-3 was used despite the imperfection.

The forming jig was held in the clamping system of the bending press, Figure 6-4, and the first bend made. The thickness of the forming jig created an offset of the laminations and the centre point of the bending mechanism. This meant the bend was formed more by forcing the laminations from a fixed contact point against the square edge of the forming jig. The bending jig is designed to slide over the part as the forming mechanism moves, forming a better bend. The result of this was a lot of spring back after the bend and the inside lamination on release had not bent the full 90 degrees. This can be clearly seen in the end tooth of Figure 6-5 (showing the laminations in the jig after the first bend) which has had no post bend processing. The rest of the teeth in the image have had post bending compression applied as was done with the three teeth trial, i.e. force was applied via a hydraulic ram downwards onto the laminations as viewed in the top of Figure 6-5. It is clear that this post bending process has finished the bending, creating a sharp right angle bend on the inside laminations.

The second bend proved problematic because of difficulties in holding the jig in the bending machine with the sprung-back teeth. Applying post-first-bend-compression solved the problem. Mounting the forming jig in the bending press clamp required compression between one of the jig bars and the laminations. This was attempted before the post-bend compression with the intention that the bending press clamp would compress the laminations enough to allow formation of the second bend. However, it was found the jig would move as the clamping pressure was applied, resulting in misalignment. The post-bend-compression resulted in a much squarer setup and the holding clamp only had to cope with a small spring back in the laminations, allowing the jig to be held in alignment and the second bend to be formed.



**Figure 6-4 the bending press**

Visual inspection of the end of the jig bars in Figure 6-6 after the second bend, reveals that the angle between the bars has been amplified by a combination of the lamination bending process and the post bend compression. This in itself is not an issue, but gives an insight into the large forces imposed and the difficulty in creating a forming jig that is rigid enough for the process while still providing adequate compression to the laminations to hold them in place.

In Figure 6-6, no post-second-bend compression has been performed. While the bending has successfully manipulated the laminations roughly into the required C-shape, the tolerances are not very good, even when ignoring the spread between the laminations from the spring-back. Figure 6-7 and Figure 6-8 are post-second-bend-compression and the result of this is that the inside lamination clearly follows the shape of the forming jig leaving only the spreading between laminations from spring-back to contend with. This greatly benefits the onward construction process as the force to overcome the spring-back is much reduced thereby simplifying assembly into the casing.

The centre of Figure 6-7 shows damage to one of the teeth resulting from the post second bend compression. The compression process has guillotined the top two laminations. This was the only tooth that received this damage so the effects in performance were expected to be minimal.

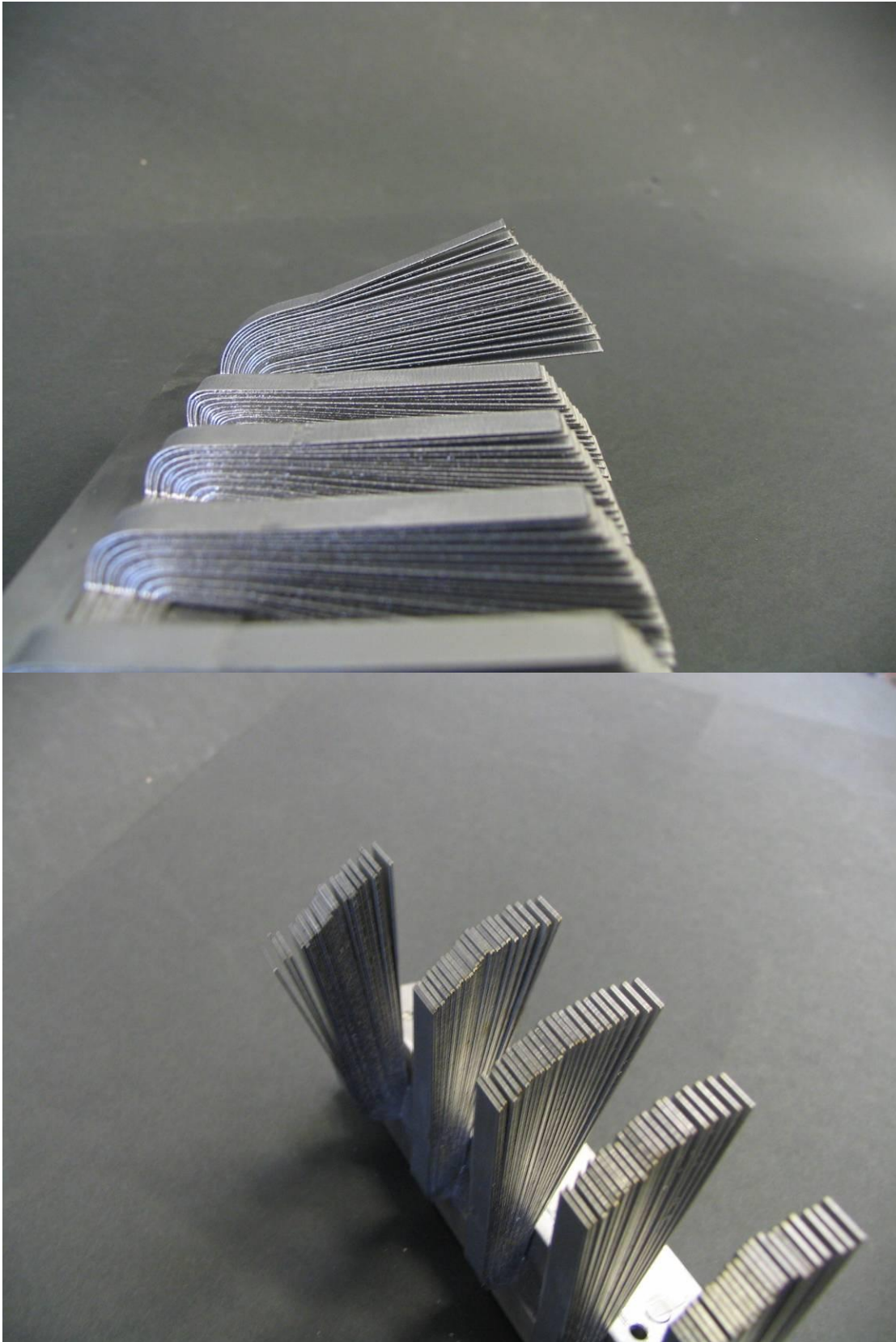


**Figure 6-5 The laminations after the first bend**

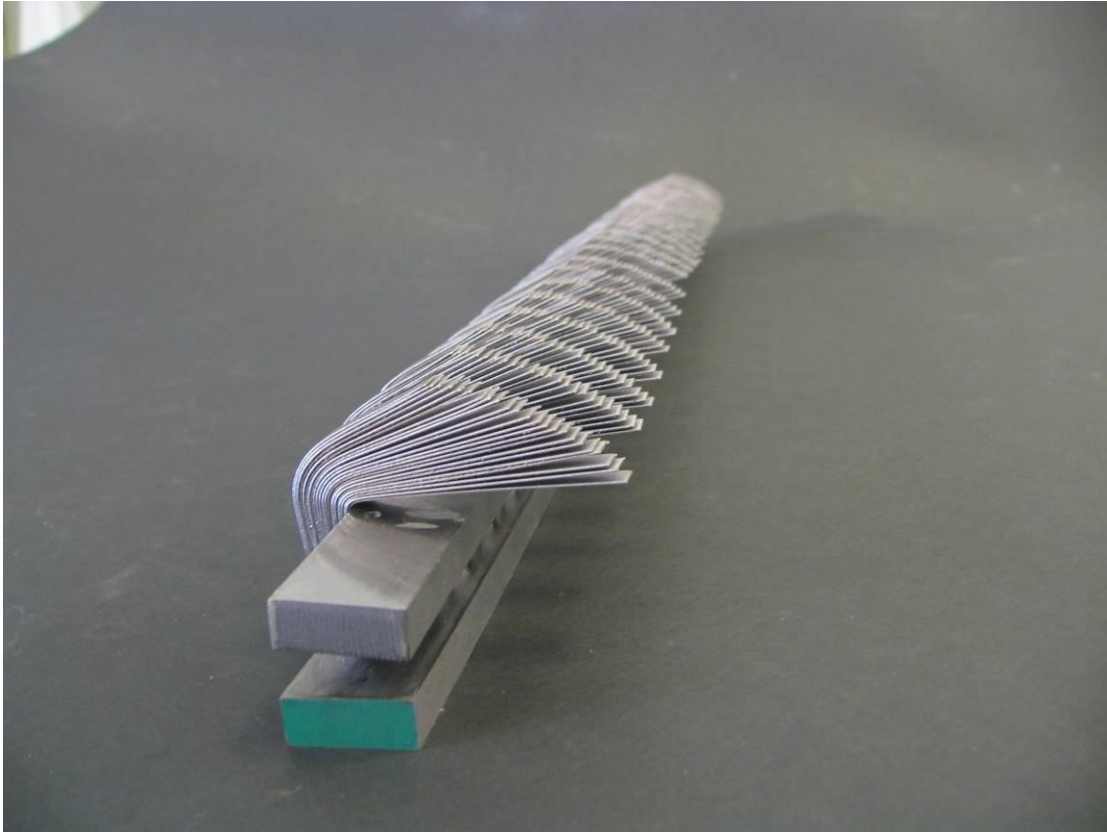


**Figure 6-6** The forming jig after the second bend.

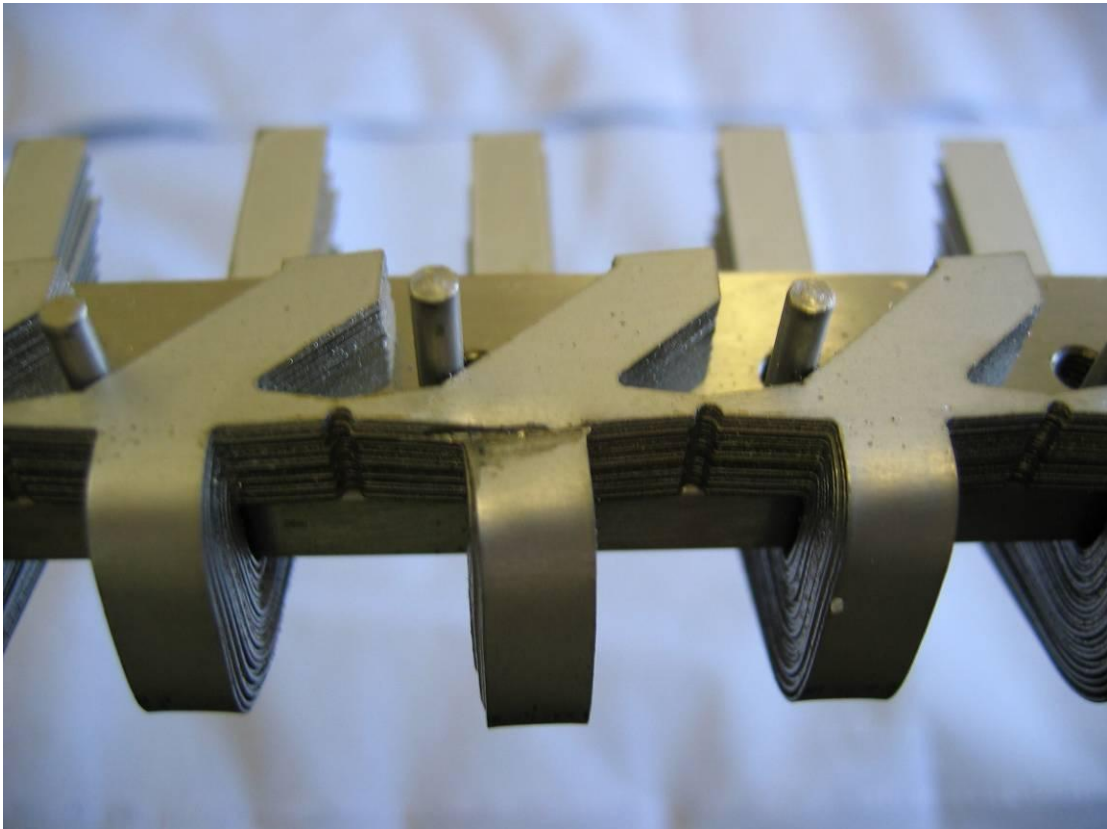


**Figure 6-7** Laminations post second bend

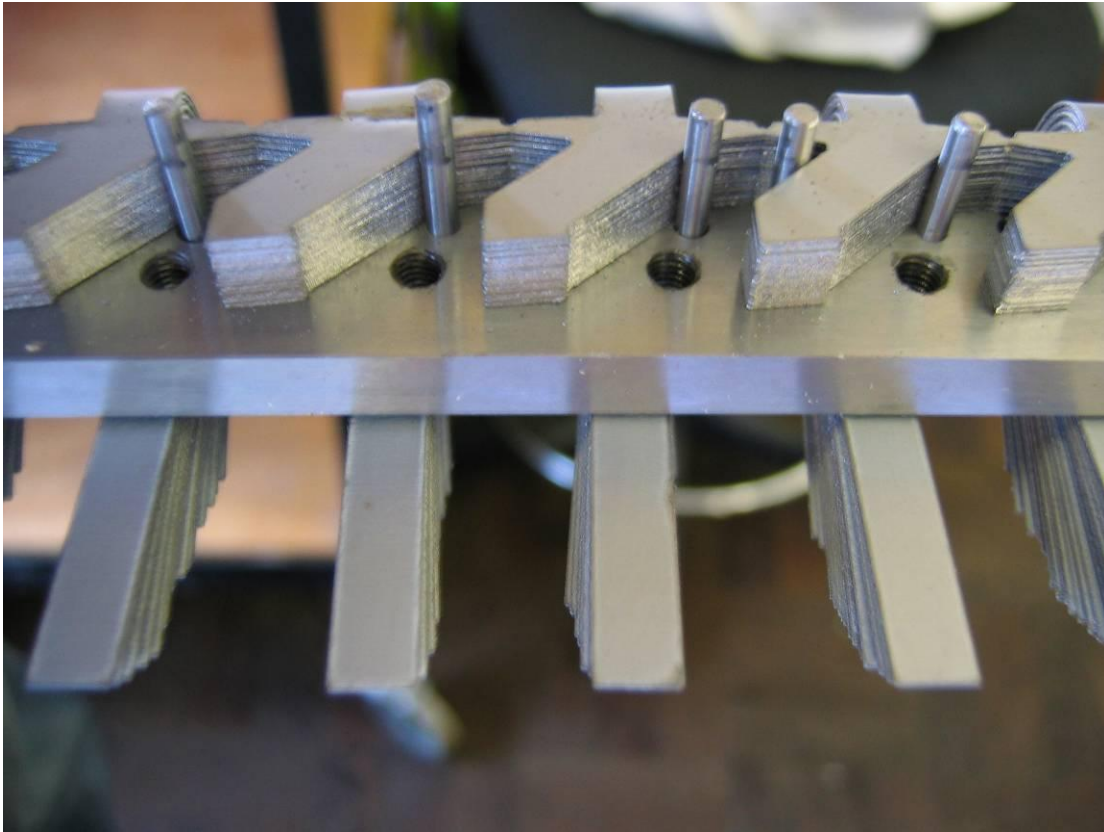


**Figure 6-8** The formed lamination in half the jig showing the pins maintaining the lamination alignment.

Overall it is clear that the laminations have been bent well enough to allow the onward construction of the machine. The conclusion can also tentatively be drawn that the process is viable as a production technique. It is also clear however that development of the bending process is likely to yield considerable improvements.

### **6.3 The Winding**

The slot opening in this prototype is deliberately the same cross sectional area as in the first prototype, allowing the same construction process to form the winding using the same aluminium former. Experience producing the first prototype's coil highlighted a problem of increased radial thickness in the region of the transition between the winding layers. This is caused by the conductor strand as it transitions from one layer to the next and the resulting radius of the bend in the conductor. To attempt to reduce the effect, a slightly thinner wire was used in the coil for the second prototype. This facilitates a sharper transition from one layer to the next by reducing the radius that the conductor forms in rising to the new layer. The new coil is shown in the winding jig in Figure 6-9 viewed circumferentially at a tangent to the point of maximum fill of the jig, i.e. the point where the conductor changes layers.

Coupled with the view in Figure 6-10 of the same point once removed from the jig, the reduction in this effect can be seen compared to the first prototype coil, where the difference could be clearly seen from such views. The result of using thinner wire is 54% more turns. There are ten turns per layer and 16 layers in the winding. The layers are offset in the same way as the first prototype i.e. the turns of one layer fit into the groove between turns of the previous layer. This offset in the layers is visible viewing the coil from the side as shown in Figure 6-11. In a real application the turns are fixed by the required terminal voltage and the choice of using thinner wire is equivalent to using more than one strand of wire and keeping the number of turns the same.

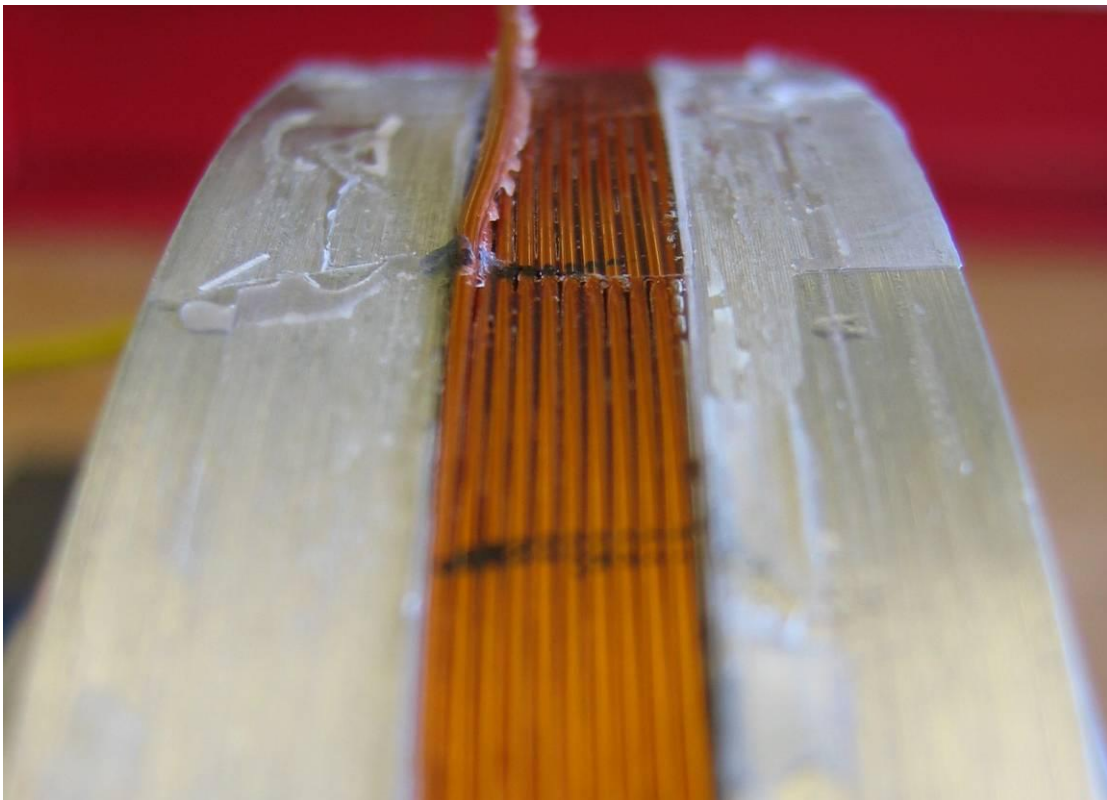


**Figure 6-9** The winding prior to removing from the forming jig.

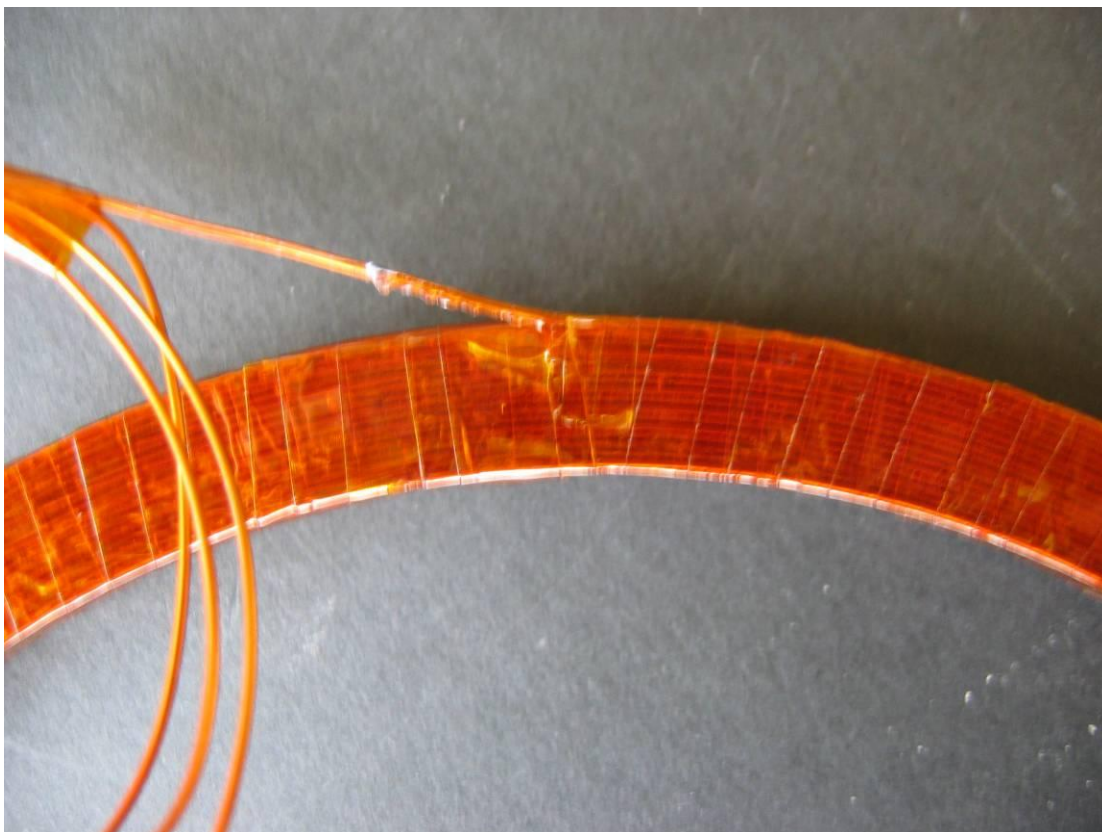


**Figure 6-10 Winding after wrapping with polyester film tape**



**Figure 6-11 Winding after removal from jig**

### **6.4 Forming the Laminations around the coil**

As was shown in the three teeth trial covered in the previous chapter, the force required to bend the laminations around the coil is small enough to be done by hand. The small amount of spring back in the lamination stack after forming in the jig means that the laminations do not create a contact fit on the sides of the coil. This non-interference fit has a side benefit in that it reduces the chance of the laminations damaging the coil insulation and creating an electrical short during forming the core around the coil.

The manual bending process concentrated on only two adjacent sections at any one time, rather than globally across all 25 sections at once. At each step, one section was held so that the coil was in maximum contact with the inside lamination at the core-back. The adjacent section was then bent by applying force to the outer lamination of the core-back till its inside core-back met the coil. Because the bend is in-plane with the laminations and rather thin (radially) the steel is quickly taken into the plastic region in this bend. This means that although the bend is a much smaller angle than the right angle made in forming the sides of the stator teeth, the spring back is much smaller and the core fits the coil snugly.

By concentrating on two adjacent sections at a time, the spring back does not tend to be cumulative around the circumference. The result is a ring that is very circular in shape but with a diameter that is slightly greater than required. If all sections had been bent at once, the likely result would have been a spiral with a good fit at the start and a poor fit at the end. The final shape is very close to the required diameter, as can clearly be seen in Figure 6-12, which shows the stator laminations bent around the coil with nothing constraining them. The small gap at the joining ends can be seen around eleven o'clock in Figure 6-12. When pressure is applied to close this gap, the laminations are in the correct position around the coil. As the gap is small, very little force is needed to shape the laminations into the final ring, making assembly into the casing rather simple. The ligature between the tooth sections did not fracture during this bending process and the teeth remained in circumferential alignment. It is clear that this forming process is simple to execute and worked well in the construction of the prototype. The "long teeth" in Figure 6-12 appear to be far too long but this is deceptive as they are the teeth formed last and they take up the extra length for the laminations on the outside of the stack. These outer laminations are close to final dimension radially, whilst those on the inside are far longer.

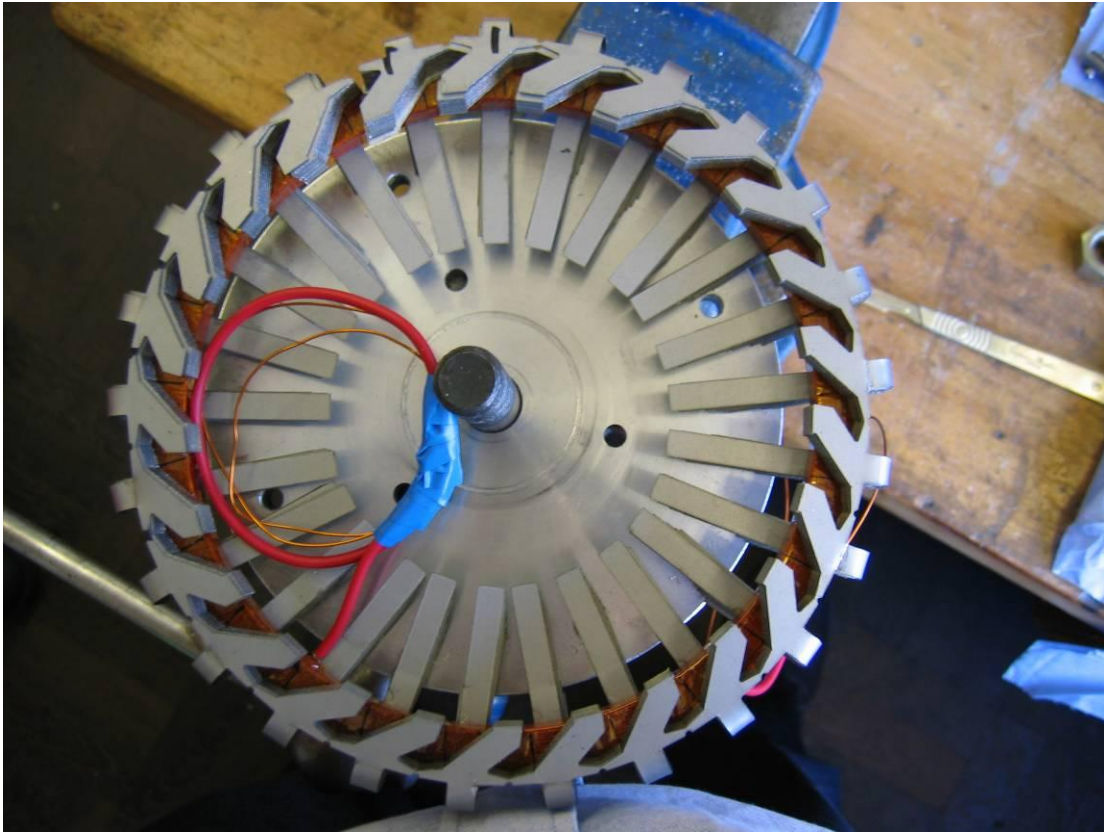


Figure 6-12 The lamination stack formed around the coil

### **6.5 Casing and end caps**

As the rotor of the first prototype is being utilised and the design of the stator is very similar, the casing of the motor takes the same form as that for the first prototype. At first it was thought that the end caps of the first prototype could be reused here. However, the folding of the laminations to form the full stator results in a thicker (radial) core-back, hence, the outer diameter is greater than that of the first prototype and no parts of the first prototype housing can be reused. On reflection, this is a good thing, as it would be very difficult to maintain concentricity of the stator and rotor when reusing the old end caps.

This casing is shown in a sectional view in Figure 6-13 which is taken from the CAD assembly drawing of the stator laminations in the casing with the end caps in place.

The inner diameter of the casing was adjusted to give a good interference fit with the stator laminations. This inference fit had the effect of consolidating the laminations in the core back, thereby removing the spring back from the first bend in the core.

As with the casing of the MH prototype, an inner flange was included in the casing, which the stator laminations locate against in an axial sense. The end cap at the opposite side to this

flange (the right hand end cap in Figure 6-13) is adjusted so that it applies axial pressure to the core and hence the spring back resulting from the second bend is taken up. With this end cap in place the active components are held firmly in the desired position.

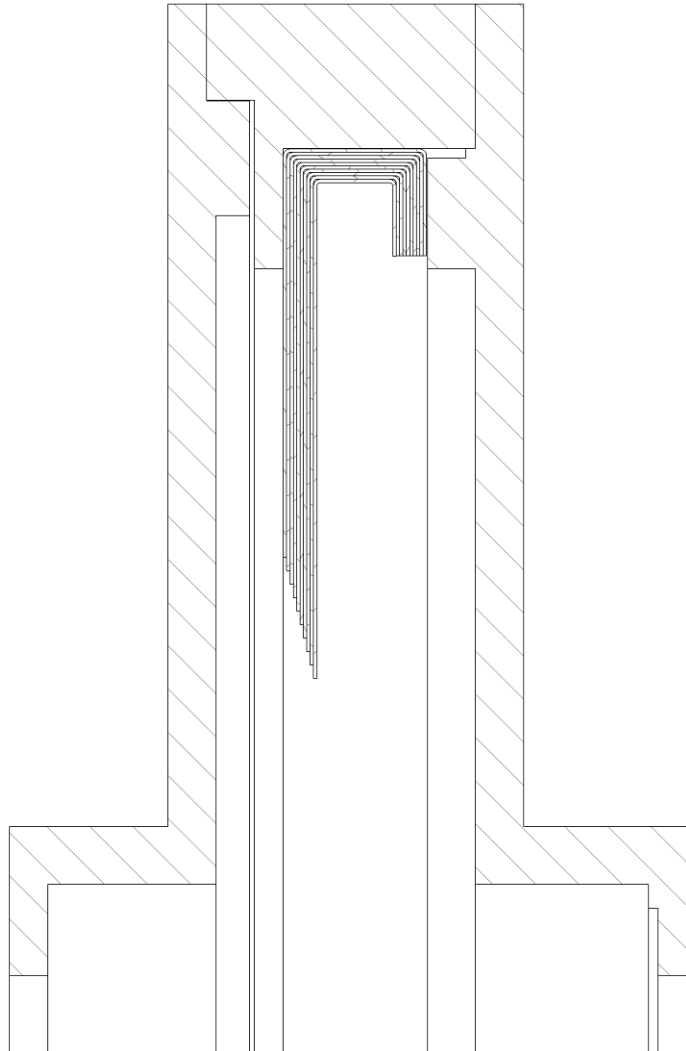


**Figure 6-13 CAD of the stator in the Casing with end caps**

### ***6.6 Assembly and Final Machining***

The stator laminations were assembled into the casing such that the staggered long teeth were against the inner flange, as shown in Figure 6-13. The end cap was then bolted on, clamping up the laminations against the coil. To hold everything in place, to give support in post assembly machining and to prevent any movement in operation, the stator was potted in-situ. For this process a temporary central cylinder was manufactured which greatly reduced the amount of epoxy needed to pot the structure. A second endplate was machined with slots into which the long lamination ends located and it mated with the inner flange in the casing and hence a volume was formed for filling with the potting epoxy. At the other end of

the casing, a ring was made to compress the laminations axially (whilst the end cap was removed for the potting process. The core is shown in the left of Figure 6-14 with the potting epoxy in place. The right hand side of Figure 6-14 shows the core after removal of the clamping ring.

Once the epoxy had cured, the temporary end plate and the inner cylinder were removed. They had been coated with a mould release agent before potting to allow minimal force to be required to do this. The end cap which applies axial pressure to the stack was then bolted in place to form a solid structure for machining the final stator air gap surface. A section of the finished stator is shown in Figure 6-15. A tooth just to the right of the centre of the picture has an end lamination that has been bent slightly towards the coil during machining. This occurred during machining because an air pocket had formed during potting, reducing support to the lamination at this point. This shows how important the support provided by potting is in the final machining process. Some form of bond between laminations is clearly necessary to avoid movement during machining.

Potting is not a desirable feature of a production process but perhaps plastic injection over-moulding could be envisaged as being a rather better substitute as it would not only provide good hold for the laminations it would also apply the pressure to take up the spring back and may also be used as the slot liner.



**Figure 6-14 stator potting jig**

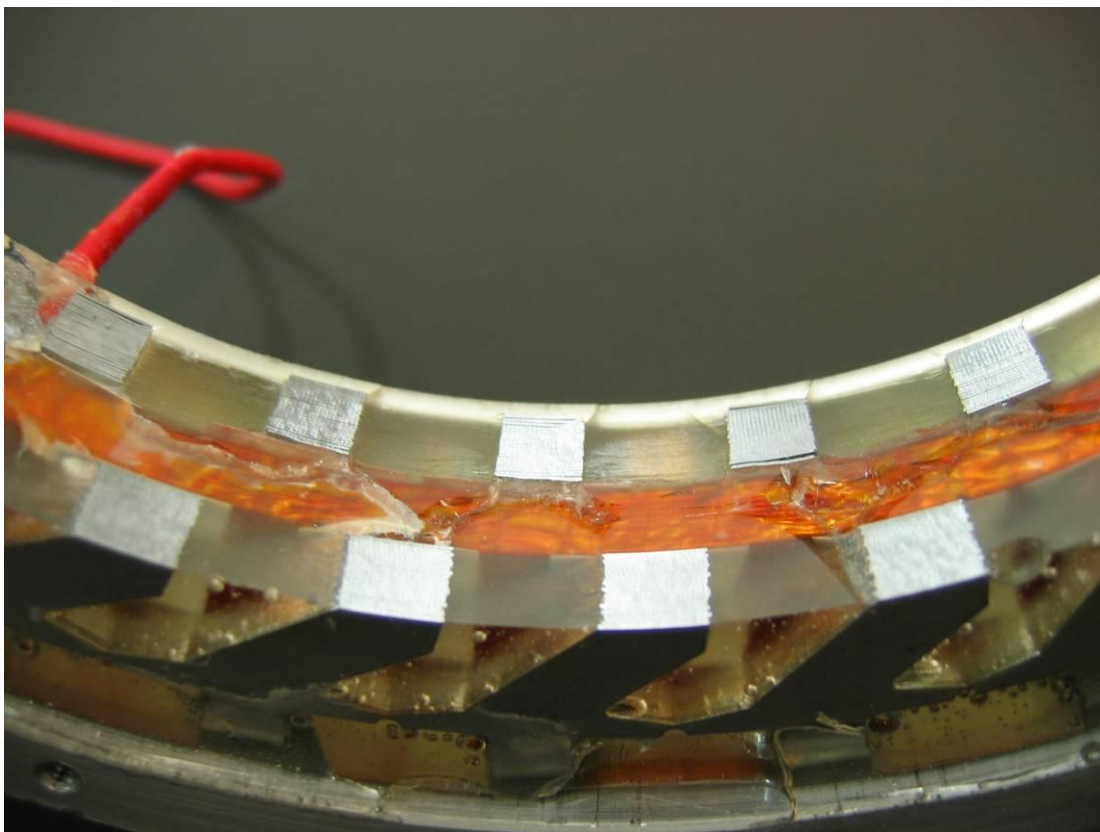


**Figure 6-15** The final machined stator bore

## Chapter 7. Testing of Formed Lamination Prototype and Comparison with the MH Prototype.

As with the first prototype there is no specific application directing the design of the formed lamination (FL) machine and the prototype is aimed at attempting to quantify how practical the formed laminations are as a method of manufacturing a modulated pole machine.

The following sections present the results of a series of measurements taken from the machine that help build a general picture of the properties for the machine. A prediction of a suitable operating condition is also given. Finally the machine is compared with the material hybrid machine and differences discussed.

### 7.1 Thermal Testing

The thermal data presented here is of the same measuring technique and format as with the first prototype presented in chapter 4. A brief overview of the test method is now given to refresh the reader's memory. With the rotor static, the winding of the machine was fed with a dc supply, the resistive heating of the winding is the only source of heat energy in the system. By measuring the change in resistance of the winding, an average temperature can be calculated using equation (7-1) and a good estimation for a thermally limiting current can be attained (ignoring transient and motion losses). The data for the two thermal tests performed with two different levels of winding current are presented.

The results of the first thermal run are presented in Figure 7-1. This test used a rather high current of 3.64 Amps and the temperature of the coil was reaching a level that was likely to affect the strength of the adhesive used in the rotor, so the test was stopped prematurely. The short run of the test reduces the accuracy of curve fitting and extrapolation to predict the final winding temperature. None the less using equation (7-2) to produce a curve fit to the temperature results gives the curve plotted on top of the results in Figure 7-1. The following values are for the variables in equation (7-2):  $T_w=36$ ;  $\tau_w=200$ ;  $T_c=45$ ;  $\tau_c=3500$ . The lowest time constant,  $\tau_w$  relates mostly to the thermal inertia of the winding and the longer,  $\tau_c$  to the core and case. Subsequent examination showed the rotor component bonding was indeed damaged by the test and a major rebuild was necessary. The issue of the rotor mechanical failure is covered in section 7.2 below.

$$\Delta T = \frac{1}{\alpha} \left( \frac{R}{R_o} - 1 \right) \quad (7-1)$$

$$T = T_w \left( 1 - e^{-\frac{t}{\tau_w}} \right) + T_c \left( 1 - e^{-\frac{t}{\tau_c}} \right) \quad (7-2)$$

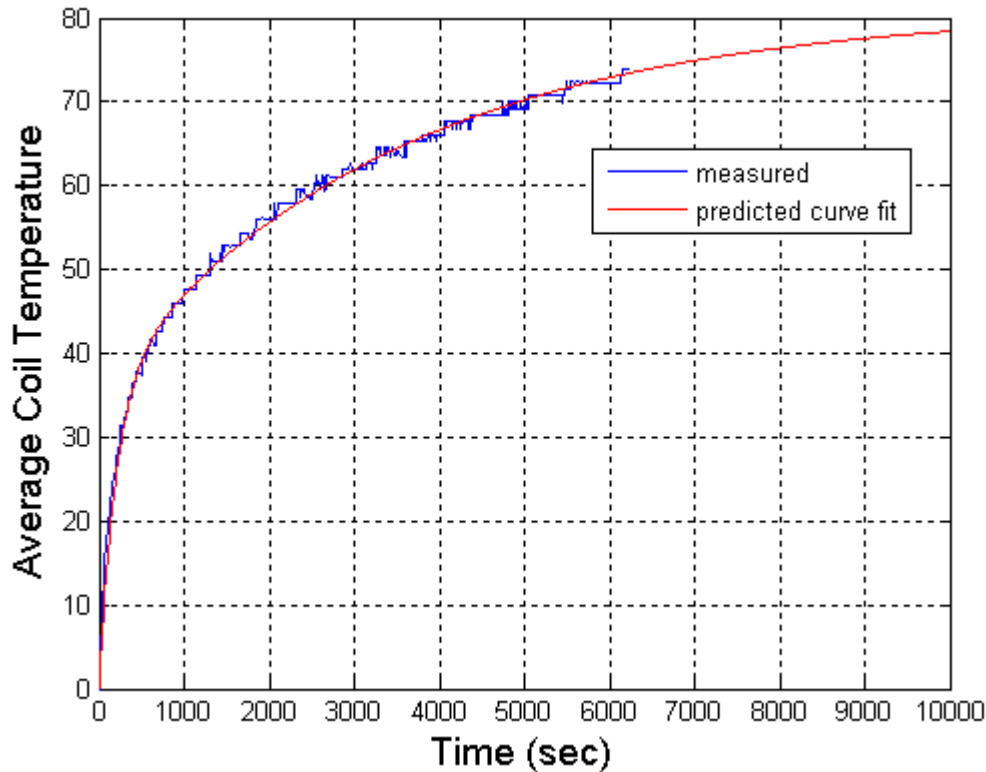
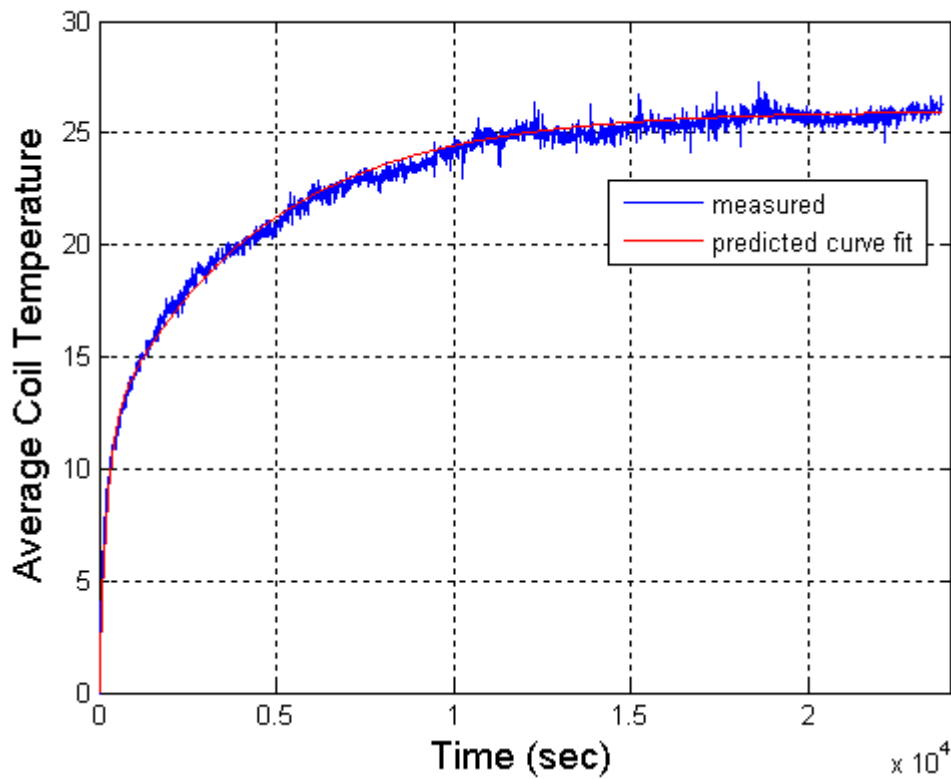


Figure 7-1 temp rise due to 3.65Amps (run 1)

After the rotor rebuild the second thermal test was carried out with a lower current of 2.11Amps. As the heating effect is proportional to the current squared, equation (7-3), this is only 33% of the power of the first run. As the temperature was much lower, the test could be run for much longer. This allowed more confidence in fitting the exponential curves using equation (7-2), for which the following values were determined,  $T_w=11.5$ ;  $\tau_w=220$ ;  $T_c=14.5$ ;  $\tau_c=4500$ . The measured change in temperature and the fitted curve using these values are presented in Figure 7-2. The results match well in that the final winding temperature is 26°C, which correlates with the reduction in the current (the first test had a rise of 81°C with 3 times more power loss  $81/3 = 27^\circ\text{C}$ ). The time constants for this curve are slightly longer than in the first test. This is to be expected as the motor was coupled to the torque measurement rig, which adds thermal mass.



**Figure 7-2temp rise in coil due to 2.11A (run 2)**

Using the thermally rated current of 4.14A calculated in equation (7-4) for a 100°C rise above ambient as the maximum allowable, and a room temperature resistance of 4 ohms it can be predicted using equation (7-3) that the motor is capable of dissipating 68.6 Watts of heat. This is 74.9% of what the MH prototype could dissipate.

$$P_{resistive} = I^2 R \quad (7-3)$$

$$I_r = 2.11 \times \sqrt{\frac{100}{26}} = 4.14 \text{ amps} \quad (7-4)$$

The reduced ability to dissipate heat in comparison to the MH prototype is a result of the castellated structure in the core-back of the machine. Assuming that the thermal path from the coil out of the machine is dominantly via the core-back and outer casing, there are two clear possible bottlenecks. Firstly the castellated structure by geometry reduces the cross section area of contact between the electrical steel laminations and the outer casing of the machine. The second effect is poor conductivity normal to the plane of the laminations. The in-plane thermal conductivity is around 20W/m/C for 3% silicon steel [54]. However, the thermal conductivity across the lamination is more in the region of 1W/m/C. The poor thermal conductivity normal to the plane is the result of the insulation on the surface of the

laminations, air-gaps which exist between adjacent laminations and touching points/areas (because the laminations are not truly flat). In the bent sections of the prototype there will be large air-gaps between laminations due to the bending process. This all means that the reduced ability to dissipate the winding loss when compared to the material hybrid is not surprising. A more detailed study of the thermal paths of the stator coupled with a refined process for the folding technique of the laminations and castellated casing to match the stator and reducing the thermal resistance between the stator and casing could easily be envisaged to improve the ability to dissipate this heat.

## **7.2 Rotor Failure**

The structure of the rotor comprises an aluminium inner to which the SMC pole pieces and the magnets are glued. The magnets and SMC pole pieces are also glued one to another. Over this assembly epoxy impregnated glass fibre tape was wound under tension. The glue used in the prototype was a common bonding formulation designed to set at room temperature. This means that the glass transition temperature of the glue was only 85°C even using optimal post curing heat treatment (which was not possible in this case). Hence any temperature approaching 80°C could be expected to soften the glue. In the first thermal test the average winding temperature reached 81°C and it is clear in retrospect that glue softening is the reason for the bond failing between the magnets/SMC pieces and the aluminium hub. The glass fibre ring did not fail but the tension was not sufficient to restrain the magnets/SMC pieces in position and they were drawn by the magnetic forces towards the stator teeth when assembled in the machine. When the rotor was not in the machine the rotor appeared to be sound to a superficial examination it was only with the rotor in the stator that the problem became apparent.

In operation with the rotor rotating, the increased natural ventilation coupled with the fact that losses induced in the rotor are rather small, means that high rotor temperatures are not generally experienced. A static heat test will however allow heat from stator losses to soak into the rotor. In a commercial motor the use of epoxy with such a low glass transition temperature is clearly not viable.

The rebuild involved recovering and then re-gluing the original rotor magnets and SMC pieces and finally over-binding the rotor with (this time) Kevlar thread at a much higher tension than the original glass fibre banding. With this construction no further mechanical problems have been encountered across all of the test programmes.

The failure highlights the inherently weak nature of this style of rotor and the importance of achieving sufficient tension in the over-banding or sleeve arrangement.

## 7.3 Back EMF

### 7.3.1 Measurements

The back EMF is the rate of change of magnet flux which links the armature winding, so giving a direct measurement of how good the magnet circuit is and an indication of the torque capability of the machine from the product of back EMF/unit speed and the current. A back EMF waveform measured at 240rpm (which corresponds to an electrical frequency of 100Hz) is presented in Figure 7-3. A pure sine wave is also plotted on the graph and it is clear to see that the measured waveform is very close to a sinusoid. This is important as this will help minimise harmonic degradation of the power factor when the machine is driven with a sinusoidal current.

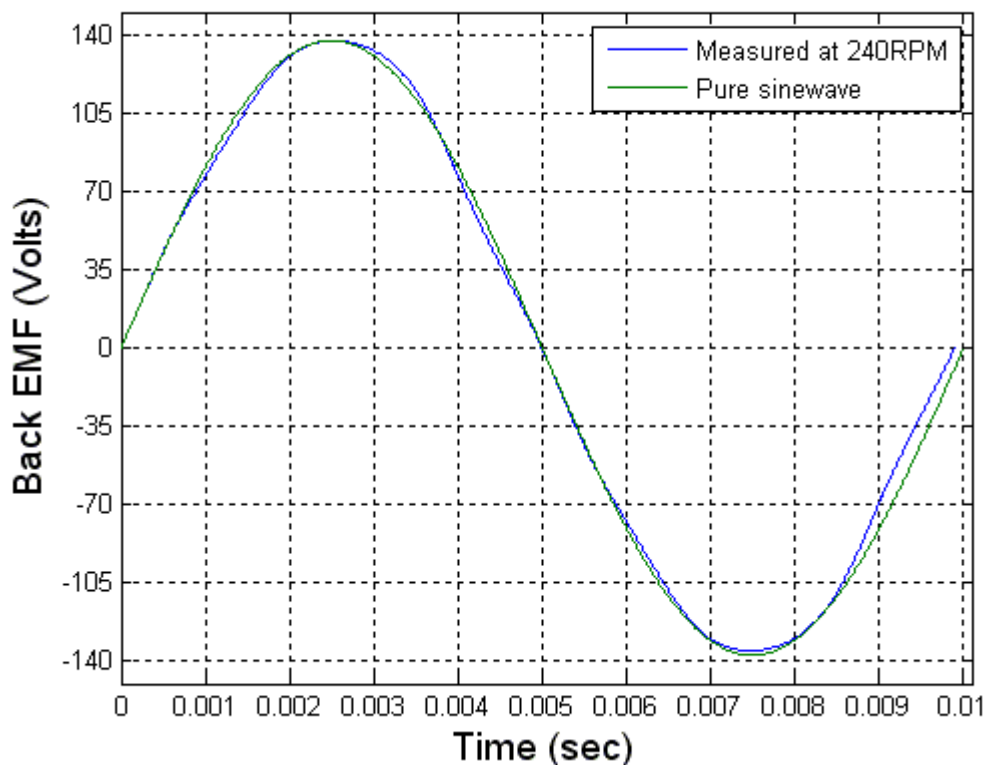


**Figure 7-3 Back EMF measured before realignment compared to a true sine wave**

The peak value of the waveform in Figure 7-3 is 137.5V. This is only 89.3% of the MH prototype when the ratio of the winding turns difference 160/104, is taken into account. It was postulated that the construction method of this machine would improve the magnitude of the magnet flux which links the armature winding due to the elimination of construction gaps in the stator compared to the MH prototype. Clearly this is not the case and further investigation was undertaken to understand the reason for the difference.

The first action was to disassemble the machine to check that the rotor had not suffered any more failures. A visual inspection flagged no concerns, but to confirm the rotor magnetic circuit had not deteriorated in its reconstruction, it was assembled back into the stator of the MH prototype and the back EMF measured. In the process of disassembling the FL machine, it was discovered that there was a 2.8mm misalignment of the stator and rotor axially. This was corrected, the machine reassembled and the back EMF re-measured.

The results of the back EMF re-measurement of both prototypes at 100Hz are presented as waveforms in Figure 7-4. It was found that the back EMF in the first prototype was the same, 100V at 240rpm, proving that the rotor magnetic structure had not been altered as a result of the rebuild. The realignment of the rotor and stator in the second prototype resulted in an increase in the back EMF of this machine. It rose from 137.5 to 142.5V at 240rpm. This puts the back EMF of the FL machine at 92.6% of the MH machine.

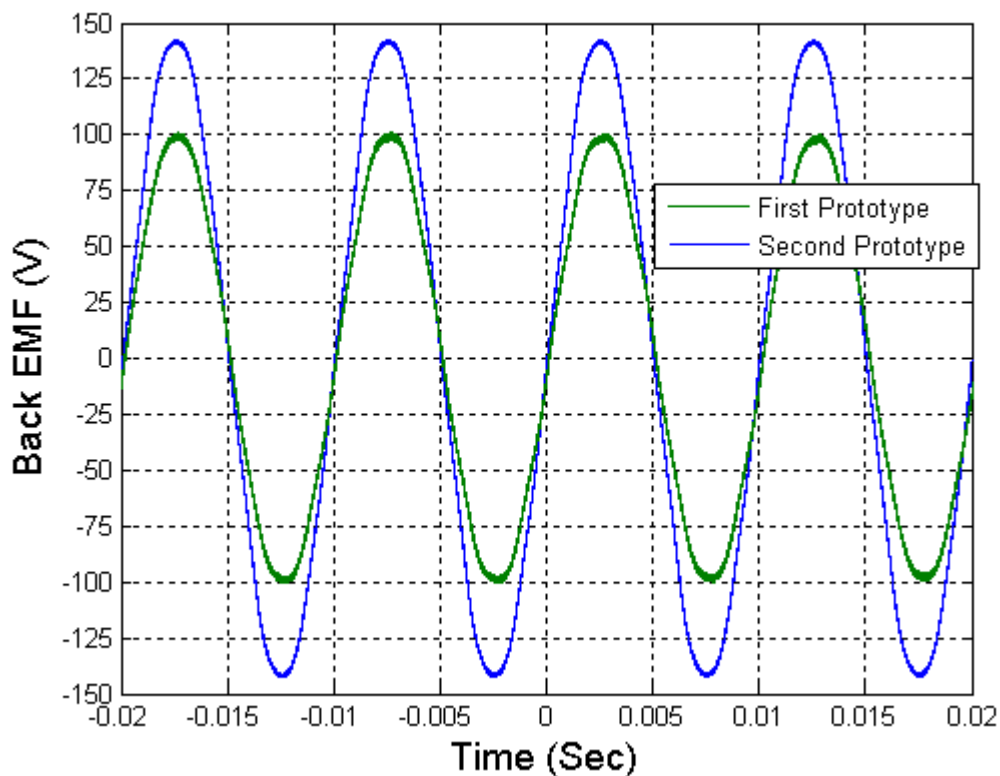


**Figure 7-4 Back EMF comparison of the first prototype (100) and the second prototype (142.5) after realignment of the rotor.**

### 7.3.2 Air-gap measurement

The other parameter that is simple to assess and could account for the differences in back EMF of the two machines is the magnetic air-gap between the rotor and the stator. At a distance of ~0.5mm (the physical air-gap being less due to the wrapping of the rotor), a small

difference of the order of 50 $\mu$ m could result in a measurable difference of back EMF. The bores of both machines were machined to size post assembly using a milling machine rather than turning on a lathe to reduce the axial forces on the teeth ends. The milling process will never be able to give as high a circularity tolerance as is achievable by turning on a lathe. The FL machine was also heated in the first thermal test to a level which possibly resulted in softening of the adhesive and may have allowed some movement driven by stresses held in the laminations from the jugged assembly. The result of these two processes means that a difference of the order of 50 $\mu$ m between the two stator bores is plausible.

The odd number of teeth on each side of the stator means that there are no opposing teeth and the bore could not easily be measured with a micrometer. So both machines were measured using a co-ordinate measuring machine (CMM). The distance of the centre of each tooth from the central axis was measured. The bore of each machine was then calculated as an average of all these measurements. It was found that there was a 0.092mm difference between the average diameter of the bores of the two machines (the FL machine having the larger bore), this means a 0.046mm difference in the air-gap between the stator and rotor. As the same rotor is used in both machines, its value is a constant and hence there was no requirement to measure it.

Other interesting data that results from the measuring of the stator bores, was the circularity or roundness of the bore. The FL stator had a much greater deviation of circularity with 0.111mm difference between the largest and smallest tooth on the side with skewed teeth and mechanical link between adjacent teeth. While the side created by the forming of the laminations had better circularity at 0.062mm. The MH machine had a much better circularity altogether at 0.031 and 0.036mm for the two sides of the stator. This fits with the fact that the modular assembly of the MH stator resulted in a much stiffer, less stressed structure compared to the FL machine.

### **7.3.3 Finite Element Calculated effect of air-gap differences**

The measured average air-gap difference of 0.046mm between the two machines was used in an FE model of the FL machine to compute a prediction of how much effect it would have upon the back EMF. A model of the rotor that was developed in FE for the MH machine was used as a basis for the FE model of the FL machine, as this part is common to both the prototype machines. To refresh the reader this model modelled air-gaps representative of glue joints between the magnets and flux concentrating blocks and the width of these gaps was used to calibrate the model against measured results.

The laminations of the stator of the FL machine were modelled with isotropic B-H properties as it would have been very difficult to model the anisotropic properties resulting from the laminations as the axis of anisotropy constantly changes as the laminations 'wrap' around the coil. The representation of the stator laminations in the model is shown in Figure 7-5, the obvious difference of this shape from the true stator is the square shape (as opposed to a more realistic constant volume of revolution curve in the bent lamination stack case) as the lamination wraps around the coil. This was considered an acceptable compromise as it is the effects of changes in the air-gap size that is under investigation and the extra material is out of the main flux path around the coil. However, not modelling the anisotropic permeability of the laminations will allow the flux to flow more freely and have a locally higher cross section and this will tend to produce a slight overestimate of the flux linkage.

When the model was run, it was found that it greatly over-predicted the back EMF compared to the measured results. This induced a rethink in the way in which air-gaps had been used in the first model to calibrate it against the measured results. Returning to the FE model of the MH machine, the extra air-gaps in the rotor and the stator were removed. The permeability of the SMC in both the rotor and stator was then reduced by a quarter via increasing the magnetic field strength by a factor of four for the same level of flux density. The justification for this is that the machining of SMC is known to have a substantial effect on the permeability of the material because of the formation of micro-cracks as a result of machining induced stresses. The SMC pole pieces are small in cross section and long in axial length and require substantial machining of an already weak shape and hence they might be expected to have significantly reduced maximum permeability. Using this modification it was found that the predicted back EMF and cogging torque profiles were similar to those achieved by using gaps as in the modelling shown in Chapter 4. However, this moved the dominating cause of the low flux levels, away from the stator and into the rotor.

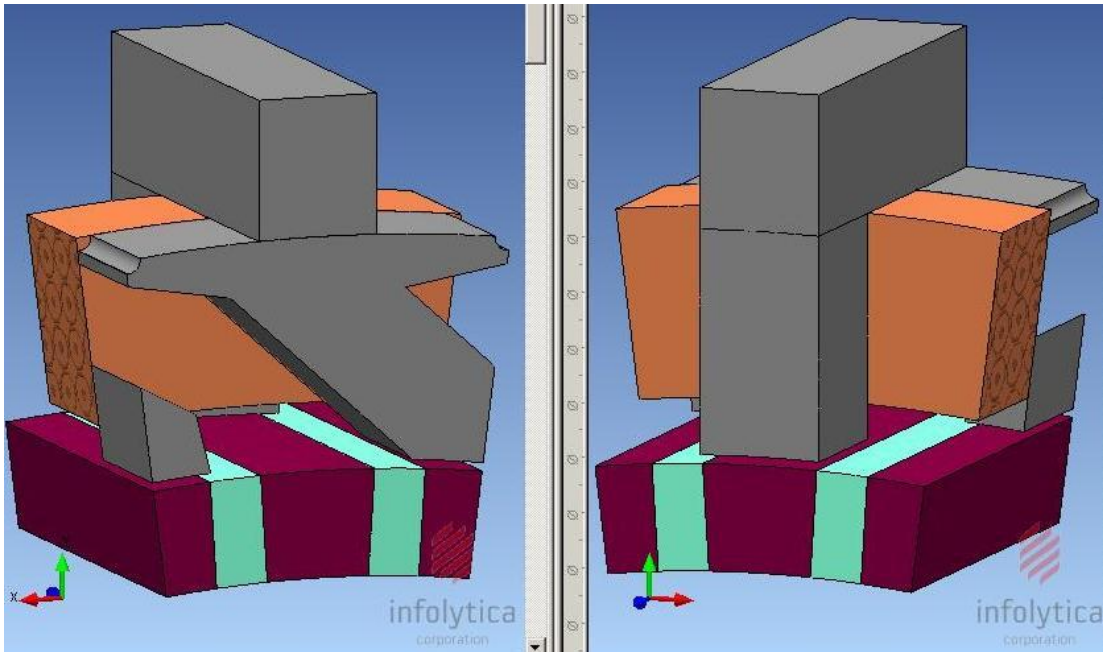


**Figure 7-5 the solid components (shown from both sides) of the 2 pole FE model for the FL machine**

To help understand the effects of changing the permeability of the SMC in different locations (rotor or stator) a similar graph to the one presented in Chapter 4 is presented in Figure 7-6. The iron parts of the FE model of the MH machine were given a linear permeability of 1000. Then the same model was run with the permeability of the rotor SMC parts (i.e. the flux concentration blocks) reduced to 200. The model was then run a third time with the permeability of the rotor SMC back at 1000 and the permeability of the SMC stator core-back decreased to 200. The graph in Figure 7-6 shows the Co-Energy against rotor position, the derivative of which is the cogging torque. Lowering the permeability of the machine's stator core-back, lowers the co-energy greatest around the aligned position (0 degrees and 180 degrees) and doesn't affect the co-energy in the unaligned position. It is this effect that controls the ratio of the peaks of the cogging torque. Lowering the permeability of the rotor flux concentrating blocks, reduces the co-energy for all rotor positions, however, it reduces the energy more in the aligned position than in the unaligned position. The result is the permeability in the rotor dominates the overall energy in the system but in a way that also accounts a lot towards the shape of the cogging torque.

Changing the permeability of the rotor SMC pieces affects the profile of the co-energy variation with rotor position. This differs from using an air-gap to reduce the effective permeability which gives a more linear change in co-energy for all rotor positions and a cogging torque variation further away from the measurements. It is impossible to be certain but it does seem from these later studies that the reduction in performance was more related

to damage caused by machining the SMC reducing its permeability than to the gaps inherent in the construction.

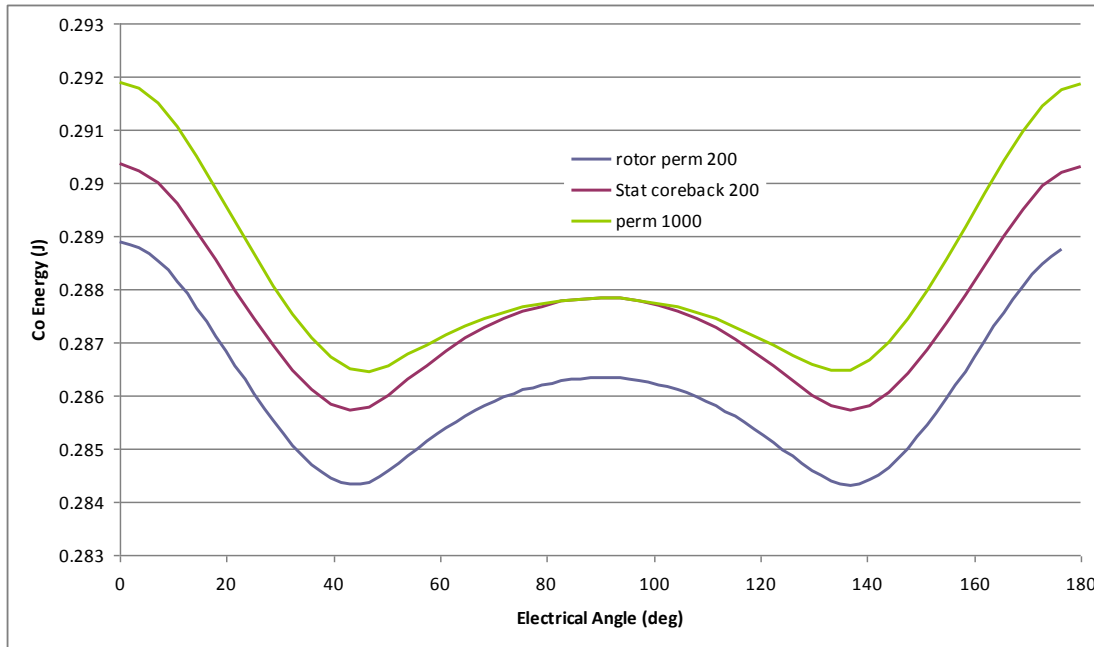


**Figure 7-6 Effect on Co Energy in the system for changing the permeability of the stator core-back or the rotor flux concentration blocks**

The new low permeability rotor model was integrated into the model of the FL machine. This model was then run to produce back EMF profiles for air-gaps of 0.5mm and 0.55mm. The results are shown plotted along with the measured back EMF in Figure 7-7. There is a peak difference between the two simulated results of 6V. This suggests that if the air-gap of the two machines was the same the measured peak back EMF would increase to 148.5V, which is 96.5% of the MH machine when the turns are taken into account. This is starting to be within the levels of material property and measurement tolerances. It is inevitable that properties of the lamination steel will have been degraded slightly in the bending process and this looks like it may be the reason for the missing 3.5% but it is impossible to be certain of the performance of the bent lamination stator given the uncertainty surrounding the rotor. The lack of performance in both machines seems to be attributed mostly to degrading the permeability of the SMC caused by introducing micro-cracks in the machining process. This feature would not be present in a production machine using only pressed parts.

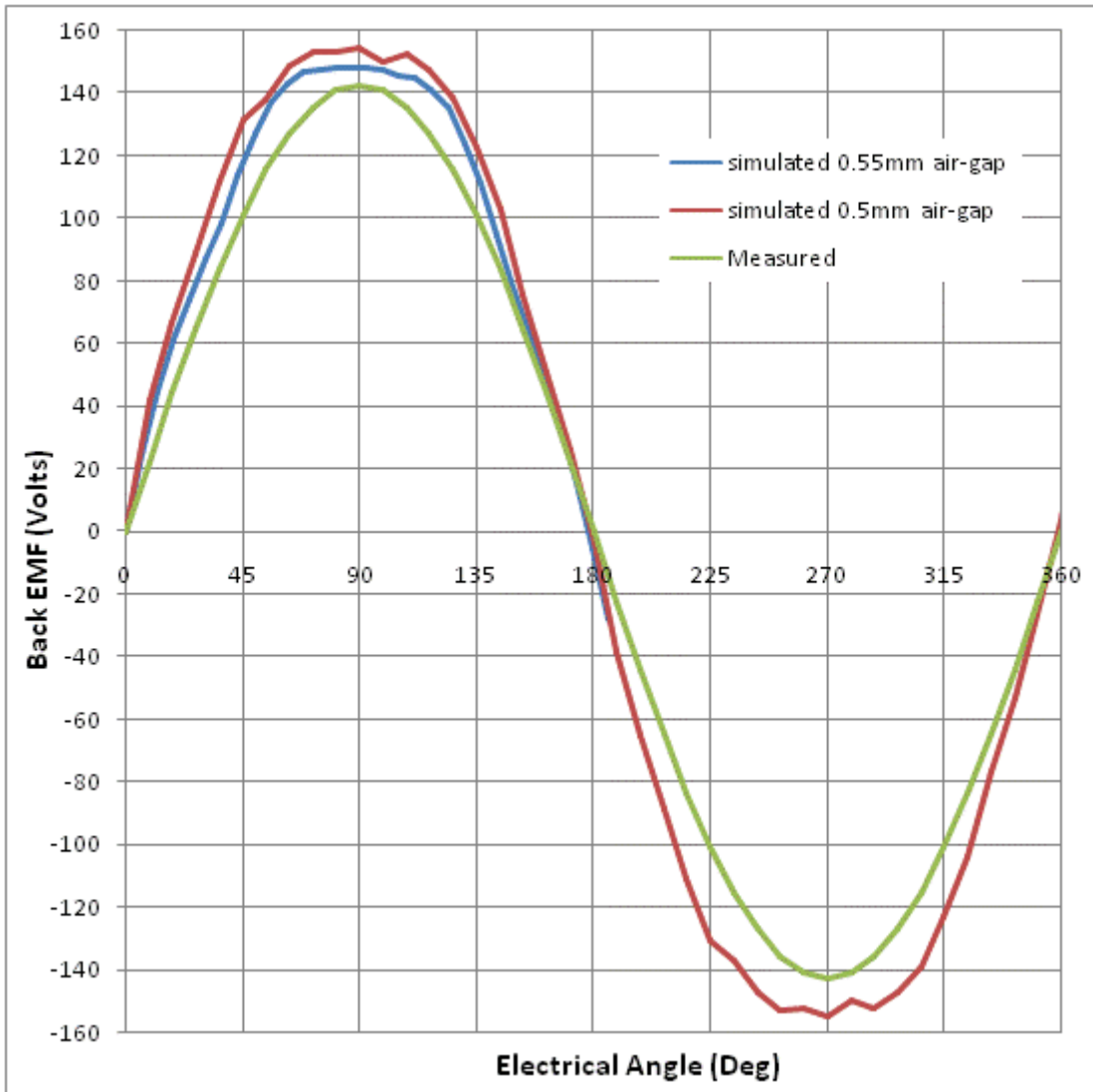


Figure 7-7 Measured back EMF along with simulated back EMF for different air-gap thicknesses

## 7.4 Static Torque Measurements

### 7.4.1 Cogging Torque

The measured cogging torque of the prototype is graphed against electrical angle in Figure 7-8 along with the measured value of the first prototype for comparison. It can be seen that there is a substantial difference in magnitude, but that the profile in terms of ratios of adjacent peaks is very similar. This is confirmed clearly in Figure 7-9 in which the measured data for the MH prototype has been scaled to 72% of the real value and as a result the two profiles follow each other closely.

The change in magnitude of the cogging can largely be attributed to the difference in air-gap size of the two machines, specifically the effect this has upon the flux that leaves the magnet

and reluctance of the path it takes. Equation (7-5), taken from Hanselman [55], shows the relationship that the flux interacting with the high permeable stator parts,  $\phi$ , and the reluctance of the path it takes,  $R$ , has with the cogging torque,  $T_c$ .

A good indication for the expected order of magnitude for the change in the cogging can be attained from the change in back EMF of the two machines (after the turns ratio is taken into account), as this is directly related to the flux that links the stator core-back. The ratio of the difference in the back EMF squared for the two machines is 0.8, which is greater than that of the cogging torques, but accounts for a large proportion of the difference. The flux linking the core-back does not account for all of the flux that the magnet produces. Some of it fringes back into the magnet linking with the high permeable teeth but not linking the coil via the core-back. As was explained in more detail in Chapter 4, this is responsible for the smaller peaks in the cogging centred around the unaligned position, or 90 degrees in Figure 7-8.

The larger air-gap in the FL machine, besides resulting in less co-energy in the machine, also affects the reluctance paths which the flux takes. The rate of change of reluctance relates directly to the cogging as shown in equation (7-5). In a conventional machine these reluctance paths are relatively simple and they can be approximately quantified with some confidence. However, the very nature of flux modulated machines means that the complexity of these reluctance paths greatly increases and understanding would require an in-depth FE analysis which is beyond the scope of this thesis.

$$T_c = -\frac{1}{2}\phi^2 \frac{dR}{d\theta} \quad (7-5)$$

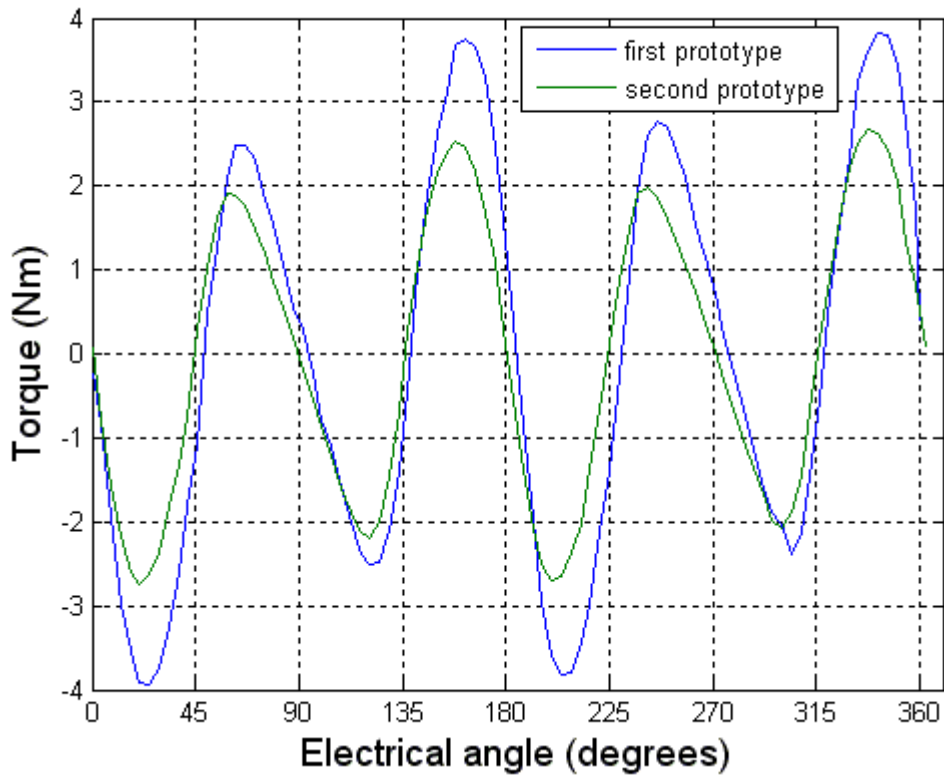


Figure 7-8 comparison of the cogging torque from the two prototypes

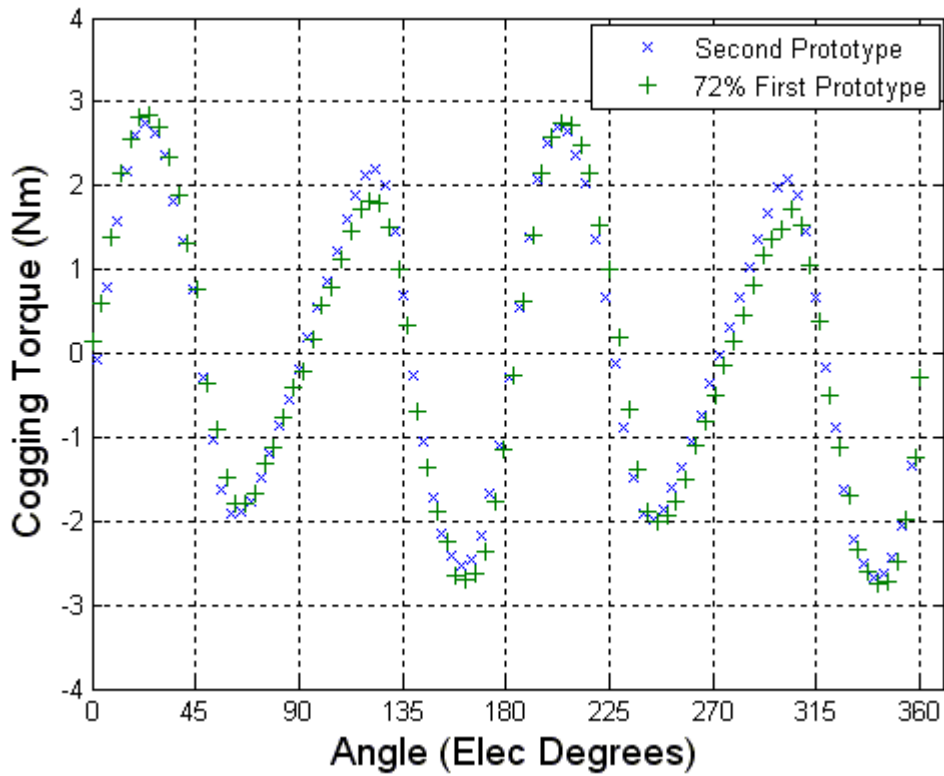


Figure 7-9 comparison of the cogging torques with the first prototype scaled to show the similarity in shape.

A comparison of the phase of the cogging torque of the two machines focusing on the zero torque crossing points, Figure 7-9, shows that the machines match up very well. The forming of the lamination around the coil might have been expected to be more likely to lead to not aligning the teeth of opposite sides of the stator correctly. There is a ratio of 25:1 for electrical to mechanical degrees in the machine, the crossing points of the zero torque axes in Figure 7-9 are within 10 electrical degrees of where symmetry would place them, i.e. every 45 degrees, which suggests a construction tolerance on the circumferential alignment within 0.4 mechanical degrees for all parts.

#### **7.4.2 Armature Excited Torque**

These measurements and the cogging torque data previously, were performed in the same setup that was used for the MH machine as described in Chapter 4. To refresh the reader, the shaft of the FL machine was coupled to a rotary table with a torque transducer in series between the two. The casing of the motor and the rotary table were held in a fixed position allowing the alignment of the rotor and stator to be adjusted by altering the rotary table. The armature was then fed a fixed DC current correlating to the values in the legend of Figure 7-10.

As was seen with the MH machine, the torque profile over one pole pitch (180 electrical degrees) is asymmetric in profile. This results from the sum of the cogging torque, which has no net value over one pole pitch, and the mutual torque resulting from the interaction of the magnet flux and the armature current. No comparison of these torque profiles for the two machines is shown here, as for an accurate comparison the armature MMF in both machines would need to be identical and no such result has been measured.

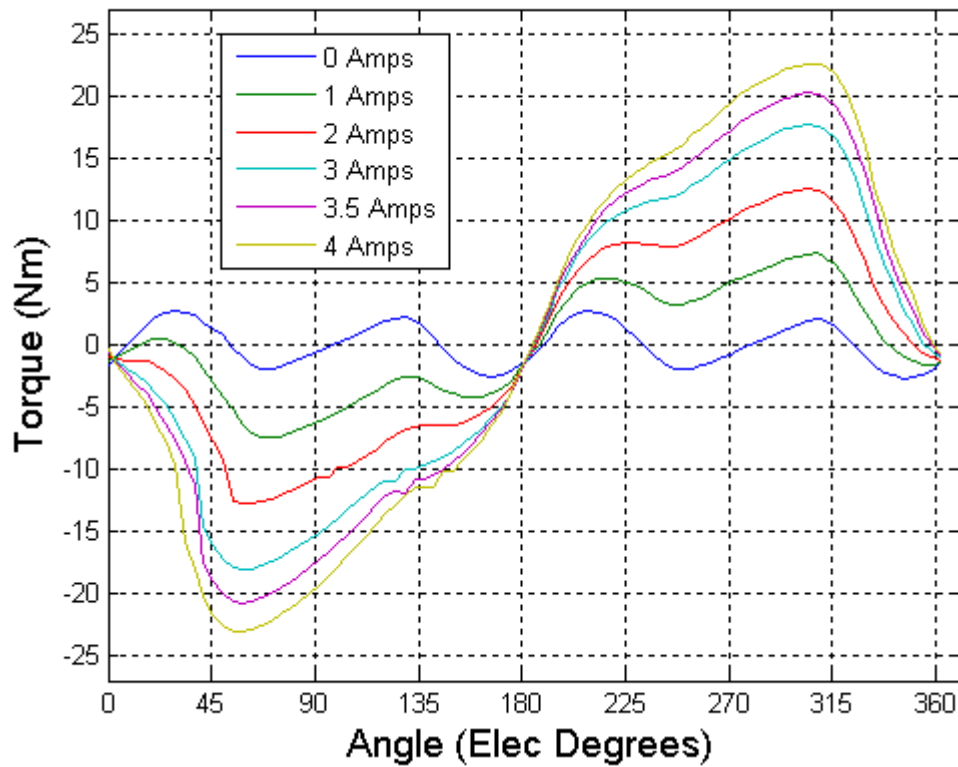


Figure 7-10 Armature excited torques

### 7.4.3 Average torque

To allow a fair comparison of the two machines the average torque over one pole pitch was calculated for the range of currents presented in Figure 7-10. The resulting average torque was then plotted for the two machines as shown in Figure 7-11 against MMF (thereby allowing a direct comparison). Figure 7-11 also has the average torque of the MH machine reduced to 88%, over plotted as points. 88% is the difference in the back EMF of the two machines and shows that the reduction in torque performance of the FL machine is directly a result of this loss of magnet flux linking the winding.

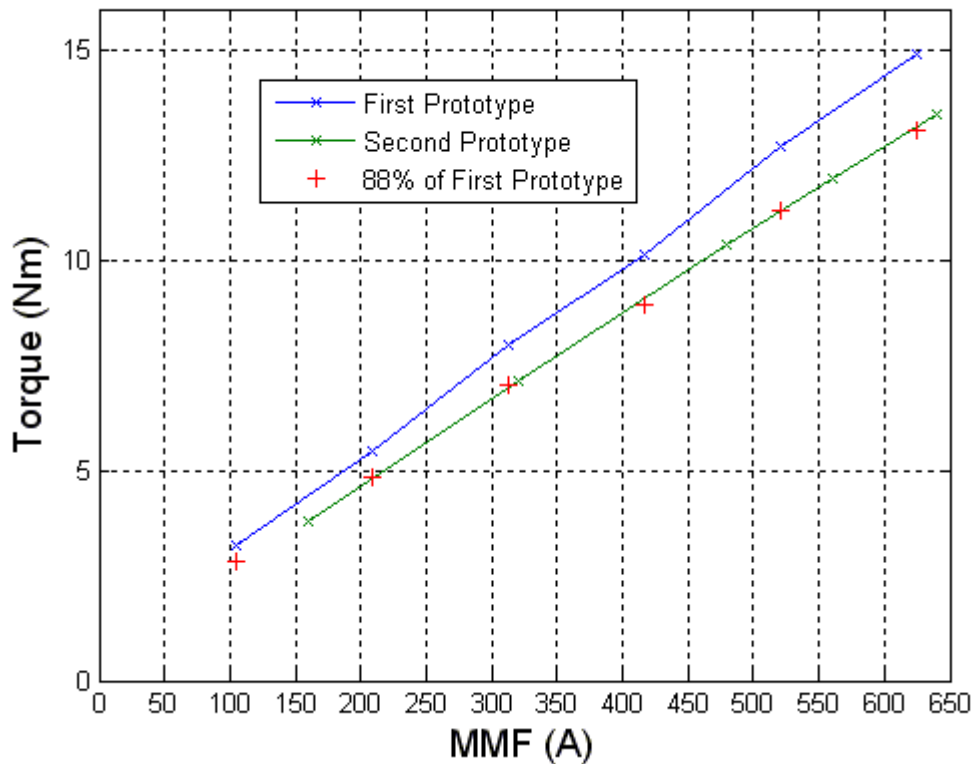


Figure 7-11 Average torque over a range of MMF of the two machines

## 7.5 Loss Measurements

The construction of this machine by folding the laminations raises the concern of loss of electromagnetic performance resulting from the stress imposed on the laminations. Loss data for the overall machine is presented in Figure 7-12 and was measured as follows. The prototype machine was coupled to a drive motor via a torque transducer. The transducer was able to measure instantaneous shaft torque and speed. This data was fed directly to an oscilloscope and internal software of the oscilloscope was used to take the rolling mean of the values. This was then recorded and the shaft power calculated as the product of the mean torque (Nm) and mean speed (rad/s) at each operating point.

The loss data is presented using a log scale in Figure 7-12. The gradient of a linear trend line fitted to the data is very close to 1. This suggests that the loss at these speeds is dominated by iron hysteresis loss which has a linear relationship with the frequency of the flux. At 100Hz /240rpm the motor is “producing” 15.1W of loss.

Using the loss data available from material manufacture in Table 7-1 and the weights of the parts presented in Table 7-2 an estimate for the iron loss of the machine can be made. For the stator, the estimated post machining weight is 630g and the average peak flux density of 1.3T at 100Hz would result in  $4.5 \times 0.630 = 2.8\text{W}$ . The rotor with an SMC mass of 342g and an

average peak flux density of 1.3T would result in  $16 \cdot 0.342 = 5.5W$  assuming a linear relationship between the data points available in the loss data in Table 7-1. This results in a total loss of 8.3W which is 55% of the loss measured. The measurement does not take into account losses in the magnets but FE results suggest that the change in the magnet flux density would be of the order of 0.02T which taking the data suggested by Fukuma et al [56] presented in Table 7-1 would give a loss of  $\sim 0.5W/kg$  and with the mass of magnet being only 162g, this loss will be negligible. There is also no account made for frictional losses such as windage and bearing loss as these are related to the square of the speed and the test speed is very low.

The difference of a factor of two in the measured and predicted loss from data sheets does fit with the idea presented earlier that the rotor SMC parts have been damaged in machining. Experience of this in the past has shown that this will increase the hysteresis loss of the SMC. In addition the bending of the laminations is also likely to increase hysteresis. It is not possible to separate the two.

**Table 7-1 Loss data for materials at 100Hz**

Material	Flux Density	Loss
Laminations (M270-35A)	1.0T	2.5W/kg
	1.3T	4.5W/kg
Somaloy 700	1.0T	9.5W/kg
	1.5T	20W/kg
NdFeB (source [56])	0.01T	0.04W/kg
	0.1T	4.0W/kg

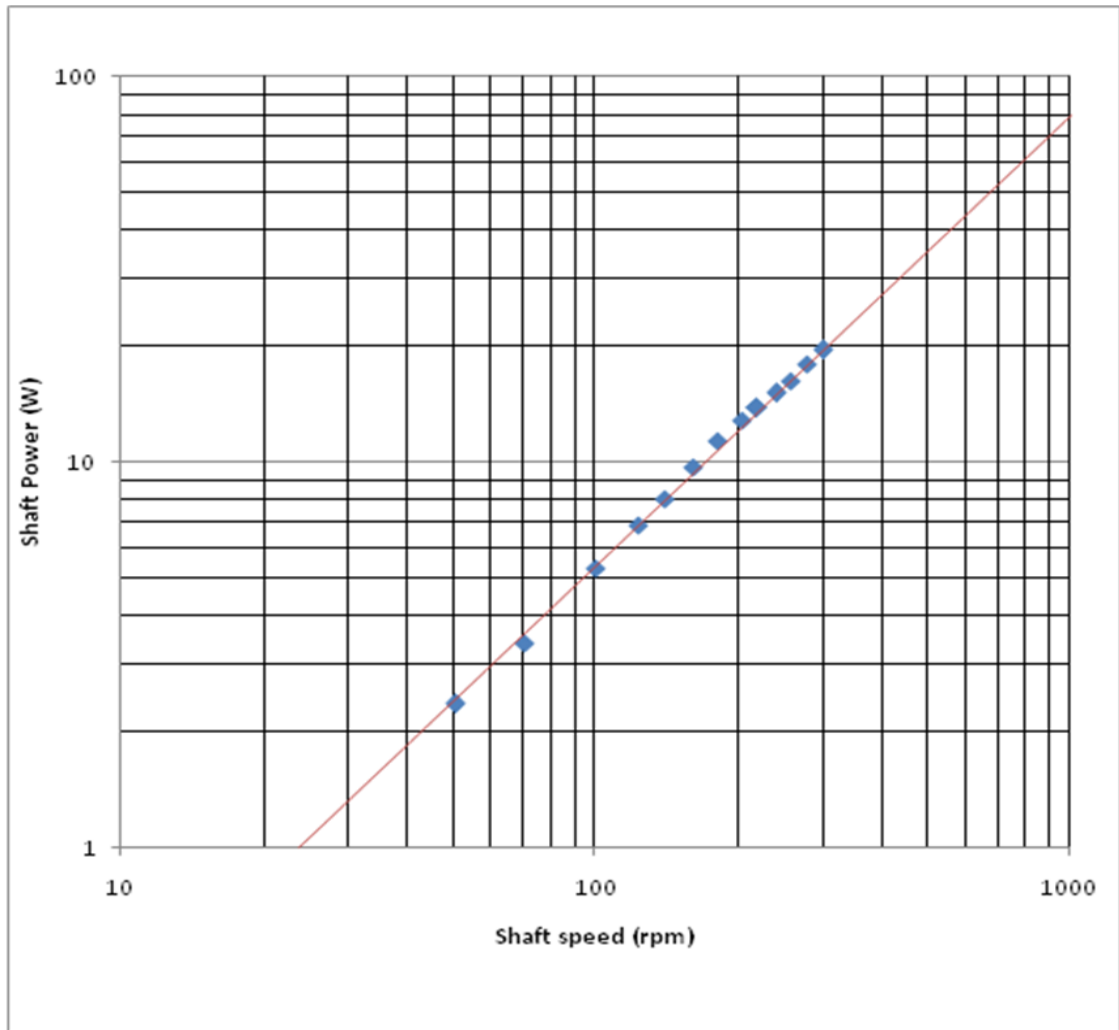


Figure 7-12 Loss data measured from the machine

## 7.6 Torque per unit Mass

The active weight for the FL machine consists of the SMC and magnets of the rotor and the laminations and coil of the stator. It totals 1.419kg, which is 88.5% of the MH prototype. This saving in mass is due to the removal of the need for mechanical links between teeth on both sides of the stator and that the SMC in the stator of the MH prototype was over engineered electromagnetically for mechanical reasons.

The average torque for the machine when square wave fed at the thermal maximum current of 4.1 amps (MMF=656) is 13.9Nm. That gives a torque per kg of active mass at 9.8Nm/kg. This value rises to 10.7Nm/kg when the correction of back EMF due to axial alignment and increased air-gap compared to the MH is taken into account, giving the two machines very similar Nm/kg capabilities. It should be noted that 10Nm/kg is a very respectable figure for a machine of this size which is naturally cooled (conventional machines might manage something more like 5Nm/kg at this size and pole number when naturally cooled).

**Table 7-2 List of the mass of different components**

Component	Weight (grams)
Single lamination (25 section)	36.6
Coil(potted)	285.1
Total Stator steel	<842 (less as material machined away
Stator steel post machining	~630 (estimate from CAD)
Total Rotor SMC	342
Total Rotor NdFeB	162

### ***7.7 Inductance measurement and Computed Power Factor***

The inductance of this machine was measured slightly differently from the first machine due to the availability of a new LCR bridge. The rotor is salient so the inductance varies with rotor alignment to the stator. The measured result is shown in Figure 7-13. The average value of the inductance is 40.2mH. The inductance of the two machines should be similar and should be related by the ratio of the turns squared. The MH machine average inductance was 19.7mH, so it would be expected that the FL machine inductance will be  $\sim 160^2/104^2 * 0.0197 = 46.6\text{mH}$ . The FL machine's per unit inductance is thus 86% of the MH machine

It should be noted that the bridge could only supply 2V, so the current was very low at  $\sim 0.13\text{A}$ . At this level it is possible that the measured results shown in Figure 7-13 are prone to hysteretic effects and probably lower than the true value.

The FL machine's stator has less surface area and leakage flux created by near adjacent surfaces may be lower. In addition the back emf results also indicate that the FL machine's stator may have a higher reluctance. It is not possible however to draw any really firm conclusions and in reality the differences are relatively small.

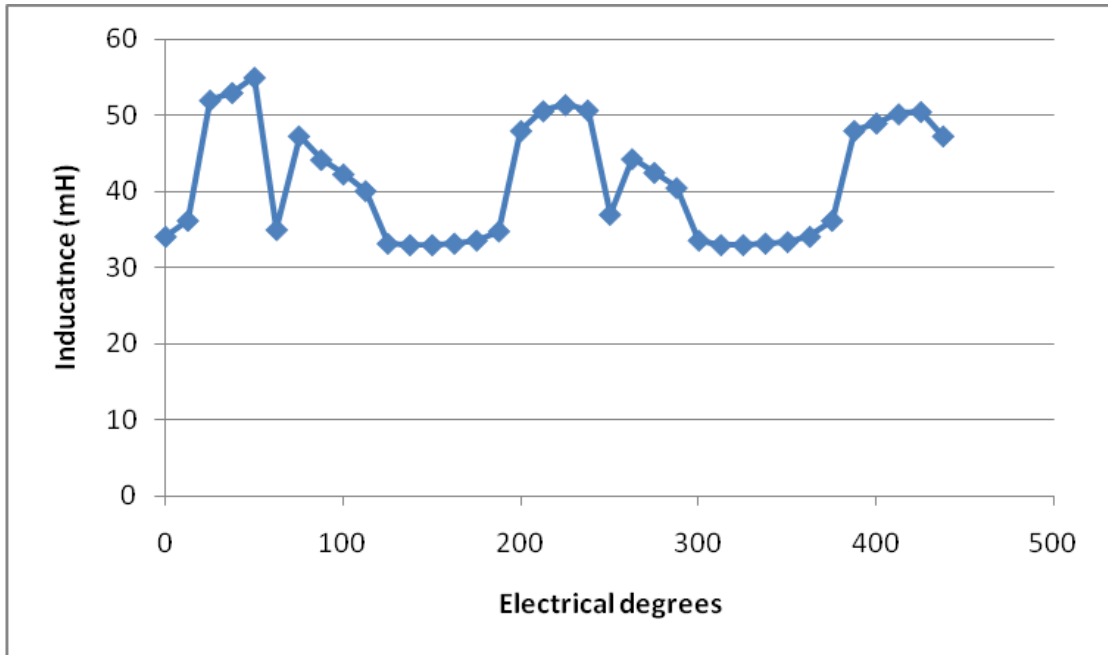


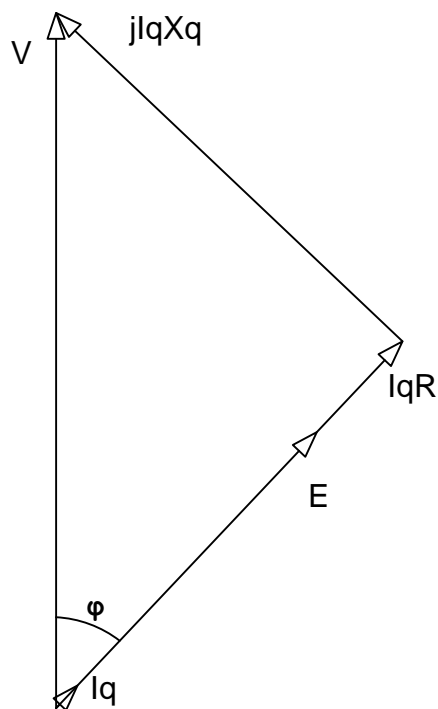
**Figure 7-13 Measured inductance of the FL machine**

Considering the machine in its maximum torque operating condition, which is when the back EMF leads the armature current by 90degrees, and assuming that the current is sinusoidal, it is possible to make a prediction for the power factor angle. The values used for making this calculation are shown in Table 7-3, and the prediction is  $\varphi=43.5\text{deg}$ . A voltage vector diagram for the machine operating in this condition is shown in 7-14, and it is clear to see that the machine's reactance is significant (1.25pu taking the back EMF as 1pu). This angle means that the converter power electronics VA will have to be over-rated to 137% as compared to the output power of the machine.

Whilst a reactance of 1.25pu is a lot larger than would typically be found in a naturally cooled conventional permanent magnet machine it is very competitive when compared with machines with equal torque density (which need forced cooling and hence much higher current densities and resulting armature fields).

**Table 7-3 Values to calculate power factor**

Parameter	Value
L average	0.038
$L_q$	0.0486
Frequency	50
$X_q$	15.27
R	4
$I_{rms}$ thermally rated	4.14
$E_{rms}$	50.38
$I_q X_q$	63.21
$I_q R$	16.56
$V_{rms}$	92.07
Theta	43.5
Power factor	0.73

**7-14 Voltage vector diagram for maximum torque at 120rpm, 50Hz**

## Chapter 8. Conclusions

### 8.1 Design

The design of the first prototype using FE showed that the material hybrid design concept with 12 poles would have a similar torque density to the 24 pole claw pole machine built by Jack et al [23]. The work also indicated that this pole number was suboptimum and that a 50 pole machine would be a much better choice to improve the torque density that could be achieved without the fine detail of the topology making construction difficult.

For fixed outer dimensions of the machine, FE was used to calculate the values of stator tooth and coil width in the axial direction such that a flux density of 1.3-1.4T could be achieved in the air-gap between the stator and the rotor. The apparent natural shape for the teeth is to make them wider circumferentially with radial distance from the air gap to start to spread the radial flux out circumferentially and hence allow a thinner core back. However this resulted in a core-back which was much thinner than would be practically possible to manufacture. Making the core-back thicker for mechanical purposes, the design was altered to utilise the extra core-back material magnetically by removing the radial taper of the teeth and allowing the isotropic permeability of SMC to take more of a role in spreading the flux circumferentially. It was shown that this helped in reducing armature reactance by minimising the crossover of flux axially between teeth of opposite polarity. The reduction in reactance was shown to be substantial, as well increasing the amount of field flux linking the winding which both lead to an overall improvement in the machine's performance.

This early work illustrated just how complex the interaction between the dimensions is and how difficult it is to achieve anything like an optimum. A first conclusion therefore is that there is a great deal of scope for further improvements in the design and in the process of the design for instance by exploring methods to automate the design optimisation, such as that performed by Dickinson et al [25] for a claw topology modulated pole machine. In chapter 2 the effect of only a few variables is considered, but there are a multitude of dimensions to which the machines performance is very sensitive.

### 8.2 Construction of the first prototype

At the end of Chapter 2, a suggested design was proposed for the manufacture of a prototype. Chapter 3 presented the detail of realising the prototype. The material hybrid concept that was presented is modular allowing all components to be manufactured individually and then brought together at the end to form the finished assembly. With the exception of the cutting of the laminations, all of the individual components were

manufactured in-house and were challenging to manufacture. However, the stator laminations were probably the most challenging as there was little or no experience in firstly producing such long strips and even less in the proposed method to assemble them into a stack. Whilst the methods of manufacture were basically successful the size of the SMC pieces raised concerns for micro-cracking during the machining process, and the small radial thickness of the SMC arcs resulted in substantial deformation in the post machining heat treatment process. The method of bending the ligatures in the laminations to form a circle relies on a plastic deformation process which is beyond adequate computation and hence extra material was added to allow the final outer diameter to be machined post bending and the inner diameter to be machined post assembly.

If the bending lamination concept was to be used in production, it is the author's view that refinement of the procedure along with improved jig design could produce parts which would allow construction of the lamination stacks and their assembly without the need for machining steps.

The biggest area of known risk within the prototype was the build-up of tolerances of the SMC wedges and magnets for the rotor. There was a real risk of these resulting in either a lot of significant gaps or insufficient space when assembled onto the rotor mount. The final assembly was adequate, although some of the gaps between adjacent components would preferably have been less. However, considering this in a large scale production the problem of compound tolerance in stacks is a big issue. The pressing production method of the SMC wedges should result in high tolerance parts with an even higher level of consistency between parts. On the other hand the production of sintered NdFeB magnets always requires considerable amounts of machining due to the large deformation in the sintering process. This means that high tolerances usually result in a heavy levy on the unit cost.

It would be interesting to see future work on the rotor looking at different magnetic materials in the same structure. Compression bonded NdFeB magnets for instance have a very high tolerance, possibly better than SMC parts as there is no heat treatment process in the post pressing of the powder. While a bigger radial depth of active material may be needed to compensate for the lower residual flux density to achieve similar flux densities in the air-gap of the machine; this might be compensated by the ability to reduce construction gaps which in turn may allow a lower working air-gap between the rotor and stator, increasing the magnetic loading of the machine. Alternatively, it may just win on a cost basis, depending which is more important for the specific application.

The final winding had a very good copper fill factor in the region of 80% for a given cross sectional area of the winding. However, the circularity on the outer diameter was not very

good, resulting in a poor thermal contact with the SMC of the core-back. The extra air-gap between the winding and the core-back shows that the true fill factor of the slot is probably less than 80%, but it is still very high. The principal cause of the lack of circularity was a bulge in the coil in the region of the crossover between layers in the winding. It is likely that precision computer controlled winding machines common in commercial practice could help to improve this point.

The final assembly of the stator was demanding as the span of one pole was only 7.2 degrees. This meant that a good tolerance of alignment between the lamination stacks either side of the winding was critical. The similarity of the measured cogging torque between pole spans suggested that this had been achieved. If a higher pole number was chosen to increase the torque density, achieving this alignment will become increasingly difficult.

### **8.3 Measured Results**

The thermal limiting current of the machine, (which was taken to be the dc current which results in a 100°C average winding temperature rise above ambient), was predicted from the measured data to be 7 Amps which correlates to the machine dissipating 91.6Watts. At this level the machine does not saturate magnetically, meaning a higher specific torque could be achieved by higher electrical loading. This would require either optimisation of the slot and iron axial length ratio or improvement of the thermal paths by refined production processes.

The machine torque was measured statically over a range of positions. The cogging torque was measured over a full revolution and its regularity (as noted above) confirmed the good concentricity in the manufacture of the machine. The FE design of the machine was performed on an aligned D-axis flux co-energy basis which meant that the profile of instantaneous torque was not predicted. When measured, the profile of the cogging produced a shape that oscillates at four times fundamental torque, double what is seen in a conventional surface mounted permanent magnet machine. This had been observed in previous work by Maddison [24] but no detailed explanation was given. With the availability of better software, the causes of the profile of the cogging were able to be investigated. It was shown that the shape results from the salient rotor topology. Peaks around the aligned position are governed by the reluctance of the path the flux takes in the iron around the coil. The peaks around the unaligned position are governed by the reluctance of the path the field flux takes without linking the coil. From this, suggestions for the size of air-gaps between adjacent components could be made which would allow the cogging torque profile to be controlled (either maximised to create *détente* torque in an actuator or minimised for smooth running). Interestingly, an improved machine construction with reduced construction gaps

and higher permeability SMC would result in the cogging being dominated by the peaks around the aligned position.

The armature excited torque was measured over two pole pitches with a dc current feeding the winding, (which is representative of a square wave feeding the machine in a continuous rotation situation). The results show that the initial FE prediction for average torque was considerably more than the true measured value. The FE study retrospective of the measurements being taken showed that this could be attributed to air-gaps of the order of 0.1-0.2mm in the glue joints of the stator of the construction. That is those between the magnets and SMC concentration blocks in the rotor and between the laminated teeth and the SMC core back of the stator. On the other hand further investigation when considering the second machine showed that the reason for the reduction in torque was more likely due to a reduced permeability of machined SMC pieces.

The profile of the measured armature excited torque is asymmetric across a pole width, even though the geometry is symmetrical. This is a result of the cogging torque interacting with the torque resulting from mutual flux between the rotor and stator.

The measured data was not taken to the full value of the thermally limiting current because of fears of further rotor failures (see later explanation). The average torque shows good correlation between the measured and that predicted from the retrospective FE work. It is also noted that the machine is showing no evidence of saturating over the measured range (and in the predictions beyond the measurements). This means that the torque at the thermally rated current can be confidentially predicted at 16.78Nm which gives a torque per active mass of 10.49Nm/kg.

The inductance of the machine alters with alignment of the stator and rotor due to the salient nature of the rotor. The value in the unaligned position is of most interest as this is (near to) the angle that the excitation would need to be applied to get maximum torque per ampere. Based around this value and a supply frequency of 50Hz (which corresponds to a rotor speed of 120rpm) a voltage vector diagram can be established to predict the power factor angle (i.e. between the supply voltage and current). This was calculated at 44.6degrees. The cosine of this angle is the displacement power factor, this is important as it tells how much a converter supplying the machine must be overrated in VAs. This comes out at 0.71 meaning that the VA rating for a converter would have to be 141% of the real power capability of the machine. This is a good figure in relation to what has been achieved with modulated pole machines, but it is low in comparison to naturally cooled conventional machines which commonly achieve greater than 0.9.

### **8.4 Formed Lamination Concept**

The results of the material hybrid prototype were promising, however, the SMC core-back was thin radially and will be problematic in mass production. This led to the development of the formed lamination idea which aimed to produce the entire stator by forming a single stack of strip laminations. This (what might be termed an “origami”) approach is unorthodox and has the undesirable feature of stressing laminations during bending which can deteriorate the electromagnetic properties of the lamination. Unlike the MH machine, where the bend in the lamination was very localised and carried little flux, the formed lamination concept requires folding the lamination orthogonally to the direction of main field flux travelling within it.

Different methods of creating the stack were discussed including one length of lamination rolled up and multiple laminations of different dimensions. These were both discounted on practicality grounds even though patents for the former method exist [43, 44]. It was decided that a stack of laminations all the same shape would be best. The core-back would be much thicker than in the MH prototype, so the core back would be made of multiple short circumferential sections. To allow the same rotor to be utilised, the laminations needed to incorporate a skew of one pole pitch. The location of this was found to be best on one side of the stator hence removing it from the forming process.

To test the concept, a three section test was performed. It was found that “spring back” – the tendency of the bent section to relax slightly after removal of the bending force – was substantial. The amount of spring back relates to the severity of the bend and hence bending a stack (where each lamination in the stack has a successively larger bend radius) tends to make the lamination “fan out”. Each bend during the testing was subjected to different methods of compression during the forming to try and reduce spring back, but these were found to make only a small difference. Future work could be envisaged where over-bending is utilised to reduce the spring back effect, as this would make assembly much simpler. It is clear from examination of commercial bends in like components had a far better shape than was realised here and that therefore there is much that can be learned. Notwithstanding the problem it was clear from the three section test that a core could be bent to shape and that the spring back could be overcome by clamping during assembly.

Following this success a full 25 section prototype stator was manufactured using the same techniques developed with the three section test. It was found more difficult to hold the lamination in a jig and hold this jig in a bending machine to form the strip-long U shaped stack. This resulted in some practical protocols being developed to achieve a relatively good shape. Although the forces used in the actual bend were low, some compression applied after bending to reduce spring back did result in damage to one of the lamination teeth.

The coil for this prototype was manufactured in the same way as that of the MH prototype. However, to try and improve the circularity of the outer diameter of the coil, thinner wire was used which resulted in a 54% increase in the turns. It should be noted here that no specific turn number was sought, the aim being simply to keep excitation current requirements within the available supply limitations. It was found that this did improve the circularity of the winding, but a noticeable bump still existed in the region of interchange between layers.

The final shape of the laminations was formed around the winding using it as a jig and thereby encasing the coil in its final position. It was thought that achieving a symmetrical shape would be difficult, but it was found that a good result could be achieved if only two adjacent sections were considered at any one time. The final assembly was potted into the case with a jig compressing the laminations axially to remove the spring back and create the correct alignment. The final bore was machined using a milling machine. It had been a worry that machining the laminations would result in problems but in practice the machining process was benign and no local or global failures resulted. The integrity of the core remained good across all of the tests. The rolling up of the laminations onto the winding also resulted in a better fit between the core-back and the winding than the MH prototype.

### **8.5 Measured Results FL prototype**

The testing of this second prototype was undertaken in the same fashion as the MH prototype. First a thermal test was performed to allow the calculation of a thermally limited current which resulted in a 100°C rise above ambient temperature. The first attempt to do this was performed with a current that was too high. This allowed the machine to reach a temperature in the mid seventies, which is around the temperature that the room temperature cured adhesives used starts to soften, causing a rotor failure. The second test was run at a much reduced current. It was found that this machine could dissipate 68.6Watts which is only 74.9% of the MH prototype. This was not a surprise as the major heat path is across the plane of the laminations in which direction there is a much lower thermal conductivity because of the interlaminar gaps. The castellated core-back also has a large part to play in the reduced thermal performance, as the area of lamination in contact with the casing was of the order of a third of the first machine. Future work should look at improving the case geometry to mimic the castellation giving an improved thermal path out of the machine. Alternatively, the case may be designed to fit between the core-back laminations, exposing them to the ambient air directly.

It was discovered that the high temperature in the first thermal run had allowed some of the rotor glue joints to fail. However, the glass fibre wrap prevented considerable movement of the parts and it was not discovered until static torque measurements were taken with current

in the armature. The increased forces involved in this test allowed the glass fibre to stretch and the active parts of the rotor moved away from the aluminium mount and interfered with the stator. This required a rebuild of the rotor in which all the active parts were recovered and then re-glued onto the mount, this time wrapped with Kevlar thread with a much higher pre-tension. Thereafter there was more caution exercised to make sure rotor temperatures were kept low. In retrospect far higher glass transition temperature adhesives should have been used and this issue should not be seen as a limiting problem in a production machine.

The static torques were measured over a range of currents and it was found that the average torque per MMF (which takes into account turns difference) was only 88% of the MH machine. A back EMF test confirmed that this was a result of less field flux. This instigated accurate measurement of the stator bores of the two machines using CMM and highlighted a 0.092mm difference between the two the FL machine having the larger bore. This may be compared with a nominal air gap of 0.5mm – in other words the air gap in the FL machine was nearly 10% larger. In disassembling the FL prototype it was also discovered that there was an axial misalignment. This was corrected and resulted in an increase in flux. It was then shown with FE that the remaining difference could mostly be attributed to the difference in stator bore.

In discussion on the first prototype it was suggested that the difference in performance of the FE predictions and measured results was a result of the relatively large gaps in the construction of the stator between the core back and teeth. If this was the case, it would be expected that the FL machine with no gaps in the stator would outperform the MH machine, but actually the results are very similar when differences such as turns and air-gap size are taken into account. This resulted in the proposal that the reduced performance of the MH machine was a result of the reduced electromagnetic properties of the SMC resulting from machining. The FE showed that changes in the permeability of the large volume of SMC in the rotor dominates the performance and could account for the difference between the measured results from the MH prototype and the original FE prediction. This theory was backed up with the measurement of loss in the machine, produced purely as a result of rotating the rotor. It was found that this was predominantly hysteresis loss, which is the prevailing form of loss in SMC at low frequencies and increases when damage occurs in machining.

The FL machine is only 88.5% of the mass of the MH machine as a result of being able to remove the mechanical link on one side of the lamination stack. However, the FL machine produced slightly less average torque, even when corrections were made for the difference in air-gap size. This resulted in the two machines having very similar torque per active mass

capabilities. However, the predicted power angle is smaller for the FL machine resulting in a small improvement of the power factor to 0.73. This means that there would be a small saving of 4% in the VA overrating requirement of the converter feeding the machine.

## **8.6 Closing Statement**

At the onset of this thesis the aim was to develop methods for constructing modulated pole machines that are realisable for low cost production. One of the key ways it was thought that this could be achieved was by reviewing the specific properties of SMC and laminated steel by utilising each material where it is best suited. Based on this aim, two designs have been developed and constructed. Testing of them reveals very similar performance, and results compare favourably against other modulated pole machines and they have characteristics which may suit some industrial applications. It is the author's belief that both designs are realistic for mass manufacture although no in depth study has been performed. As a result it would be fitting for future work to refine the design of the machines, address some of the issues raised by the prototypes and perform an in-depth study of the suitability of the designs in medium to large scale production.

Both machines employ highly novel construction methods which necessarily have a very small experience base to lean on. It is clear that there is a good deal of scope for future work to improve the methods used and hence gain significant improvement in ease of manufacture and performance. One example that the author would like to see is the use of compression bonded magnets in the flux concentrated rotor. Another would be an in depth study of the effect bending the laminations in these designs has upon the loss characteristics of the steel.

---

## References

- [1] Höganäs\_Ltd, "Home page - Höganäs Ltd," [Online]. Available: [www.hoganas.com](http://www.hoganas.com). [Accessed: 2010].
- [2] H. Weh, Hoffmann, H, and Landrath, J, "New permanent magnet excited synchronous machine with high efficiency at low speed," *Proc. Int. Conf. Electrical Machines (ICEM88)*, 1988.
- [3] H. M. Weh, H, "Achievable force densities for permanent magnet machines in new configurations," *Proc. Int. Conf. Electrical Machines (ICEM86)*, 1986.
- [4] E. Hughes, *Electrical Technology*, revised by Ian McKenzie Smith, 7 ed.: Addison Wesley Longman Ltd., 1995.
- [5] A. E. Fitzgerald, C. Kingsley, and S. Umans, *Electric machinery*, 6th ed. New York :: McGraw-Hill Book Co, 2002.
- [6] W. M. Arshad, T. Backstrom, and C. Sadarangani, "Analytical design and analysis procedure for a transverse flux machine," in *Electric Machines and Drives Conference, 2001. IEMDC 2001. IEEE International, 2001*, pp. 115-121.
- [7] G. W. Mclean, "Brushless d.c. drives using claw-type stator and disc rotor," *Proc. IEE*, vol. 126, pp. 683-689, 1979.
- [8] P. G. Dickinson, "Application of Soft Magnetic Composites in Electrical Machines," Ph.D. Thesis, University of Newcastle upon Tyne: Newcastle upon Tyne, 2002.
- [9] N. Tesla, "Alternating-Electric-Current Generator," United States Patent No. 447921, 1891.
- [10] E. F. W. Alexanderson, "High-Frequency Alternator," G. E. Company, Ed. United States Patent No. 1008577, 1911.
- [11] F. A. Furfari and E. L. Owen, "Rediscovering William Stanley, Jr. Part 2," *Industry Applications Magazine, IEEE*, vol. 10, pp. 10-13, 2004.
- [12] E. L. Owen, "Rediscovering William Stanley, Jr. Part I," *Industry Applications Magazine, IEEE*, vol. 9, pp. 9-12, 2003.
- [13] W. M. Mordey, "Electric Generator," United States Patent No. 437501, 1890.
- [14] R. H. Bertsche, "Dynamoelectric Machine," United States Patent No. 2928963, 1960.
- [15] H. R. Kirchmayr, "Permanent magnets and hard magnetic materials," *Journal of Physics D: Applied Physics*, vol. 29, p. 2763, 1996.
- [16] T. Hattori, Y. Suzuki, and T. Yamada, "Analysis of permanent magnet type stepping motor with claw poles using electromagnetic field analysis," in *Electrical Machines and Systems, 2008. ICEMS 2008. International Conference on, 2008*, pp. 3539-3543.

- 
- [17] L. Seung-Bin, J. Dae-Sung, K. Ki-Chan, K. Dae-Hyun, and L. Ju, "Characteristic Analysis of Permanent-Magnet-Type Stepping Motor With Claw Poles by Using 3 Dimensional Finite Element Method," *Magnetics, IEEE Transactions on*, vol. 43, pp. 2519-2521, 2007.
- [18] M. R. Harris, G. H. Pajooman, and S. M. Abu Sharkh, "The problem of power factor in VRPM (transverse-flux) machines," in *Electrical Machines and Drives, 1997 Eighth International Conference on (Conf. Publ. No. 444)*, 1997, pp. 386-390.
- [19] R. J. Parker and R. J. Studders, *Permanent magnets and their application*: New York: Wiley, 1962.
- [20] M. Bork and G. Henneberger, "New transverse flux concept for an electric vehicle drive system," in *Proc. Int. Conference on Electrical Machines (ICEM)*, Vigo, Spain, 1996.
- [21] G. Henneberger and M. Bork, "Development of a new transverse flux motor," in *New Topologies for Permanent Magnet Machines (Digest No: 1997/090), IEE Colloquium on*, 1997, pp. 1/1-1/6.
- [22] H. Weh, "Transversal Flow Machine in Accumulator Arrangement," Germany: J. M. Voith GmbH, 1988.
- [23] A. G. Jack, B. C. Mecrow, C. P. Maddison, and N. A. Wahab, "Claw pole armature permanent magnet machines exploiting soft iron powder metallurgy," in *Electric Machines and Drives Conference Record, 1997. IEEE International*, 1997, pp. MA1/5.1-MA1/5.3.
- [24] C. P. Maddison, "Transverse Flux Machines for High Torque Applications," Ph.D. Thesis, University of Newcastle upon Tyne: Newcastle upon Tyne, 1999.
- [25] P. G. Dickinson, A. G. Jack, and B. C. Mecrow, "Improved permanent magnet machines with claw pole armatures," in *International Conference on Electrical Machines (ICEM)*, Brugge, Belgium, 2002.
- [26] B. C. Mecrow, A. G. Jack, D. J. Atkinson, P. G. Dickinson, and S. Swaddle, "High torque machines for power hand tool applications," in *Power Electronics, Machines and Drives, 2002. International Conference on (Conf. Publ. No. 487)*, 2002, pp. 644-649.
- [27] Y. P. Dou, Y. G. Guo, J. G. Zhu, and H. Y. Lu, "Effect of Armature Reaction of a Permanent-Magnet Claw Pole SMC Motor," *Magnetics, IEEE Transactions on*, vol. 43, pp. 2561-2563, 2007.
- [28] Y. G. Guo, J. G. Zhu, and H. Y. Lu, "Effects of Armature Reaction on the Performance of a Claw Pole Motor With Soft Magnetic Composite Stator by Finite-Element Analysis," *Magnetics, IEEE Transactions on*, vol. 43, pp. 1072-1077, 2007.
-

- 
- [29] R. Qu, G. B. Kliman, and R. Carl, "Split-phase claw-pole induction machines with soft magnetic composite cores," in *Industry Applications Conference, 2004. 39th IAS Annual Meeting. Conference Record of the 2004 IEEE*, 2004, pp. 2514-2519 vol.4.
- [30] J. Cros, J. R. Figueroa, and P. Viarouge, "Analytical design method of polyphase claw-pole machines," in *Industry Applications Conference, 2004. 39th IAS Annual Meeting. Conference Record of the 2004 IEEE*, 2004, pp. 1397-1404 vol.3.
- [31] C. P. Maddison, B. C. Mecrow, and A. G. Jack, "Claw Pole Geometries for High Performance Transverse Flux Machines," *Proc. Int. Conf. on Electrical Machines (ICEM98), Istanbul, Turkey*, pp. 340-345, 1998.
- [32] L. O. Hultman and A. G. Jack, "Soft Magnetic Composites – Motor Design Issues and Applications," PM<sup>2</sup>TEC 2004, in Chicago, USA
- [33] A. G. Jack, "The impact of new materials on the design of electrical machines," in *Impact of New Materials on Design, IEE Colloquium on*, 1995, pp. 1/1-1/5.
- [34] M. Persson, P. Jansson, A. G. Jack, and B. C. Mecrow, "Soft magnetic composite materials-use for electrical machines," in *Electrical Machines and Drives, 1995. Seventh International Conference on (Conf. Publ. No. 412)*, 1995, pp. 242-246.
- [35] L. Hultman, M. Persson, and P. Engdahl, "Soft magnetic composites for advanced machine design," *PMAsia2005 in Shanghai*, 2005.
- [36] P. Jansson, "Processing Aspects of Soft Magnetic Composites," *Euro PM2000 Soft Magnetics Materials Workshop*, 2000.
- [37] P. Jansson, "SMC materials - including present and future applications " in *International Conference on Powder Metallurgy & Particulate Materials*, New York, NY; USA, 2000, pp. 7.87-7.97.
- [38] A. G. Jack, B. C. Mecrow, and P. G. Dickinson, "Core Back for an Electrical Machine and Method for Making the Same " United States Patent Application, Publication Number: 2004/0212267 A1, 2004.
- [39] A. G. Jack, B. C. Mecrow, G. Nord, and P. G. Dickinson, "Axial Flux Motors Using Compacted Insulated Iron Powder and Laminations - Design and Test Results," in *Electric Machines and Drives, 2005 IEEE International Conference on*, 2005, pp. 378-385.
- [40] H. M. Amreiz, "Transverse Flux Switched Reluctance Motors," Ph.D. Thesis, University of Newcastle upon Tyne: Newcastle upon Tyne, 2002.
- [41] H. M. Amreiz, B. C. Mecrow, and C. Weiner, "Switched reluctance machines with simple hoop windings," in *Power Electronics, Machines and Drives, 2002. International Conference on (Conf. Publ. No. 487)*, 2002, pp. 522-527.
- [42] J. P. Licata and D. J. Ricker, "Strip Wound Dynamoelectric Machine Core," United States Patent No: 4365180, 1981.
-

- 
- [43] N. Miyake, A. Matsui, Y. Nakahara, A. Hashimoto, and M. Motohashi, "Stacked Stator Core And Method Of Manufacturing Thereof, And Rotary Motor And Method Of Manufacturing Thereof," United States Patent No: 7185418 B2, 2007.
- [44] Y. Ohuchi, T. Ebine, T. Ohwanda, and R. Tomozaki, "Method Of Manufacturing A Stator Core For Rotary Electric Machines," United States Patent No. 3842493, 1974.
- [45] J. B. Whiley, "Dynamoelectric Machine Means," United States Patent No. 3188505, 1965.
- [46] K. Kazama, H. Kato, K. Takinami, and M. Okamoto, "Core For Rotary Electric Machines and Method of Manufacturing The Same," European Patent No. EP 0833427 A1, 1998.
- [47] N. C. Bach\_Anderson, B. Lundsted\_Poulsen, T. Blad, and K. Hellegaard, "Blechpaket aus Segmenten," European Patent No. EP 1598918 A1, 2005.
- [48] T. Yamada, T. Kawamura, and N. Mizutani, "Stator for Dynamoelectric Machine," United States Patent No. 5986377, 1999.
- [49] H. Akita, Y. Nakahara, N. Miyake, and T. Oikawa, "New core structure and manufacturing method for high efficiency of permanent magnet motors," in *Industry Applications Conference, 2003. 38th IAS Annual Meeting. Conference Record of the, 2003*, pp. 367-372 vol.1.
- [50] H. Weh, H. Mosebach, and H. May, "Design concepts and force generation in inverter-fed synchronous machines with permanent magnet excitation," *Magnetics, IEEE Transactions on*, vol. 20, pp. 1756-1761, 1984.
- [51] A. Jack, E. Pinguey, and G. Nord, "An Electric Machine Assembly," World Intellectual Property Organization, International Publication No. WO 2007/024184 A1, 2007.
- [52] "Ansys Finite Element Suit (v8 - v11.0)," Ansys Inc. Southpointe, 275 Technology Drive, Canonsburg, PA 15317 United States.
- [53] MAGNET, "Infolytica Design and Analysis Suit for Electromagnetics," Infolytica Corporation, 300 Léo Pariseau, Suite 2222, Montréal, Québec H2X 4B3, CANADA.
- [54] D. Staton, A. Boglietti, and A. Cavagnino, "Solving the more difficult aspects of electric motor thermal analysis," in *Electric Machines and Drives Conference, 2003. IEMDC'03. IEEE International, 2003*, pp. 747-755 vol.2.
- [55] D. C. Hanselman, *Brushless permanent magnet motor design 2ed.*: Cranston, R.I., 2003.
- [56] A. Fukuma, S. Kanazawa, D. Miyagi, and N. Takahashi, "Investigation of AC loss of permanent magnet of SPM motor considering hysteresis and eddy-current losses," *Magnetics, IEEE Transactions on*, vol. 41, pp. 1964-1967, 2005.
-